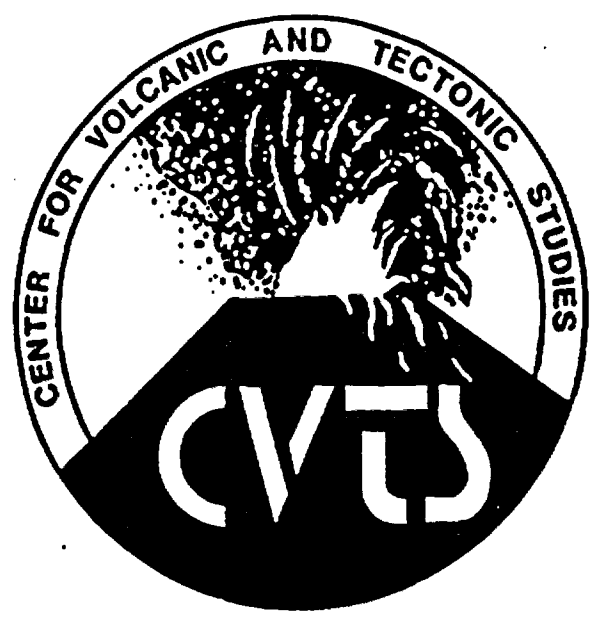


**REGIONAL IMPORTANCE OF POST-6 M.Y. OLD VOLCANISM IN THE
SOUTHERN
GREAT BASIN:
IMPLICATIONS FOR RISK ASSESSMENT OF VOLCANISM AT THE PROPOSED
NUCLEAR WASTE
REPOSITORY AT YUCCA MOUNTAIN, NEVADA**



**Center for Volcanic and Tectonic Studies¹
Department of Geoscience
University of Nevada, Las Vegas
Las Vegas, Nevada 89154**

Report No. 10

**ANNUAL REPORT for the Period 7/1/87 to 6/30/88 Submitted to
the Nuclear Waste Project Office
State of Nevada**

SEPTEMBER 1, 1988

¹Eugene I. Smith-Principal Investigator
Daniel Feuerbach-Research Associate
Terry Naumann-Research Associate
Ed Thomas-Laboratory Associate
Erin Cole-Graduate Student

Handwritten notes:
P4
P7
15
16
17
3307

INTRODUCTION

This report summarizes our activities during the period July 1, 1987 to June 30, 1988. Our goal was to develop an understanding of late-Miocene and Pliocene volcanism in the Great Basin by studying late-Tertiary volcanic rocks to the north and south of the Nevada Test Site (Figure 1). We especially concentrated on detailed stratigraphic studies and geochemistry to determine the nature of chemical changes during the lifetime of a volcanic field, and on structural studies to determine the nature of the structures that control vent location. Also, K-Ar age dating provided important new information on the duration of activity at a single volcanic center. Geologic studies were concentrated in the Fortification basalt field in southern Nevada and in the Reveille Range in central Nevada.

Our studies provide three important conclusions that have implications for volcanism about the proposed Nuclear Waste Repository at Yucca Mountain. These are:

- 1) There are no easily recognized geochemical characteristics that signify the termination of volcanism.
- 2) The location of vent areas of basaltic volcanoes are not necessarily controlled by pre-existing structures.
- 3) Volcanism at an individual basaltic center may last as long as 500,000 years.

REVEILLE RANGE-INTRODUCTION

(Terry Naumann)

Geologic mapping (scale 1:25,000) concentrated on a volcanic complex near Hyde Spring in the northeastern Reveille Range (Figure 2). Basalts of the Hyde Spring volcanic complex were emplaced through a major Tertiary ash-flow sheet; the Monotony Tuff. Studies in the Reveille Range are important because deep erosion resulting in up to 400 m of relief provides an ideal opportunity to study the internal structure of vents of polycyclic Pliocene cinder cones that were emplaced in ash-flow tuff, thus providing a close analog to the Yucca Mountain-Crater Flat area. Goals of this study are: (1) To determine the volcanic stratigraphy to serve as a framework for

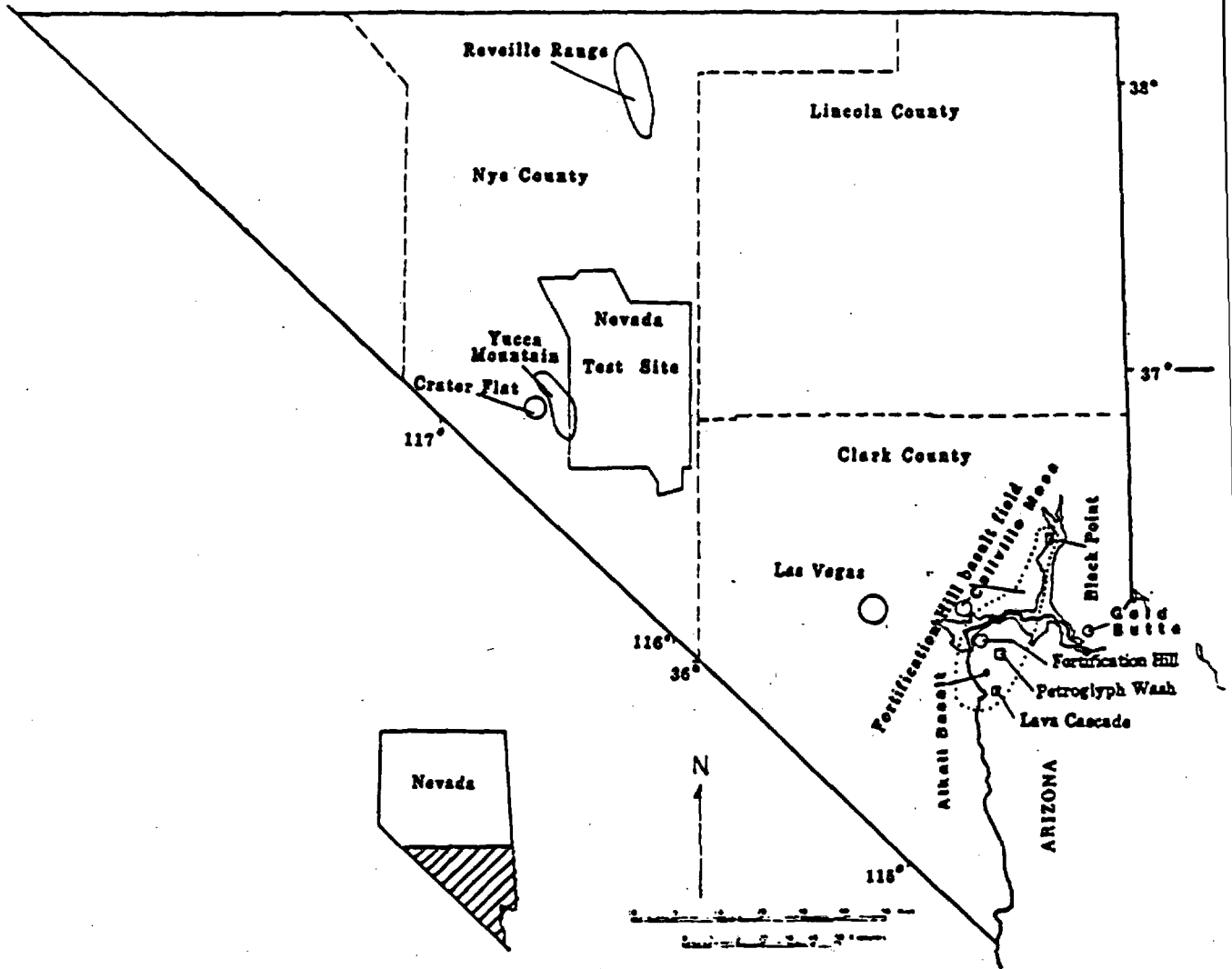


Figure 1. Index map showing locations mentioned in text.

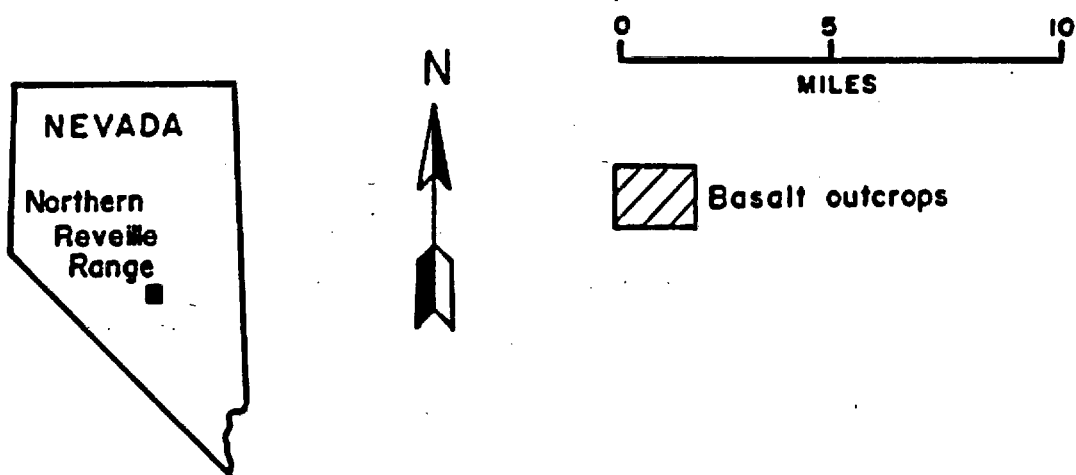
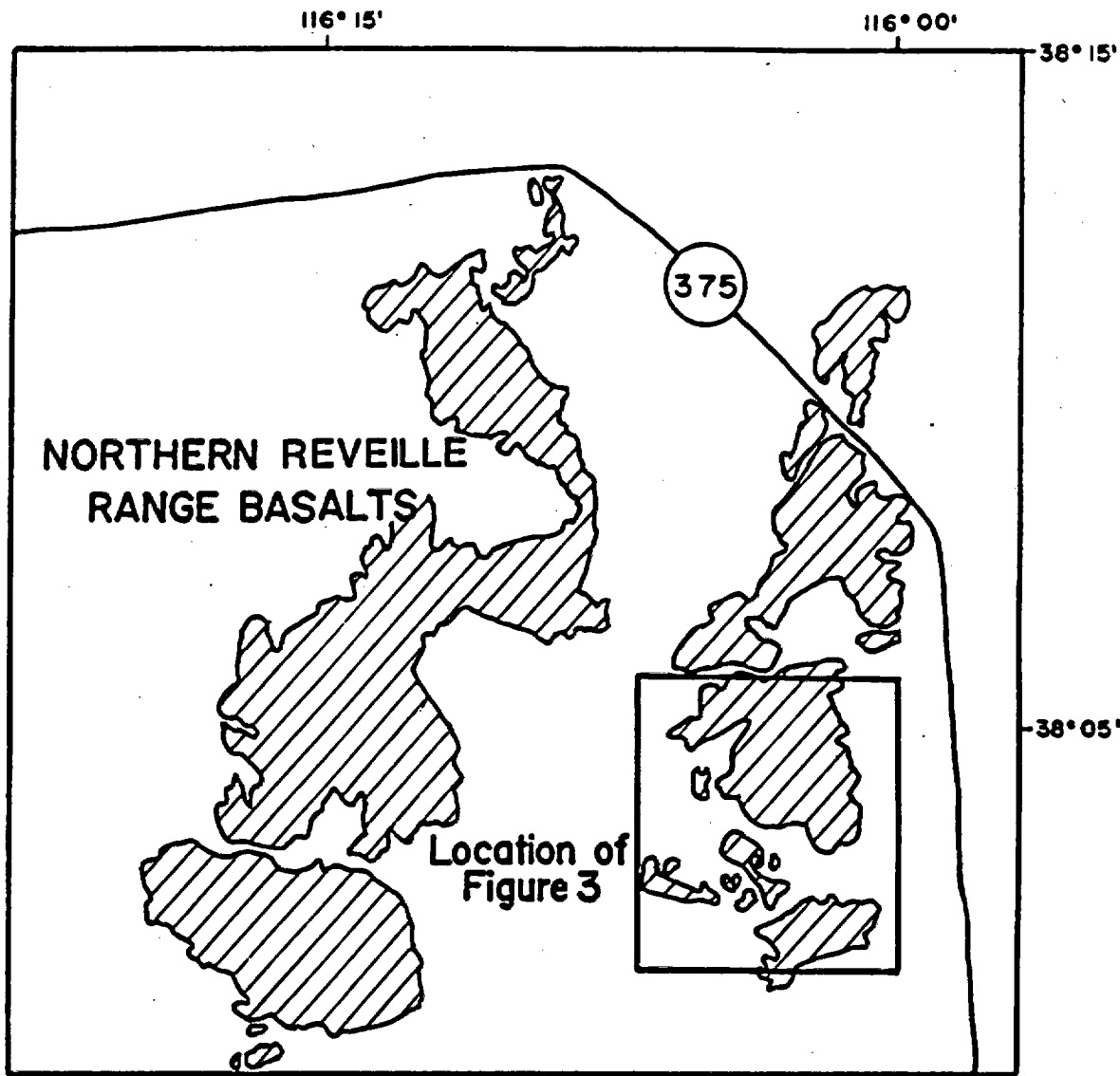


Figure 2. Index map of the northern Reveille Range, Nevada.

geochemical and geochronologic studies. Knowledge of the stratigraphy is important to accurately document changes in the composition of magma during the lifetime of the volcanic field. (2) To evaluate the effects of regional structure and basement rock type on the emplacement and localization of the vent areas.

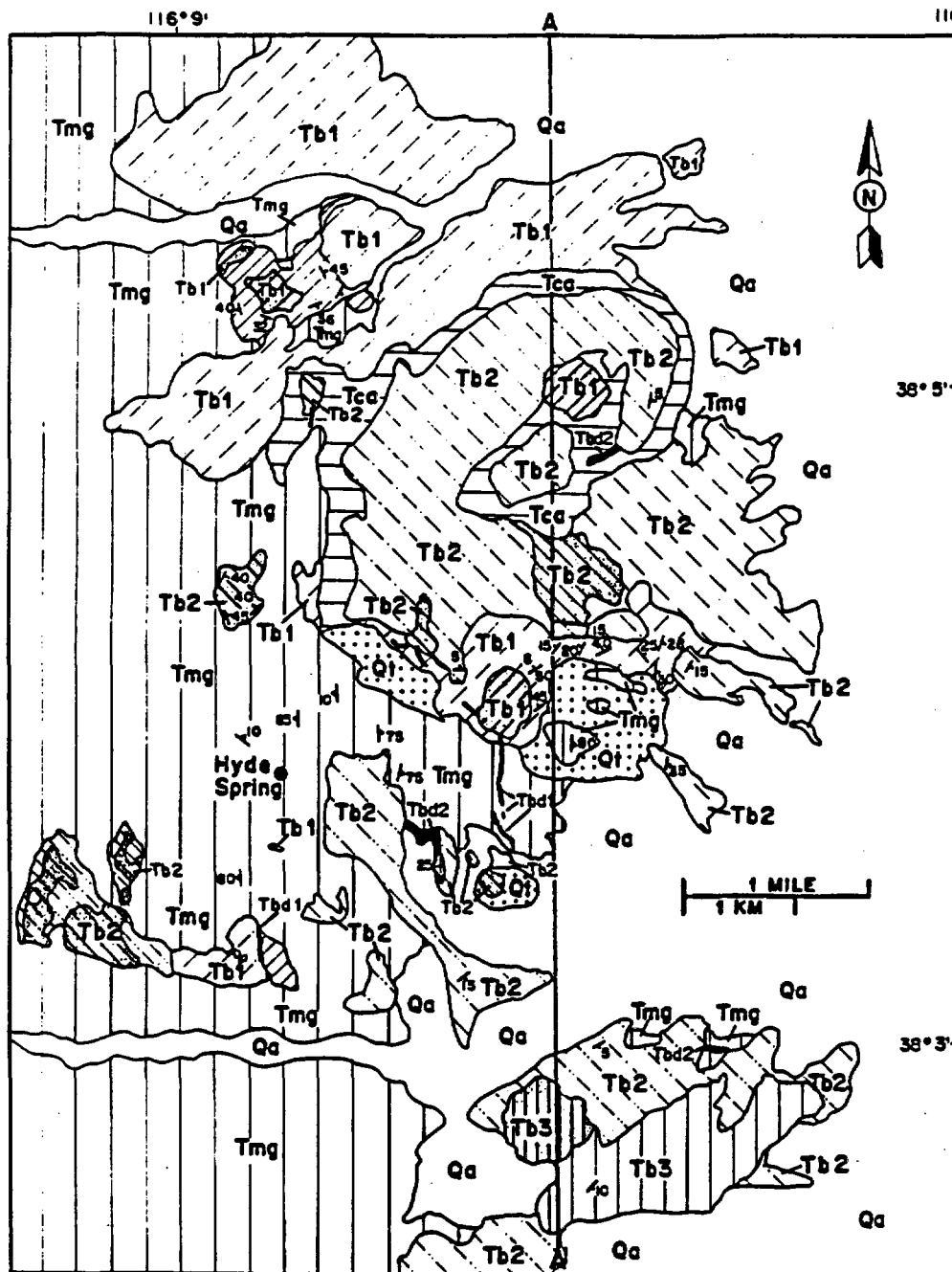
VENT AREAS

The Hyde Spring volcanic complex (Figure 3) records three eruptive episodes.

First Episode

The earliest episode of basaltic activity (Tb1, Figure 3) is represented by three highly dissected cinder cones, and related plugs, dikes and lava flows, that erupted through and are buttressed against the Monotony Tuff. Volcanic rocks of the first episode contain large (up to 2 cm in size) andesine megacrysts that form up to 40% of the rock.

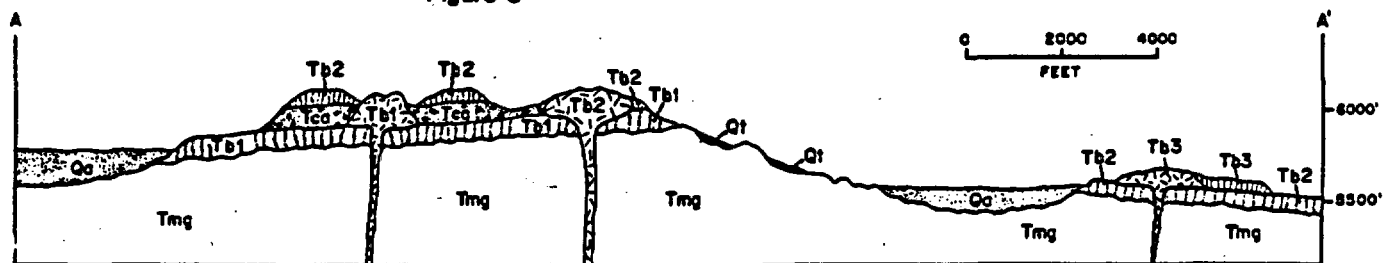
Volcanic rocks of the first episode originated from three separate volcanic centers: (1) a scoria-cone complex 2 km northeast of Hyde Spring (Figure 3). The cone is on the north flank of a paleotopographic high formed by Monotony Tuff. In this area, remnants of cinder-scoria cones and lava flows are exposed in deeply incised canyons north of the main vent area. Lavas flowed to the north and east and are now mostly covered by later eruptive products of the second episode. (2) A scoria-cone complex 2 km north of Hyde Spring (Figure 3). At this locality a scoria cone and associated plugs erupted flows that covered up to 15 km². Lavas flowed to the north, east and south. Together lavas from these two centers produced a lava field that covers an area of 50 km². Cinder cones at both centers are composed of massively bedded red to brown scoria, cinder, spatter, agglutinated scoria and ash. Locally, cinder is planar bedded, contains well formed bombs and was clearly deposited during Strombolian type eruptions. First episode lavas from these centers are commonly separated from second episode lavas by thick, poorly consolidated colluvial deposits (Tca, Figure 3), but near a scoria-cinder cone 1.5 km northeast of Hyde Spring, northwest dipping first episode lavas lie directly beneath east dipping second episode flows without intervening colluvium. (3) A volcanic center 2 km south of Hyde Spring (Figure 3) is composed of a 100 m thick sequence of plagioclase megacryst rich lavas and massively bedded red to brown scoria. The scoria was



- EXPLANATION**
- Qa Quaternary Alluvium
 - Q1 Quaternary Talus
 - Tb3 VENT } Plagioclase Megacryst Bearing Basalt (late stage)
 - Tb3 FLOW }
 - Tb2 VENT OR PLUG } Plagioclase, Pyroxene Bearing Basalt
 - Tb2 SCORIA }
 - Tb2 FLOW }
 - Tca Older Colluvium and Alluvium
 - Tbd1 VENT OR PLUG } Plagioclase Megacryst Bearing Basalt
 - Tbd1 SCORIA }
 - Tbd1 FLOW }
 - Tbd2 Basalt Dike
 - Tbd2 Basalt Dike
 - Tmg Tuff of Goblin Knobs (Monotony Tuff)
 - / Dike
 - } Contact
 - 30y Attitude
 - 45y Foliation Attitude

GEOLOGIC MAP OF A PORTION OF THE NORTHERN REVILLE RANGE, NEVADA

Figure 3



buttressed on the west by the Monotony Tuff. Lavas of this volcano were fed by a north-south striking dike and flowed west through canyons in the Monotony Tuff. Canyons were filled to a depth of up to 100 m.

Second Episode

The second episode of basaltic activity in the Hyde Spring volcanic complex (Tb2, Figure 3) is represented by eight separate volcanic centers that include cinder cones, plugs, flows, and dikes. Lavas of the second episode contain variable amounts of augite (up to 40%), amphibole (up to 35%) and plagioclase (<5%) megacrysts and coarse grained gabbroic xenoliths (up to 20 cm in size). Xenoliths of dunite are occasionally found in flows.

Several second episode dikes (Tbd2, Figure 3) served as vents for flows. A 10 m wide dike, 4 km northeast of Hyde Spring, fed flows that extend for 2 km to the north of the vent. Another 10 m wide dike, 1.5 km southeast of Hyde Spring fed flows that travelled 3.6 km to the southeast.

Six plugs of second episode basalt are exposed in the Hyde Spring area. Two plugs, 2 km and 3 km northeast of Hyde Spring, intrude scoria and are associated with dikes. The most voluminous lava flows of second episode basalt erupted from a cinder cone 2 km northeast of Hyde Spring and flowed 3.5 km to the north and east. Other flows originated from a center 3 km northeast of Hyde Spring and cascaded over the eastern range margin. Pressure ridges and large ramp-like folds form ridges on the upper surfaces of flows that trend perpendicular to flow direction. Three plugs intrude Monotony Tuff and display steep, inward dipping foliation and are associated with minor amounts of scoria. A volcanic center 2 km southwest of Hyde Spring, is a formed by four plugs that intrude a cinder cone. This cinder cone is composed of massively bedded red to brown scoria, cinder, spatter, agglutinated scoria. Locally, cinder is planar bedded, contains well formed bombs and was deposited during Strombolian-type eruptions. Cinder from this center partially buries first episode lavas to the east.

Together the total area of outcrop of second episode lavas is approximately 20 km² (13 Km² scoria-plug related, 7 km² dike related).

Third Episode

The final episode of basaltic activity (Tb3, Figure 3) is represented by a cinder cone that formed on second episode lavas. The cone formed on the distal portion of second episode flows 4 km southeast of Hyde Spring and erupted lavas that cover about 2.0 km². Third episode lavas contain variable amounts of plagioclase (up to 40%) and augite (<2%) megacrysts.

STRUCTURAL CONTROL OF VENT EMPLACEMENT

Structural analysis of the Monotony Tuff indicates a large population of north-south striking and near vertical fractures. There is also a background population of high-angle fractures with diverse orientations (Figure 4). Vents within the Hyde Spring volcanic complex are not controlled by mapped faults or joints in the Monotony Tuff. Several lines of evidence support this conclusion: (1) Ninety percent (9 of 10) dikes of the first episode strike obliquely to the trend of joints. (2) Three dikes of the second episode cut across the north-south joint set at 45 degrees. A dike 1 km southeast of Hyde Spring (Figure 3) trends north-south for 0.5 km then abruptly turns northwest. (3) Second episode plugs, 1.5 km southwest of Hyde Spring, crudely follow the north-south striking joints in the Monotony Tuff but 0.5 km to the west, plugs trend perpendicular to the north-south joints. (4) There is no consistent alignment or trend of either episode 1 or episode 2 plugs.

GEOCHEMISTRY OF THE HYDE SPRING VOLCANIC COMPLEX

Major element analyses are available for 25 samples from first, second, and third episode lavas. These include new analyses for 9 samples (Table 1). These analyses provide sufficient data to classify, determine chemical variation with stratigraphic position and discuss differences and similarities between each eruptive episode. Trace and rare-earth element (REE) analyses are available for 16 samples of the first and second episode.

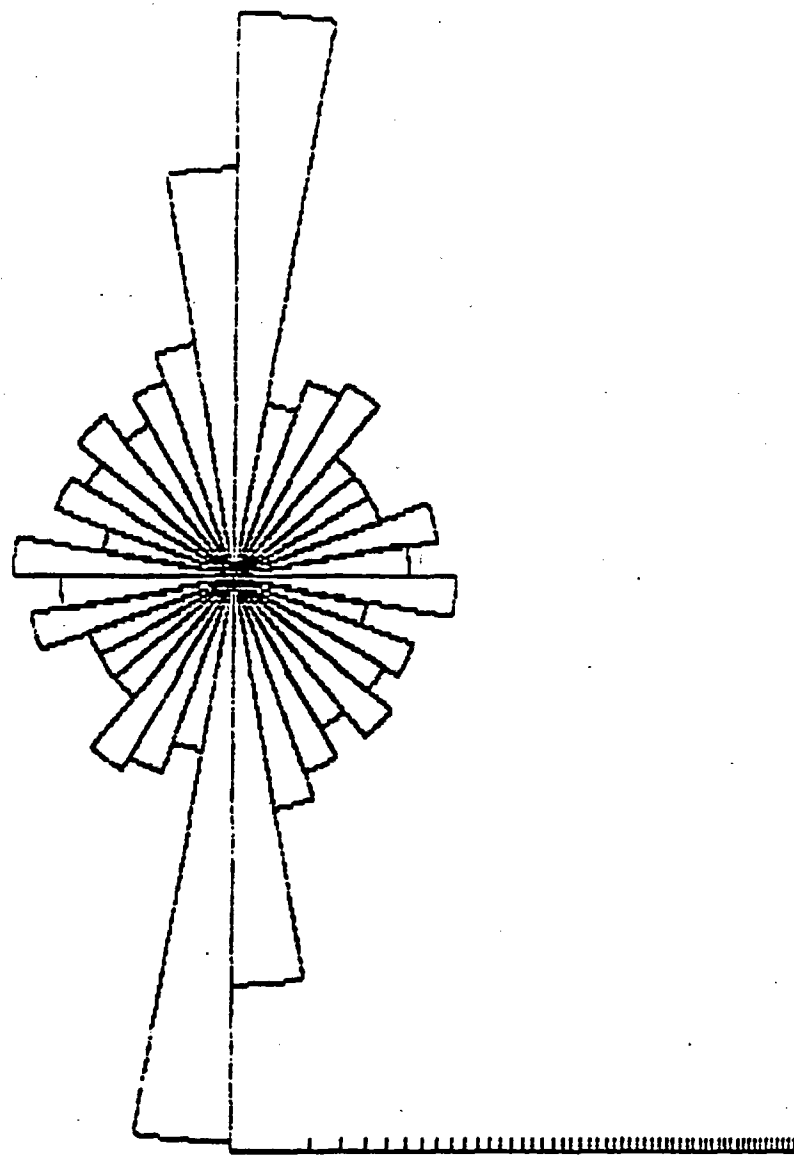


Figure 4. Rose diagram showing prominent north-south joint directions within the Monotony Tuff, Reveille Range, Nevada.

File name C:\NORMR3.ROC

Sample	R-1-17	R-1-18	R-1-19	R-1-22	R-1-23	R-1-24	R-1-25	R-1-26	R-1-27
Group #	0.00	1.00	2.00	1.00	1.00	0.00	0.00	1.00	1.00
Qual	0	0	0	0	0	0	0	0	0
Key	0	0	0	0	0	0	0	0	0
Ref	0	0	0	0	0	0	0	0	0
SiO2	47.12	46.51	46.70	45.01	43.88	47.63	46.54	44.68	44.43
TiO2	2.02	3.52	3.34	2.00	3.13	2.06	3.35	2.84	2.84
Al2O3	16.62	15.78	15.88	15.63	14.61	16.34	16.33	14.77	14.31
FeO	13.37	15.48	14.68	12.18	12.58	13.66	14.98	12.17	12.27
MnO	0.17	0.20	0.18	0.17	0.17	0.18	0.19	0.17	0.17
MgO	5.66	4.60	4.83	6.45	10.19	5.34	5.15	9.69	10.36
CaO	8.90	7.66	8.84	9.63	9.85	8.55	8.40	9.79	10.20
Na2O	3.67	4.13	3.85	3.47	3.20	3.71	3.58	3.49	3.31
K2O	1.13	1.43	1.11	1.83	1.57	1.10	1.06	1.77	1.50
P2O5	0.44	0.68	0.48	0.64	0.63	0.44	0.40	0.62	0.60
Total	100.00	100.00	100.00	100.00	100.00	100.00	100.00	100.00	100.00
AN	52	45	48	69	75	48	51	73	74
or	7	8	6	11	9	7	6	10	9
ab	23	24	23	10	7	25	24	7	7
an	28	20	22	21	20	24	25	19	20
na	4	6	5	10	11	3	3	12	11
d1	13	11	15	18	20	13	11	20	22
o1	20	21	19	22	25	20	22	23	24
tl	6	7	6	6	6	6	6	5	5
ep	1	2	1	1	1	1	1	1	1
FeO*	13.37	15.48	14.68	12.18	12.58	13.66	14.98	12.17	12.27
F/F+M	0.705	0.773	0.751	0.584	0.556	0.721	0.747	0.560	0.546
den	2.72	2.74	2.74	2.74	2.77	2.72	2.75	2.75	2.76

Table 1. New whole rock major-element geochemistry and cation normative mineral compositions for basalts from the Reville Range, Nevada.

Chemical Classification

Chemical classification is based on techniques of Irvine and Baragar (1971) and is reviewed in Table 2 and Figures 5, 6, and 7. All rocks of the Hyde Spring volcanic complex are classified as alkalic and fall within either the sodic or potassic series (Figure 5, 6, and 7).

TABLE 2
Chemical Classification of Volcanic Rocks
in the Hyde Spring Volcanic Complex

<u>Episode</u>	<u># of Samples</u>	<u>Rock Name</u>	<u>Phase</u>
1	9	alkali basalt	dike, flow
1	1	hawaiite	dike
2	5	picrite	plug
2	5	alkali basalt	dike, plug, flow
2	2	hawaiite	flow
2	1	trachybasalt	flow
2	1	tristanite	plug
3	1	alkali basalt	flow

Chemical Variation

Rocks of the Hyde Spring volcanic complex have SiO₂ contents that range from 41 to 56% (Figure 8). Rocks of the first and second episode are both hypersthene and nepheline normative while rocks of the third episode are only nepheline normative (Figure 9). There is no trend from hypersthene to nepheline normative rocks with time. Foland et al. (1987 and 1988) indicate a general tendency for the youngest basalts at any one locality in the Reveille Range to contain the most normative nepheline. However, our work demonstrates that there is not a positive correlation

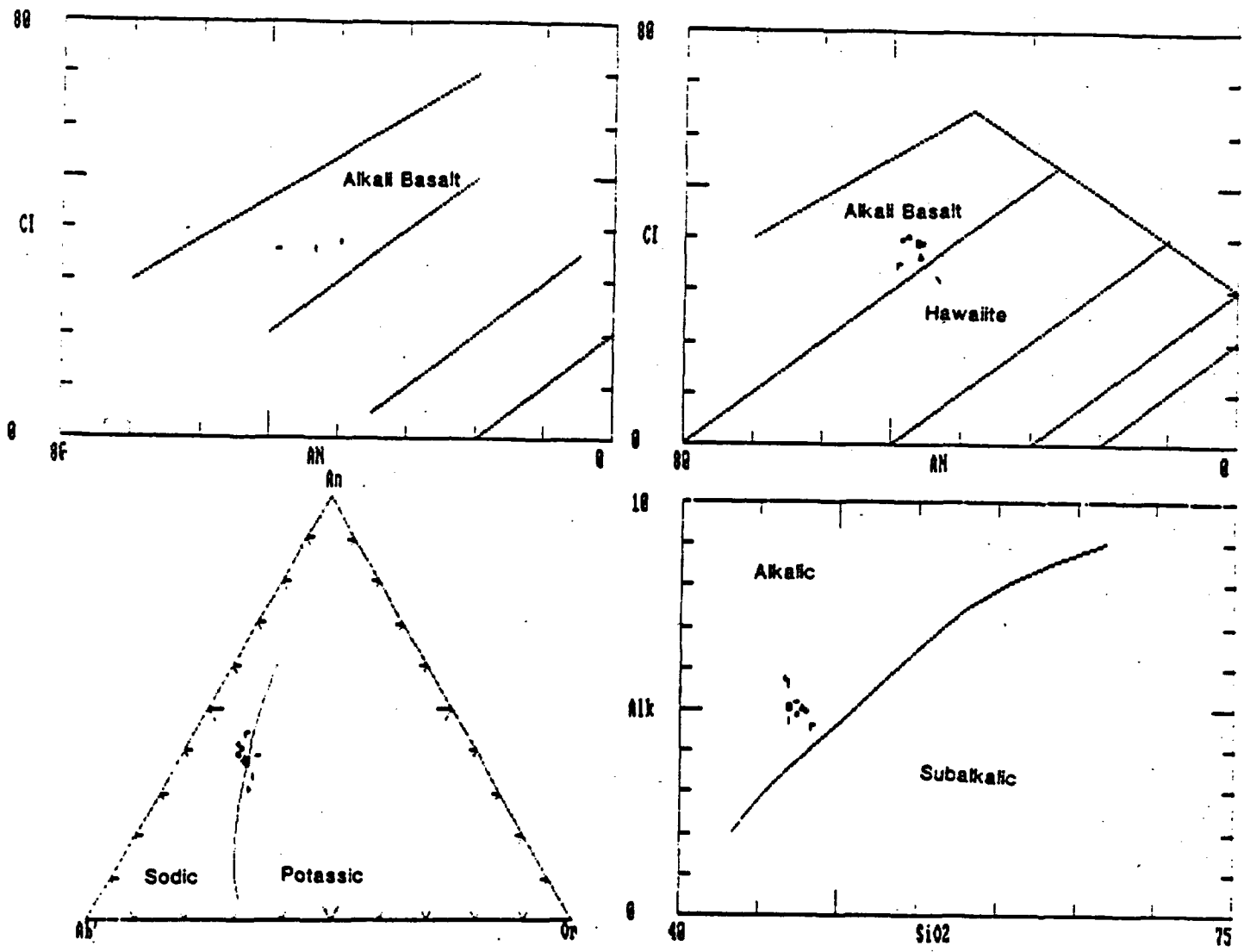


Figure 5. Irvine and Baragar classification (1971) for Reveille Range, Episode 1 basalts.

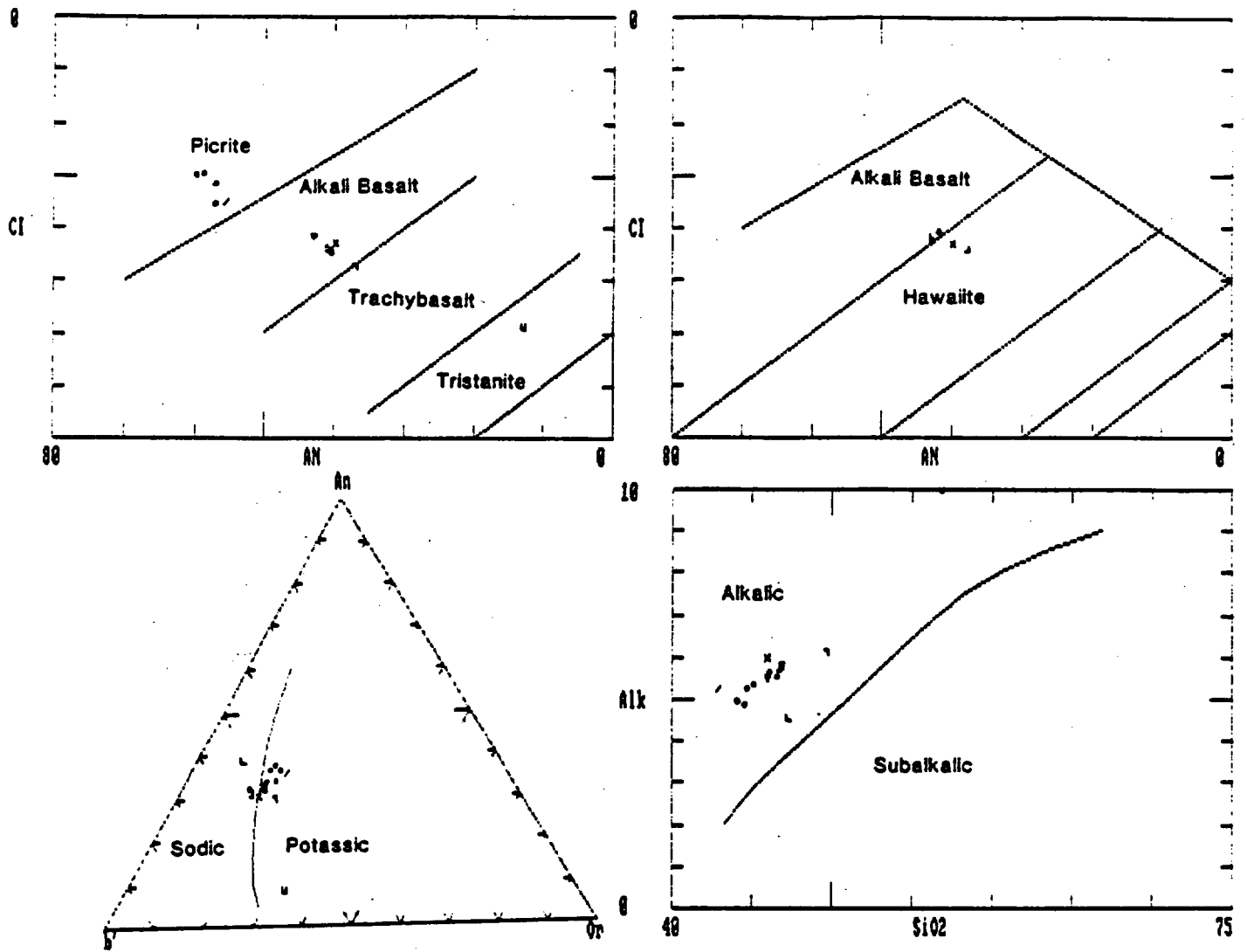


Figure 6. Irvine and Baragar classification (1971) for Reveille Range, Episode 2 basalts.

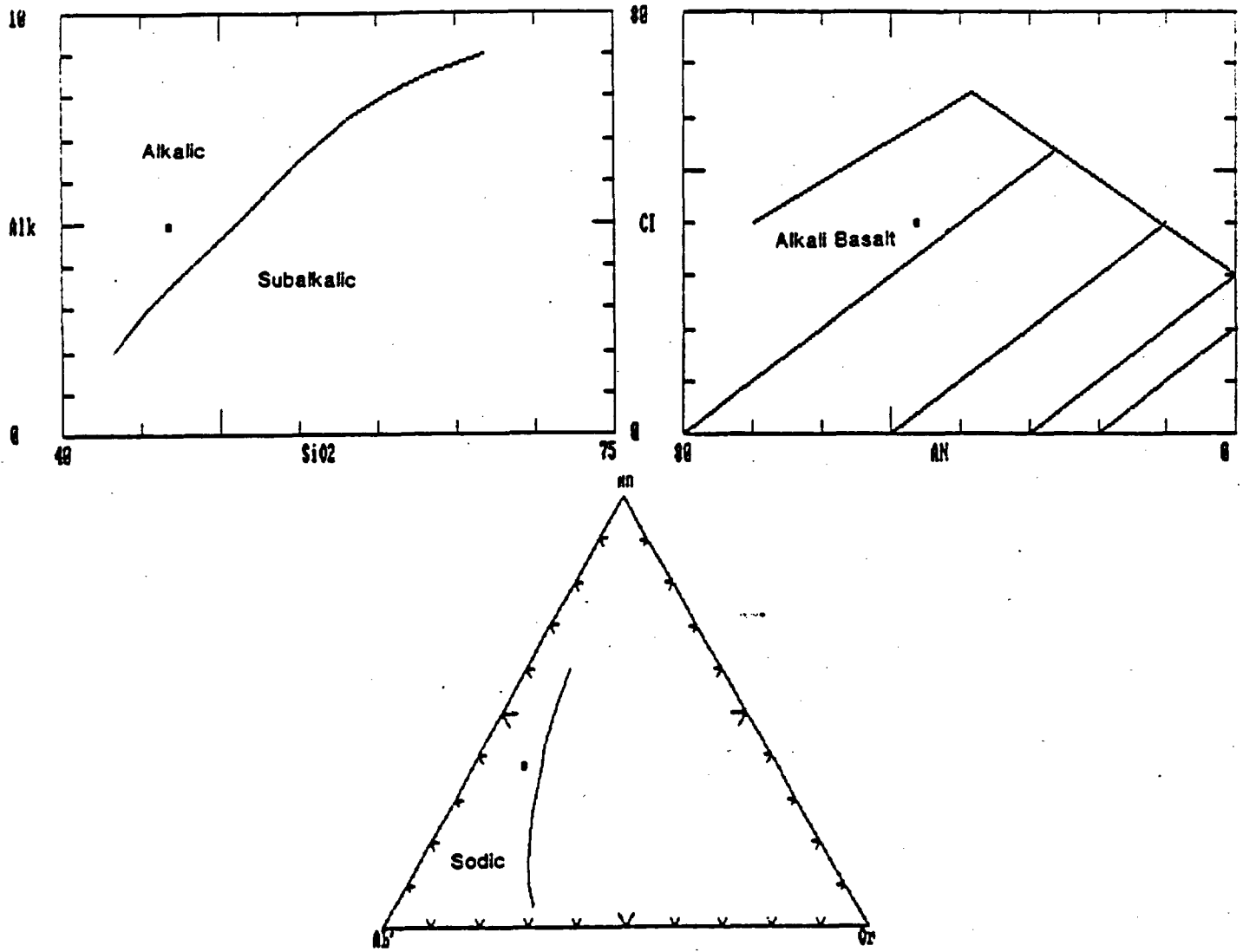


Figure 7. Irvine and Baragar classification (1971) for Reveille Range, Episode 3 basalts.

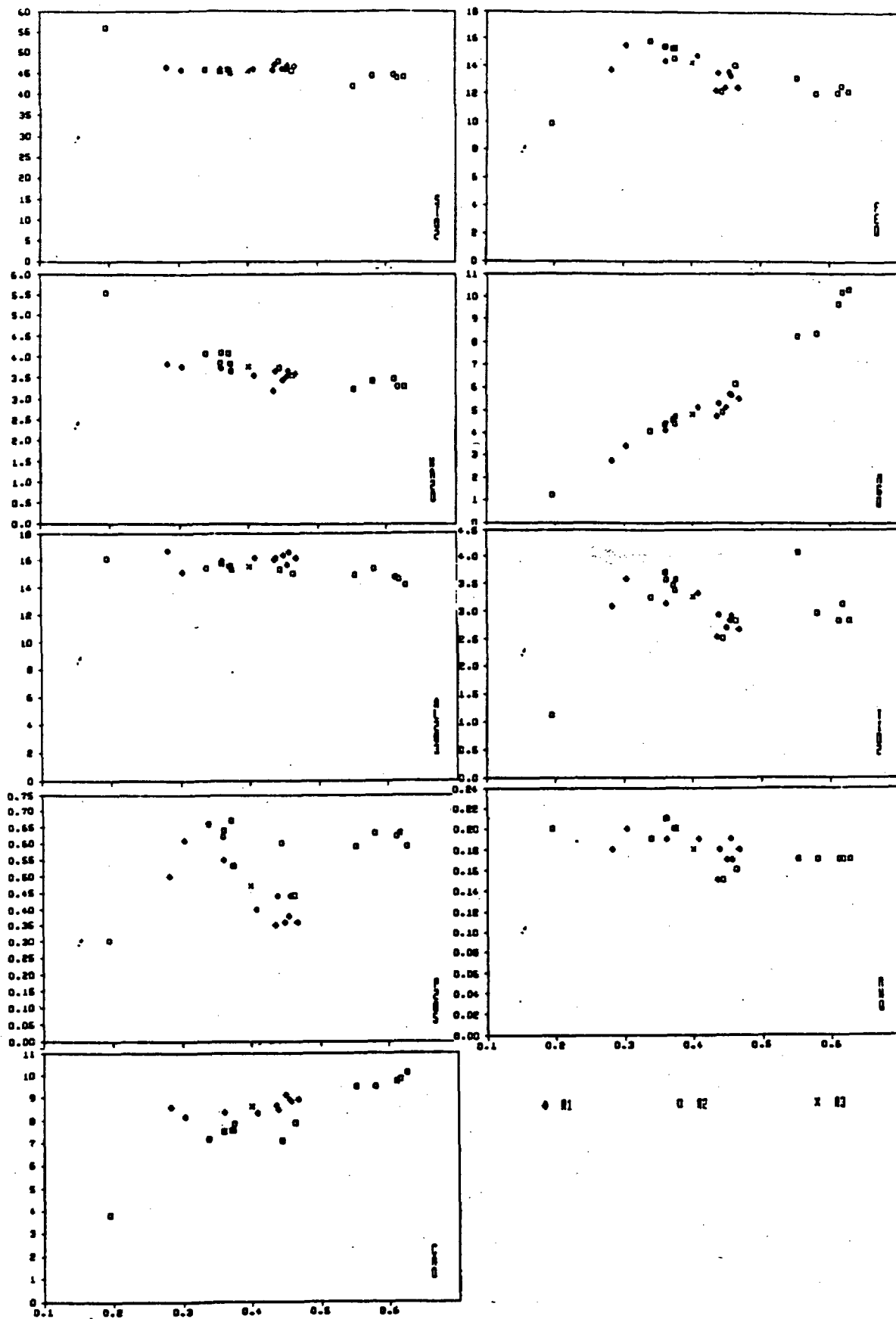


Figure 8. Harker variation diagrams for the Reveille Range basalts. Diamonds=Episode 1, Squares=Episode 2, X=Episode 3.

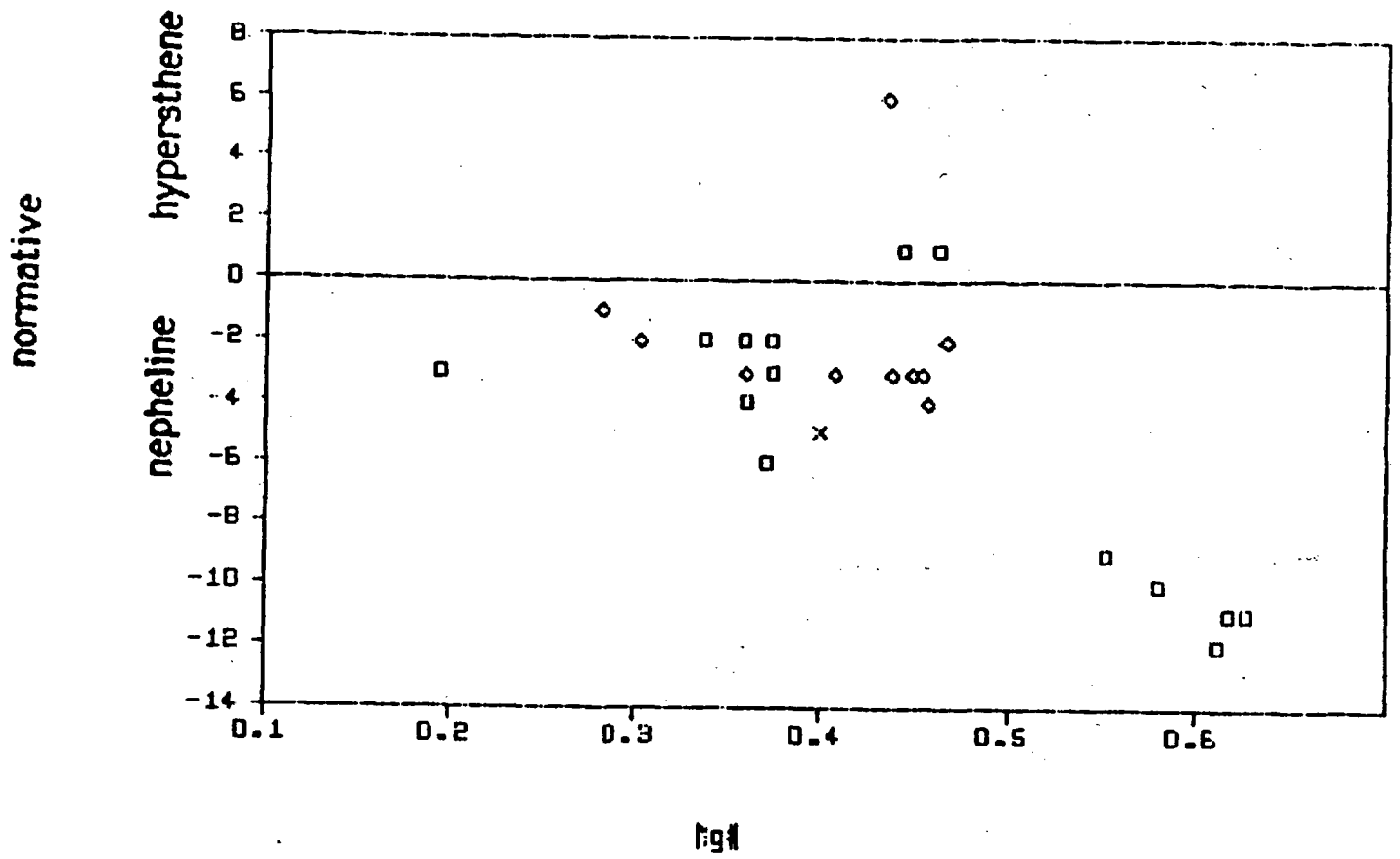


Figure 9. Cation normative hypersthene and nepheline vs. Mg# for the Reville Range basalts. Diamonds=Episode 1, Squares=Episode 2, X=Episode 3.

between normative nepheline content and age (Figure 9) or a simple trend from hypersthene normative to nepheline normative basalts with age. Therefore, in this area, the eruption of nepheline normative lavas does not signal the termination of volcanic activity.

Chemical Comparison Between Episodes

There are subtle differences in major element chemistry, rock norms and modal mineralogy that characterize the first, second and third episode lavas. These are: 1. First episode rocks (10 samples) all contain plagioclase megacrysts. All but four rocks are sodic (Figure 5). These rocks have a narrow chemical range with SiO_2 values ranging from 44 to 48% and except for one hawaiite, all are alkali basalts. First episode rocks are higher in Al_2O_3 and CaO, and lower in P_2O_5 while the remaining oxide abundances are similar to the rocks of the second episode (Figure 8). First episode rocks are hypersthene or nepheline normative (Figure 9) and are less enriched in the light REE compared to rocks of the second episode (Figure 10). 2. Second episode rocks (14 samples) either contain augite and or hornblende megacrysts. All but three rocks are potassic (Figure 6). Episode 2 rocks are more chemically diverse than episode 1 rocks, ranging in SiO_2 from 41 to 56% and include picrite, alkali basalt, hawaiite, trachybasalt, and tristanite. Second episode rocks are hypersthene or nepheline normative (Figure 9) and display higher overall enrichments in the REE (Figure 10). 3. Third episode rocks (1 sample) contain plagioclase megacrysts. This sample is a nepheline normative (Figure 9), K-rich alkali basalt (Figure 7) and plots within the range of first episode rocks on all variation diagrams.

COMPARISONS WITH CRATER FLAT

Several comparisons can be made between the basalts of the Reville Range and the basalts at Crater Flat-Yucca Mountain:

1. Basaltic volcanoes in the Reville Range lie within the belt of volcanism that stretches from Death Valley in the south to the Pancake Range in the north and that also includes Crater Flat (Vaniman and Crowe, 1981).
2. Basalts of the Hyde Spring volcanic complex were emplaced in a major Tertiary ash-flow sheet; the Monotony Tuff. Basalts at Crater Flat were also emplaced in

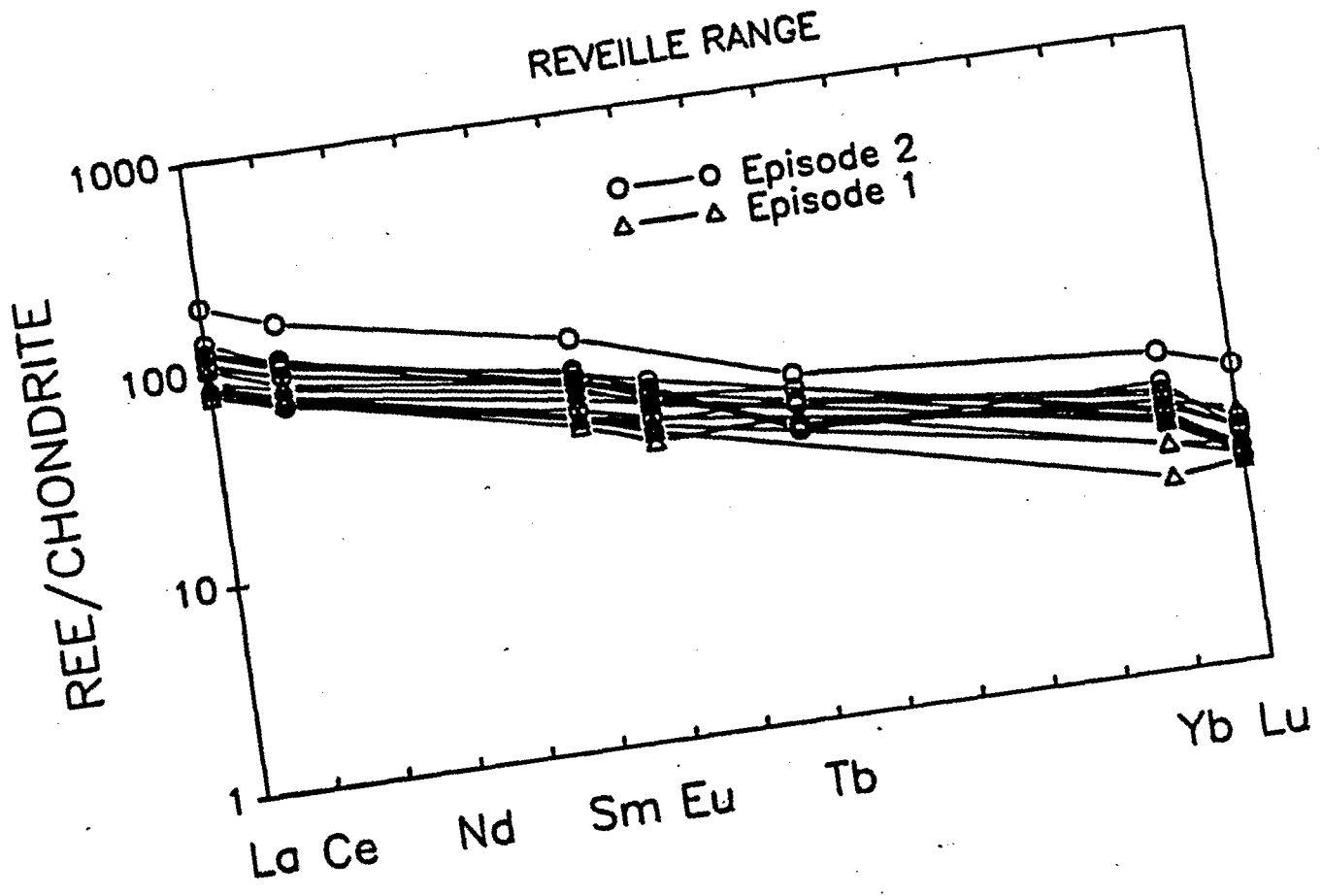


Figure 10. Rare-earth element plot for the Reveille Range basalts

ash-flow tuff (Carr, 1982).

3. Volcanic activity occurred at approximately the same time in both locations (< 4 Ma) (Vaniman and Crowe, 1981; Dohrenwend et al., 1985).

IMPLICATIONS

Conclusions based on the study of the Reveille Range basalts that have a direct bearing on the proposed Yucca Mountain repository are:

1. Feeder dikes and plugs do not use existing structures during emplacement.

2. Rocks of the Hyde Spring volcanic complex are both hypersthene and nepheline normative, however there is no trend from hypersthene to nepheline normative rocks with time. Therefore, at least in this area, the eruption of nepheline normative lavas does not signal the termination of volcanic activity.

INTRODUCTION-FORTIFICATION HILL FIELD

(Dan Feuerbach)

The nature of the change of the chemistry of igneous rocks during tectonic transitions is highly debated. Studies by Lipman et al., (1972), Christiansen and Lipman (1972), and Suneson and Lucchitta (1978) and other authors suggested that in the Basin and Range province of the western United States, volcanism changed from calc-alkalic intermediate to bimodal rhyolite-basalt during the transition from crustal compression to extension. However, Anderson (1978) and Smith et al. (in press) demonstrated that in the Lake Mead area of Nevada and Arizona, calc-alkaline intermediate volcanism persisted throughout major extension. Only after major extension did basalt erupt (9-4 Ma). Volcanic activity in the Lake Mead area provides an almost continuous record of changing volcanism during the transition from active crustal extension to relative crustal stability. In the Lake Mead area, active extension

lasted from approximately 15 to 10 Ma (Anderson, 1978; Anderson, 1982; Bohannon, 1983 and 1984). The Hamblin-Cleopatra volcano (12.5-13.1 Ma) (Anderson, 1973; Thompson, 1985) erupted during major extension and represents some of the latest calc-alkaline intermediate volcanism in the Lake Mead area. Changes in character of volcanism began during the waning stages of extension with the eruption of the basalt and basaltic andesite at Callville Mesa (10.3 to about 11 Ma) and continued with the post-extension eruptions of the Fortification Hill basalt (9.7-4.7 Ma). During this transition period, calc-alkaline volcanism (Hamblin-Cleopatra Volcano and Callville Mesa) was replaced by eruptions of alkali basalt (Fortification Hill and Lava Cascade).

This report discusses the petrogenesis and structural control of vent emplacement of basalts at Fortification Hill and of basalts and basaltic andesites at Callville Mesa and provides the first modern description of these volcanic fields. We describe petrography and field relationships, and present major and trace element chemistry and new K-Ar age dates. The report also documents and models changes in the style of volcanism in the time interval between a period of active extension and tectonic quiescence.

GEOLOGIC SETTING

The Fortification Hill and Callville Mesa volcanic fields lie in the southern part of the Basin-and-Range physiographic province. The major structures are mid- to late-Miocene low-angle and high-angle normal faults. Low-angle faults formed during maximum extension, and high-angle block faults may be related to a deep crustal detachment fault (Deubendorfer et al., in press). The Lake Mead Fault Zone consists

of a series of west-southwest trending left-lateral strike-slip faults (Figure 11). This fault zone may be coeval with low-angle faulting and probably formed as an accommodation zone between differentially extending upper-plate blocks (Bohannon, 1983; Weber and Smith, 1987).

South of Lake Mead is a series of north-northwest trending high-angle normal faults that cut Miocene volcanic and plutonic rocks and Miocene to Pliocene clastic intrabasinal sediments of the Muddy Creek Formation (Feuerbach, 1986; Mills, 1985; Anderson, 1978). Small allochthonous blocks of tilted Paleozoic sedimentary rocks also crop out. The area north of the Lake Mead Fault Zone is composed of highly tilted Mesozoic sediments and Miocene intrabasinal sediments of the Horse Spring and Muddy Creek Formations (Bohannon, 1983). The area within and immediately adjacent to the Lake Mead Fault Zone consists mainly of volcanic rocks of the Hamblin-Cleopatra and Callville Mesa volcanoes.

The Fortification Hill basalt field forms a north-northeast trending belt 75 km long that extends from Malpais Flattop, Arizona to Black Point, Nevada (Figure 11). Basalts of Fortification Hill age periodically erupted from late-Miocene to early-Pliocene time (9-4.5 Ma). These include the volcanic rocks of Lava Cascade, Petroglyph Wash, Fortification Hill, Black Point, and the alkalic basalt dikes and flows along U.S. 93 (Figure 11). Stratigraphically, the basalts of the Fortification Hill field lie within and above intra-basinal conglomerates, sandstones, and siltstones of the Muddy Creek Formation.

The Callville Mesa basalts and basaltic andesites crop out in the middle of the Fortification Hill Basalt belt, just to the northwest of the Lake Mead Fault Zone. These

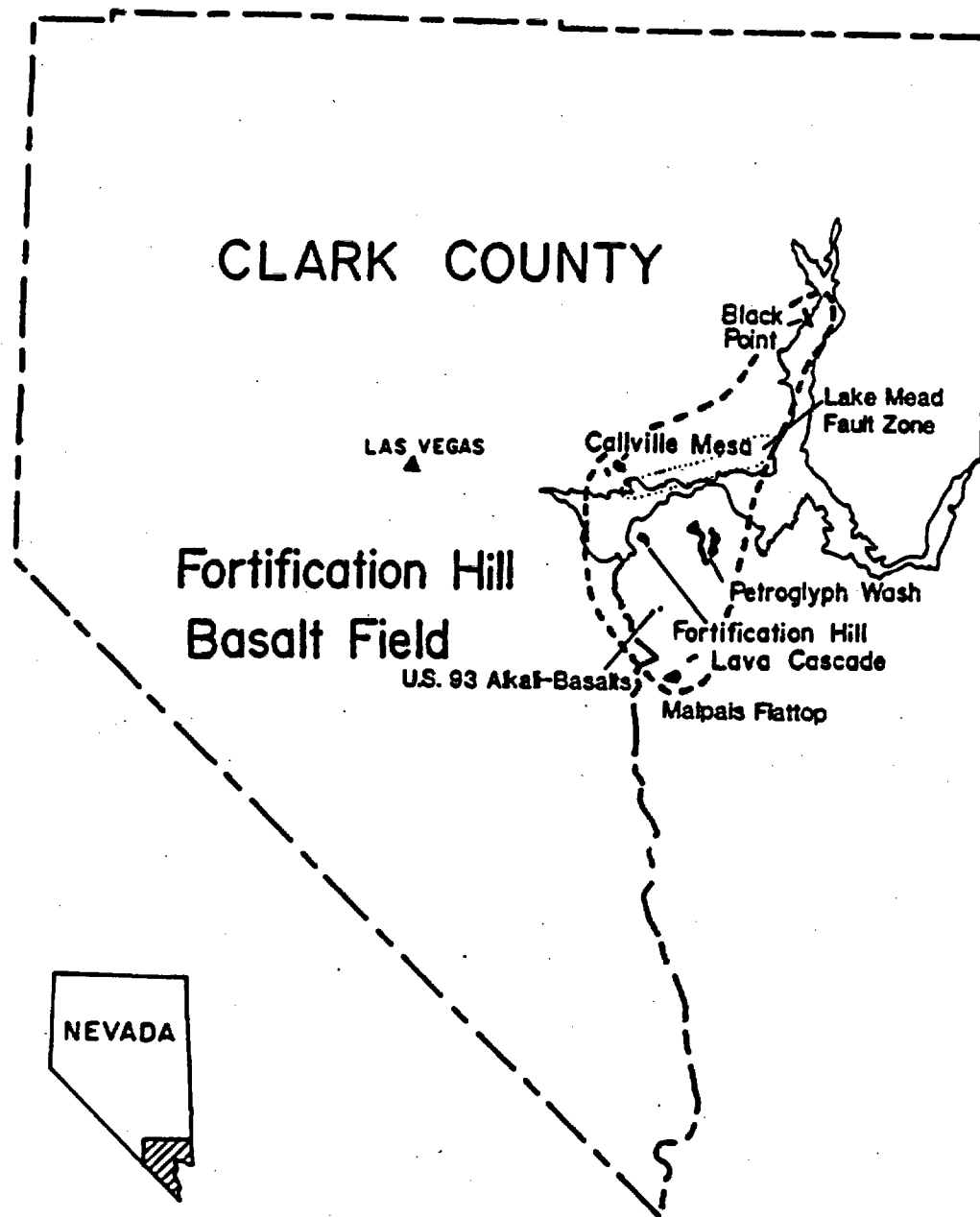


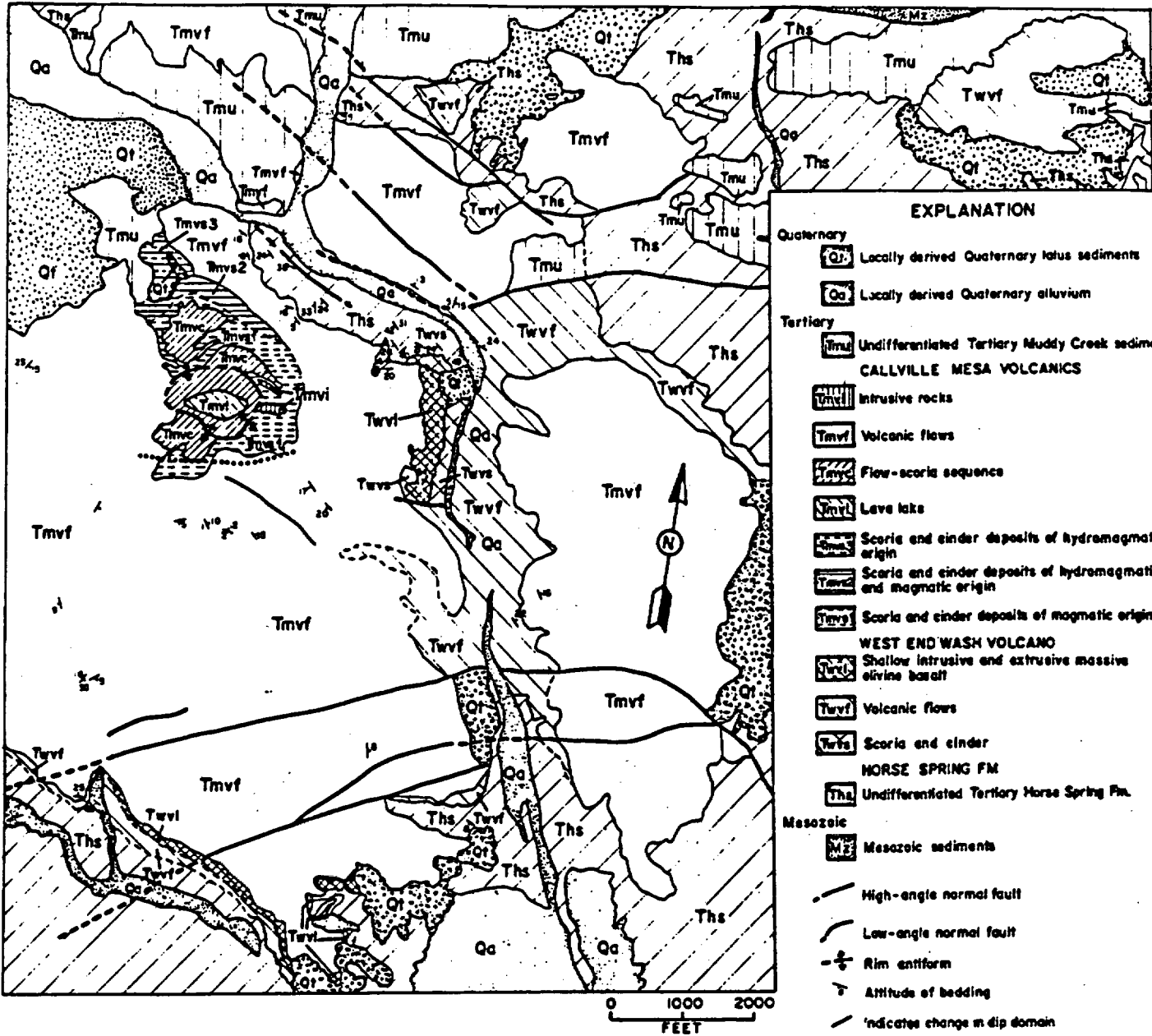
Figure 11. Index map of the Fortification Hill basalt field and locations mentioned in text.

rocks erupted 12?-10 Ma from volcanoes located at Callville Mesa and West End Wash (Figure 11). Flows from these volcanoes cover an area of at least 20 km². They lie on clastic intrabasinal sediments of the Thumb and Lovell Wash members of the Miocene Horse Spring Formation and may be intercalated within the Red Sandstone Unit (Bohannon, 1983). Two volcanic sections are recognized; an older set of flows that erupted from the West End Wash volcano and a younger set of flows that erupted from the Callville Mesa volcano. Rocks of the West End Wash volcano were structurally disrupted during the waning stages of east-west extension. Flows from the Callville Mesa vent cascaded over existing faults, however, locally flows are offset by east-west trending normal faults.

DESCRIPTION OF VOLCANIC CENTERS

Callville Mesa

Composite volcanoes were the source of the basalt and basaltic andesite at Callville Mesa and West End Wash (Figure 12). The best preserved cone is at Callville Mesa. Here, activity began with Strombolian eruptions and ended with Surtseyan-type eruptions. Its volcanic history is: 1) pyroclastic activity forming scoria of magmatic origin containing volcanic bombs, blocks (sample number F8-24-46-LN), scoria, cinder, ash, and rootless flows; 2) intermittent pyroclastic eruptions and extrusion of lava forming interbedded scoria (1-10 m) and flows (1-3 m) on the flanks of the volcano; 3) eruption of lava through dikes on the flanks of the volcano (sample numbers F8-24-48-LN and F8-24-49-LN); 4) filling and draining of a lava lake (sample number F8-24-51-LN) at the summit followed by collapse of flows inward creating a rim antiform; 5) pyroclastic eruptions of a wet magma forming scoria of combined



GEOLOGIC MAP OF CALLVILLE MESA

Figure 12.

hydromagmatic and magmatic origin comprised of quenched blocks, volcanic bombs and blocks, and scoria; 6) hydromagmatic eruptions producing scoria comprised of quenched blocks of magma ejected from the vent and accretionary mudballs in a matrix of mud and ash. The hydromagmatic eruptions occurred when magma contacted ground water. 7) intrusion of pyroxene-olivine-bearing plugs into the core of the volcano. In some areas the axis of the rim antiform served as a conduit for emplacement (Figure 12). The West End Wash stratocone is highly eroded so its original morphology is obscured, however, a vent zone was identified and contains scoria intruded by feeder dikes and a large shallow plug.

Fortification Hill Basalts

The Fortification Hill basalts erupted from three different types of volcanic centers: 1) cinder cones; 2) fissures; 3) small diatremes and plugs.

Cinder Cones

Small to moderately large cinder cones formed by Strombolian-type eruptions are the dominant type of volcanic center associated with Fortification Hill basalts. Cinder cones are present at Lava Cascade, Petroglyph Wash, and Fortification Hill (Figure 11). The cinder cones are located where lava from near vertical dikes reached the surface. These dikes are now exposed in country rock adjacent to the cones.

Cones are round to oval, elongated in the direction parallel to the high-angle normal faults and feeder dikes (Figure 13 and 14). Flows are commonly buttressed against their source cones.

Initial eruptions of cinder cones formed scoria mounds comprised of spatter, ash, cinder, agglutinated scoria, loose scoria, blocks, and bombs. During the next phase

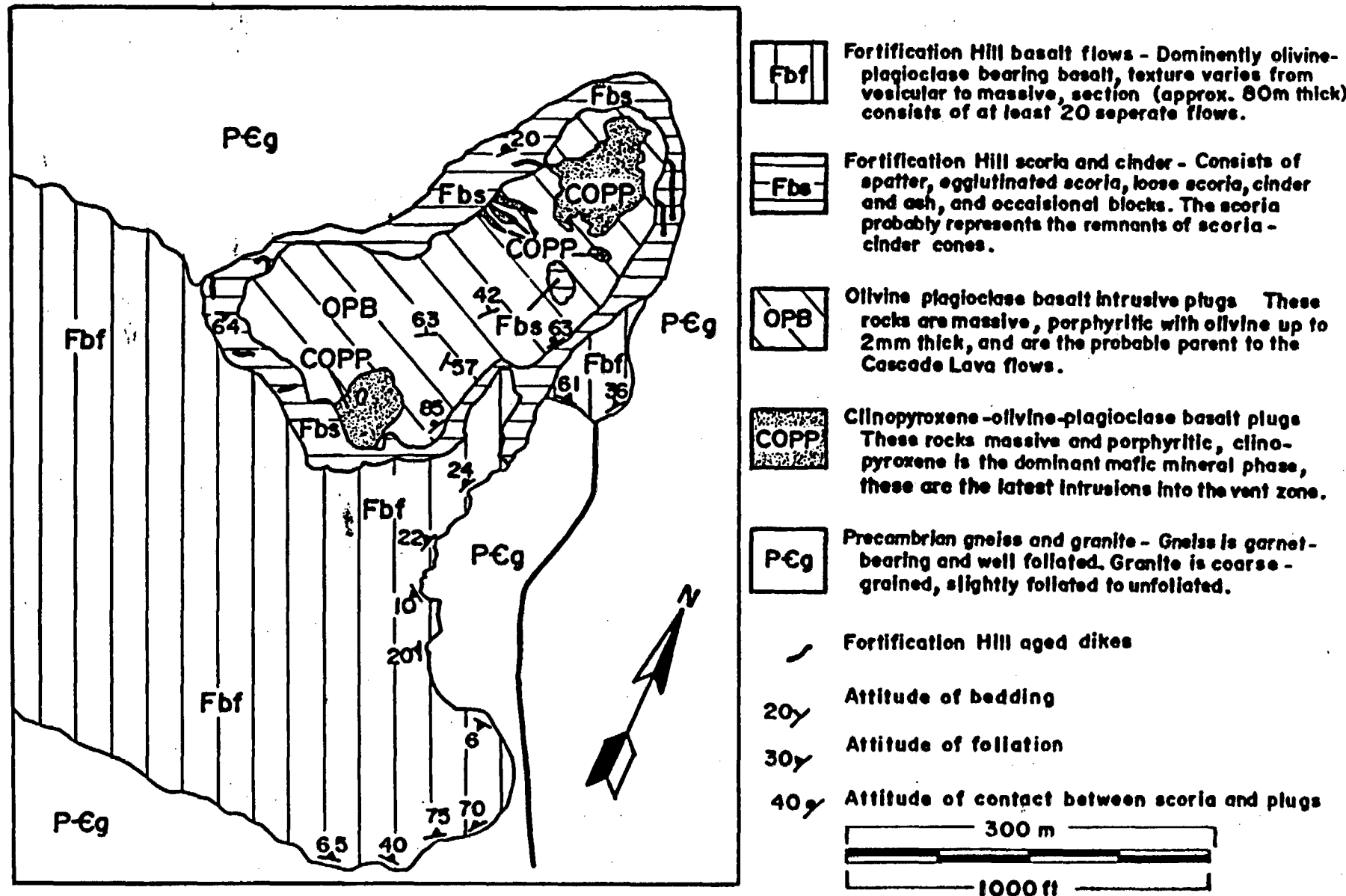


Figure 13. GEOLOGIC MAP OF THE LAVA CASCADE VENT FACIES

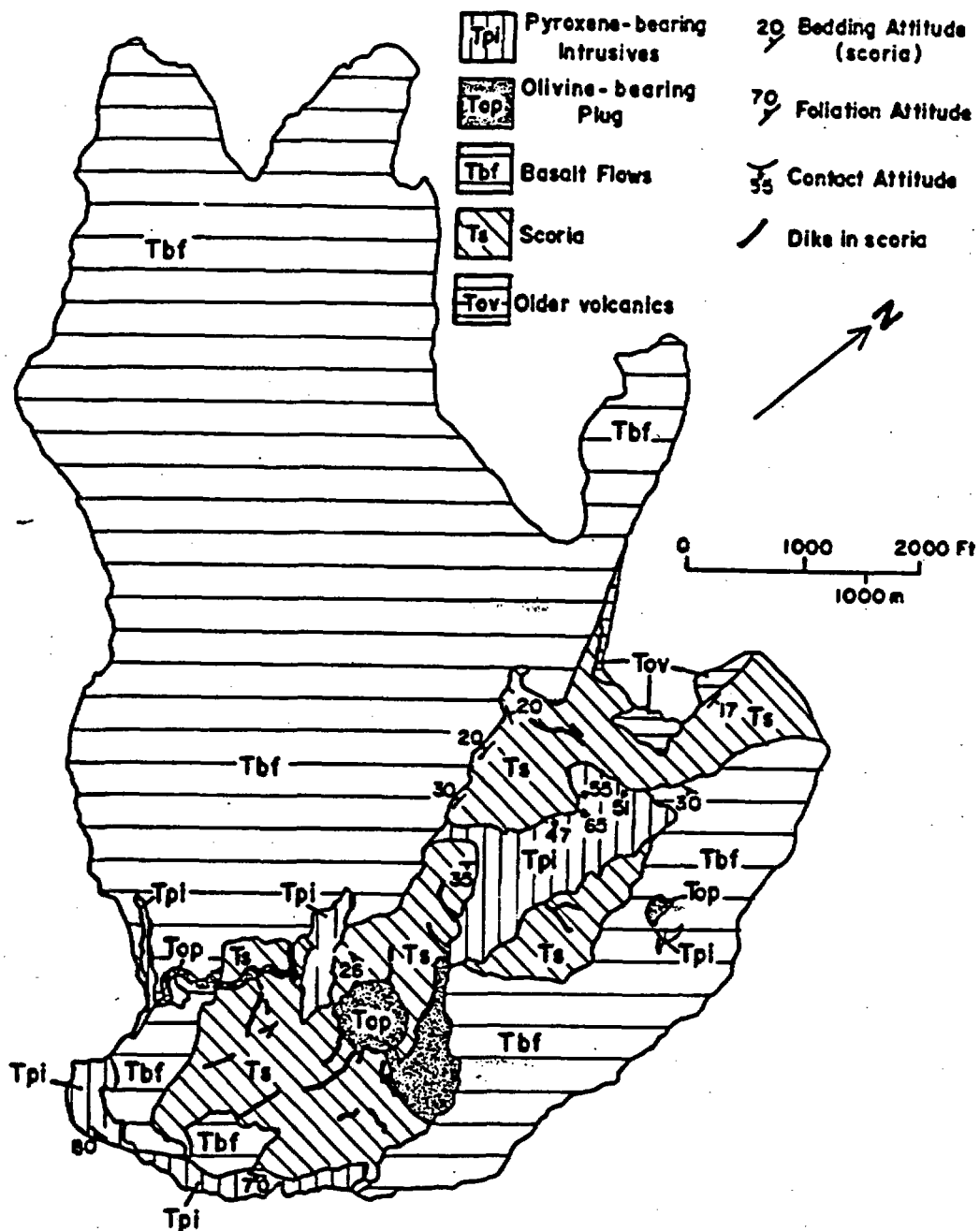


Figure 14. GEOLOGIC MAP OF FORTIFICATION HILL

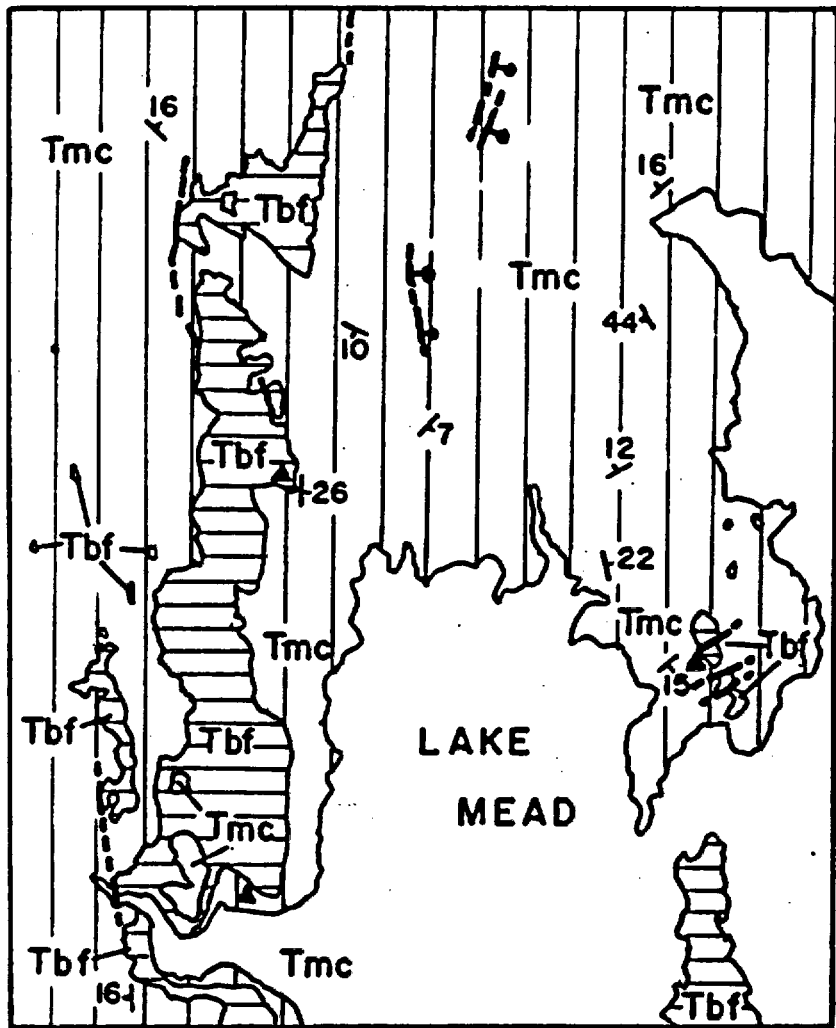
of eruption, massive olivine basalt flows erupted from the base and flanks of the cone. Dikes meander through the scoria, and vent where they intersect the side of the cone (Figure 4). The latest volcanic activity is represented by intrusion of a plug or composite plug into the scoria cone. The plug-scoria contacts usually dip 30 to 70 degrees inward (Figure 13 and 14). Plug rock displays either concentric or planar foliation. Foliation is produced by closely spaced fractures formed along zones of internal shearing.

Dikes

At Black Point, Nevada, basalt erupted from three north-northwest trending en echelon dikes (Figure 15). Feeder dikes are internally brecciated and vary in width from 1 to 4 m. The northernmost dike dips 40 degrees to the west and does not appear to feed flows, however, it intensely sheared adjacent sediments during emplacement. In a zone 0.5 m wide on either side of the dike, siltstone fragments of the Muddy Creek Formation were ripped from country rock and rotated into an orientation parallel to the margins of the dike. In a zone 15 m wide on the east side of the dike, sediments are cut by east and west dipping high-angle normal faults that probably formed during the forceful injection of the dike.

The central dike is internally brecciated and dips 40 to 70 degrees to the west. It crops out just to the west of the Black Point flows where it feeds these flows.

The southern dike is offset nearly 100 m to the west of the central dike. It is nearly 4 m wide and dips 80 degrees to the west. Here, dike emplacement resulted in zones of synthetic and antithetic high-angle normal faults in the fine-grained gypsiferous siltstones of the Muddy Creek Formation. These zones of faulting are



GEOLOGIC MAP OF THE BLACK POINT VOLCANICS

-  Tertiary Muddy Creek sedimer
-  Fortification Hill aged basalts
-  High angle normal fault
-  Dike (feeds the flow it is in contact with)
-  Attitude of bedding
-  Outcrops of ash more than two feet thick

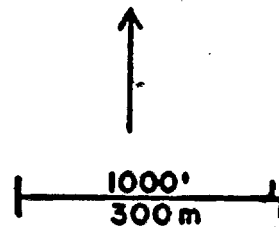


Figure 15.

accommodation zones formed by forceful injection and dilation during dike emplacement. They extend nearly 10 m to the west of the dike.

En echelon dikes were also the source of the megacryst-bearing alkali-basalts along U.S. 93 in Arizona, 13 mi south of Hoover Dam (Figure 11) (Campbell and Schenk, 1950).

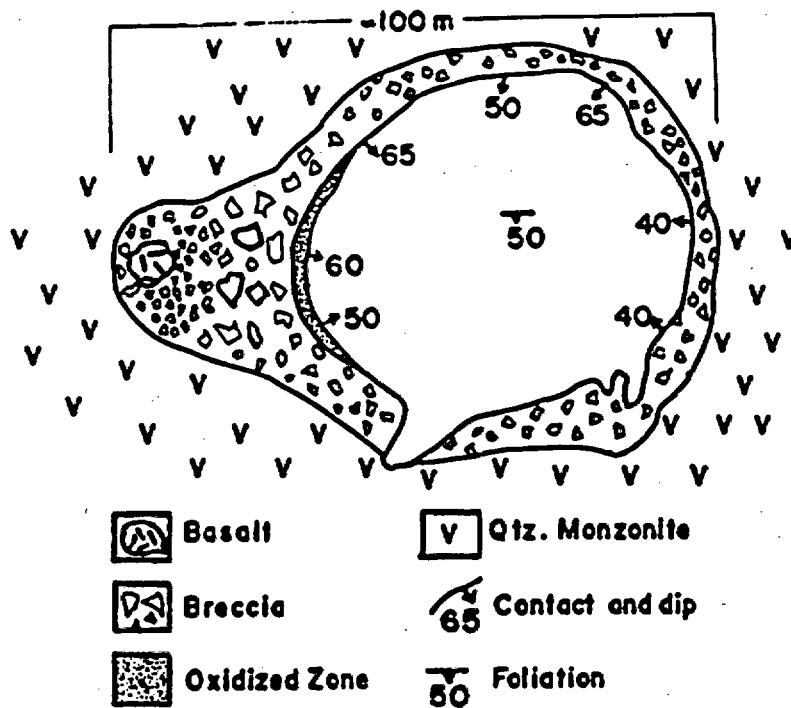
Diatremes and Plugs

A diatreme (100 m diameter) and a basalt plug (150 m diameter) crop out in Petroglyph Wash (Figure 11). The diatreme is composed of a tuff breccia intruded by a highly-foliated alkali basalt plug. The breccia contains scoria and angular clasts of Wilson Ridge quartz monzonite. The quartz monzonite is Tertiary in age (Anderson, 1973) and forms the country rock in this area (Feuerbach, 1986). Small cylindrical pipes of basalt containing pyroxene megacrysts also intrude the breccia. The contact between the plug and breccia dips inward 40 to 60 degrees (Figure 16a).

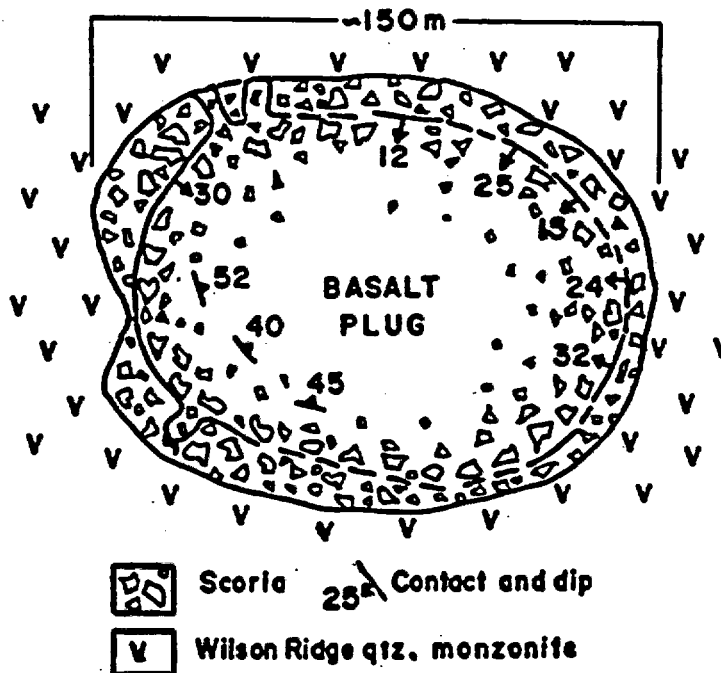
The internal geometry of the basalt plug is similar to that of the diatreme. The plug is surrounded by scoria and the plug-scoria contact is inward dipping (Figure 16b). Scoria is composed of agglutinated cinder, ash, and scoria and contains angular clasts of the Wilson Ridge quartz monzonite. The outer portions of the plug contain the same quartz monzonite inclusions as the scoria. The abundance of inclusions gradually decreases toward the center of the plug. No tuffaceous breccia was identified at this center.

GEOCHRONOLOGY

Six K-Ar dates are now available for Fortification Hill and Callville Mesa basalts (Table 3) and four new whole rock K-Ar age dates for the Fortification Hill basalt field



PETROGLYPH WASH DIATREME



PETROGLYPH WASH PLUG

Figure 16. Sketch maps of the Petroglyph Wash diatreme (a) and plug (b).

Location Information
 Fortification Hill, near Hoover Dam.
 Latitude 36 03' 18" N
 Longitude 114 48' 54" W

Potassium		Radiogenic Ar pm/g		% Atm. Ar		Reported Date +/- Err
Data	Mean	Data	Mean	Data	Mean	
0.932	0.937	9.45	9.32	50.5	51.3	5.73 +/- 0.13
0.925		9.31		51.5		
0.953		9.22		51.8		
		9.32		51.3		

Location Information
 Lava Cascade, located just east of U.S. 93 across from Willow Beach turnout. Olivine basalt flow at distal end of the Lava Cascade exposure, Clark Co., Nevada
 Latitude 35 52' 26" N
 Longitude 114 36' 06" W

Potassium		Radiogenic Ar pm/g		% Atm. Ar		Reported Date +/- Err
Data	Mean	Data	Mean	Data	Mean	
0.857	0.875	8.00	7.835	62.8	63.8	5.16 +/- 0.14
0.874		7.82		64.1		
0.892		7.74		64.3		
0.878		7.78		64.2		

Location Information
 Black Point volcanics, located approximately four miles south of Overton Beach.
 Latitude 36 24' 43" N
 Longitude 114 23' 02" W

Potassium		Radiogenic Ar pm/g		% Atm. Ar		Reported Date +/- Err
Data	Mean	Data	Mean	Data	Mean	
0.655	0.643	6.93	6.79	89.5	89.8	6.08 +/- 0.39
0.634		6.78		89.9		
0.639		6.84		89.7		
0.643		6.67		89.9		

Location Information
 Fortification Hill, near Hoover Dam
 Latitude 36 03' 02" N
 Longitude 114 48' 37" W

Potassium		Radiogenic Ar pm/g		% Atm. Ar		Reported Date +/- Err
Data	Mean	Data	Mean	Data	Mean	
1.275	1.270	11.85	11.95	55.6	55.5	5.42 +/- 0.13
1.268		11.98		55.5		
1.280		12.02		55.3		
1.256		11.96		55.7		

Location Information
 Lava Cascade, located just east of U.S. 93 across from Willow Beach turnout. Olivine basalt plug at summit of Black Mountains.
 Latitude 35 52' 38" N
 Longitude 114 35' 15" W

Potassium		Radiogenic Ar pm/g		% Atm. Ar		Reported Date +/- Err
Data	Mean	Data	Mean	Data	Mean	
0.810	0.813	6.69	6.69	53.7	53.7	4.74 +/- 0.12
0.793		6.63		54.8		
0.836		6.75		53.2		
		6.69		53.9		

Location Information
 Volcanic center
 Latitude 36 10' 37" N
 Longitude 114 44' 39" W

Callville Mesa.

Potassium		Radiogenic Ar pm/g		% Atm. Ar		Reported Date +/- Err
Data	Mean	Data	Mean	Data	Mean	
2.238	2.233	39.65	39.63	11.6	10.8	10.21 +/- 0.21
2.227		39.34		11.8		
2.234		40.48		7.6		
2.242		39.04		12.2		

Table 3. K-Ar age dates of Fortification Hill, Lava Cascade, Black Point, and Callville Mesa.

and three K-Ar age dates for the volcanic rocks at the Callville Mesa-West End Wash volcanic center will be available in September 1988. K-Ar dating was done by Dr. Paul Damon of the Geochronology Laboratory of the University of Arizona. K-Ar dates were used to determine: 1) the duration of volcanic activity at an individual volcanic center; 2) compositional changes with time; 3) time dependant migration patterns of volcanism; and 4) changes in the nature of structural control with time.

Duration of Volcanism at a Single Center

At Fortification Hill, the earliest flow and a late-stage pyroxene-bearing plug that intrudes the cinder cone were dated (Table 3). The length of volcanic activity at Fortification Hill (considering the 2 sigma error) was 5.0×10^4 to 5.7×10^5 years. An early flow and olivine-bearing plug were dated at the Lava Cascade. Volcanic activity lasted from 1.6×10^5 to 5.8×10^5 years.

Volcanism was episodic during the span of activity at each center. However, the period of time between eruptive episodes was probably short. This is suggested by: 1) the lack of soil horizons or other evidence of erosion between flows, and 2) chemically and mineralogically there is little variation from top to bottom in the flow stack.

Structural Control and Migration of Volcanism

During the time period from 13-9.5 Ma volcanism was restricted to the area along the Lake Mead Fault system (Figure 17 and 18). Left-lateral movement along the Hamblin Bay fault between the 13 and 9.5 Ma transported the northern half of the Hamblin-Cleopatra volcano 20 km to the west-southwest (Anderson, 1973).

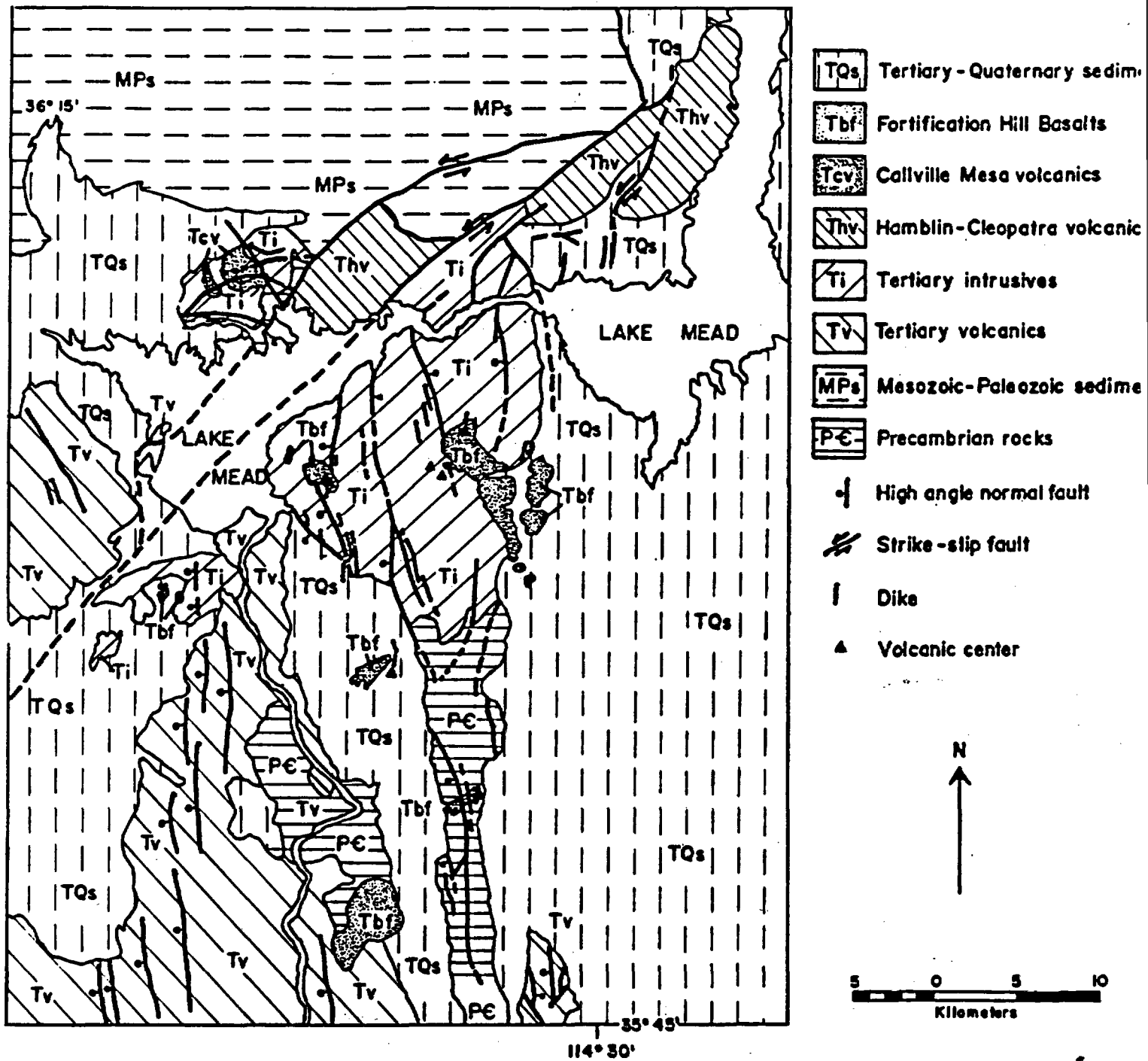


Figure 17. Generalized geologic map of the Lake Mead area.

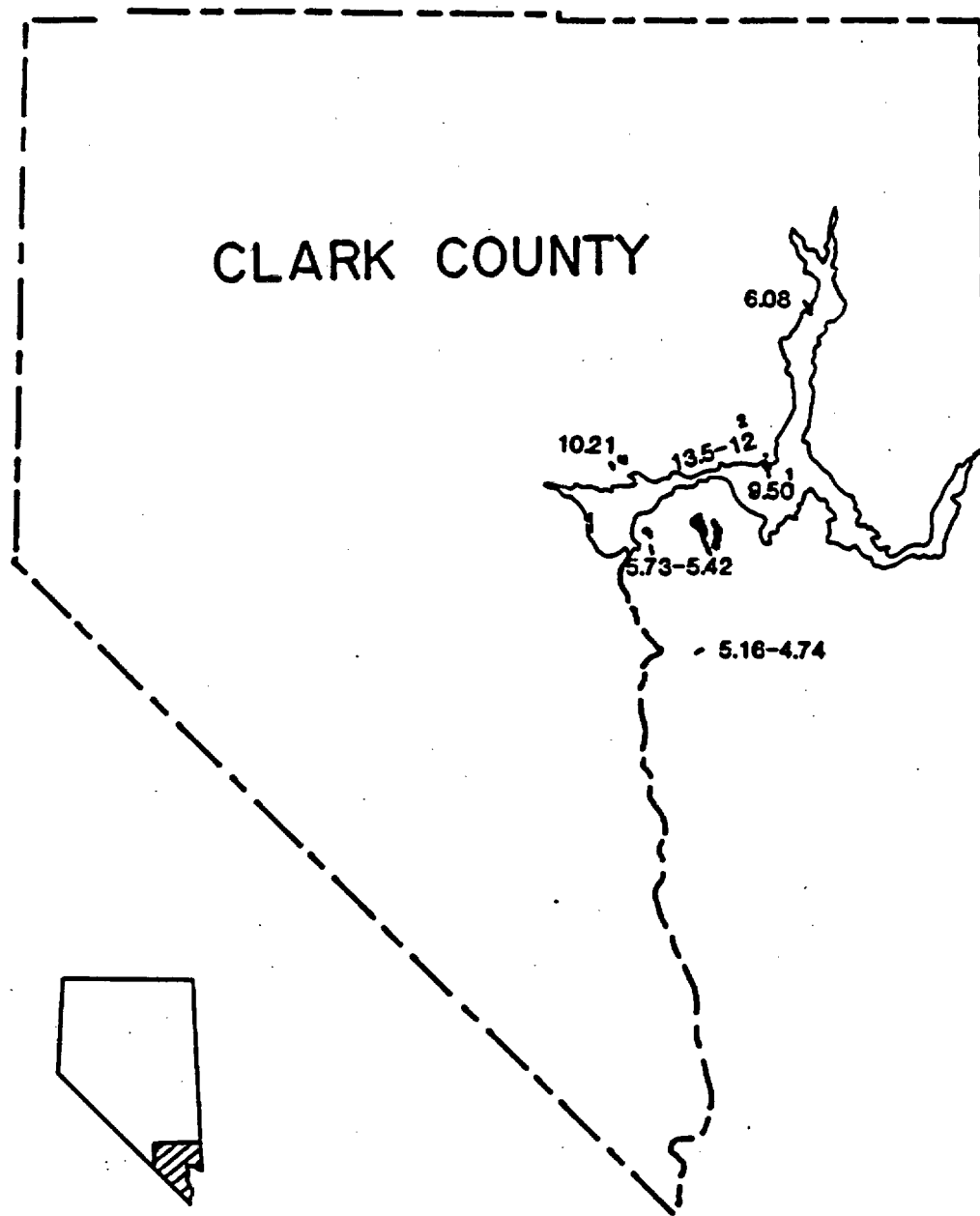


Figure 18. Locations of K-Ar age dates in the Lake Mead area. ¹ Date on Fortification Hill basalt from Thompson, (1986). ² Range of K-Ar age dates for the Hamblin-Cleopatra volcano from Thompson, (1986).

The post 6 Ma Fortification Hill basalts erupted adjacent to north-northwest striking high-angle range bounding faults (Figure 17 and 18). This period of volcanism migrated south with time (Figure 18).

Magmatism and Time

Volcanic Style

The character of volcanic eruptions appears to have changed with time. The Hamblin-Cleopatra volcano (13.5-12 Ma) is a stratovolcano formed by many quartz-normative andesite and dacite flows. The Calville Mesa-West End Wash volcanoes (11-10.3 Ma) are stratocones built of hypersthene and olivine-normative basalt and basaltic andesite. The Fortification Hill aged (6-4.9 Ma) alkali-basalts and hawaiites erupted from cinder cones and dikes and are hypersthene to nepheline and olivine-normative. These observations suggest trends toward; 1) smaller volcanic centers, 2) a larger volume of pyroclastic deposits, and 3) more explosive types of eruptions with time.

Composition

To evaluate the geochemical and mineralogical changes with time, geochemical and normative mineral contents are plotted against the average K-Ar age of the rock. MgO, CaO, and Fe_2O_3 show a continuous increase in abundance from 13.5 Ma to 4.9 Ma. SiO_2 however, decreases with time (Figure 19). TiO_2 content increases during eruptions of the Fortification Hill age basalts but decreases during eruptions of the Hamblin-Cleopatra volcano (Figure 20).

V, Sc, and Eu increase in concentration with time during Fortification Hill age basalt eruptions and decrease during eruptions of the Hamblin-Cleopatra. Cr remains

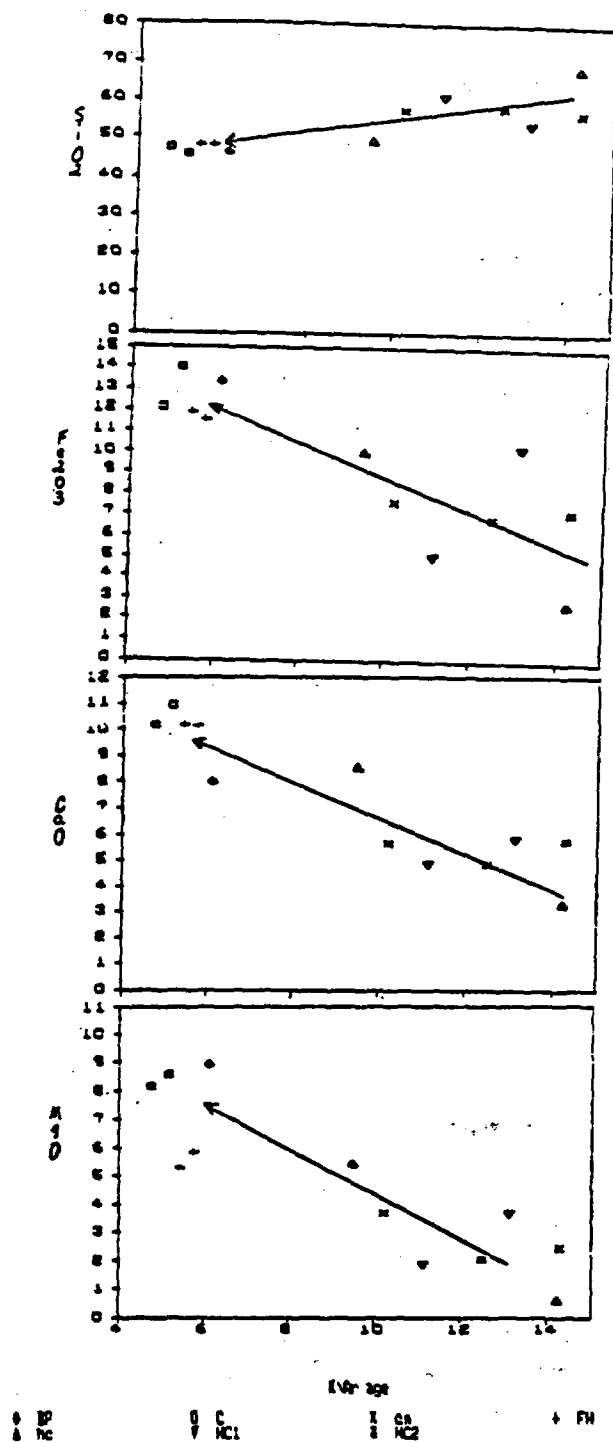


Figure 19. SiO₂, Fe₂O₃, CaO, and MgO plotted against K-Ar age dates for Miocene to Pliocene volcanic rocks in the Lake Mead area. BP=Black Point, C=Lava Cascade, FH=Fortification Hill, CM=Callville Mesa, HC=Fortification Hill age basalt (from Thompson, 1986), HC1=First sequence lava, Hamblin-Cleopatra volcano (from Thompson, 1986), and HC2= Second sequence lava, Hamblin-Cleopatra volcano (from Thompson, 1986).

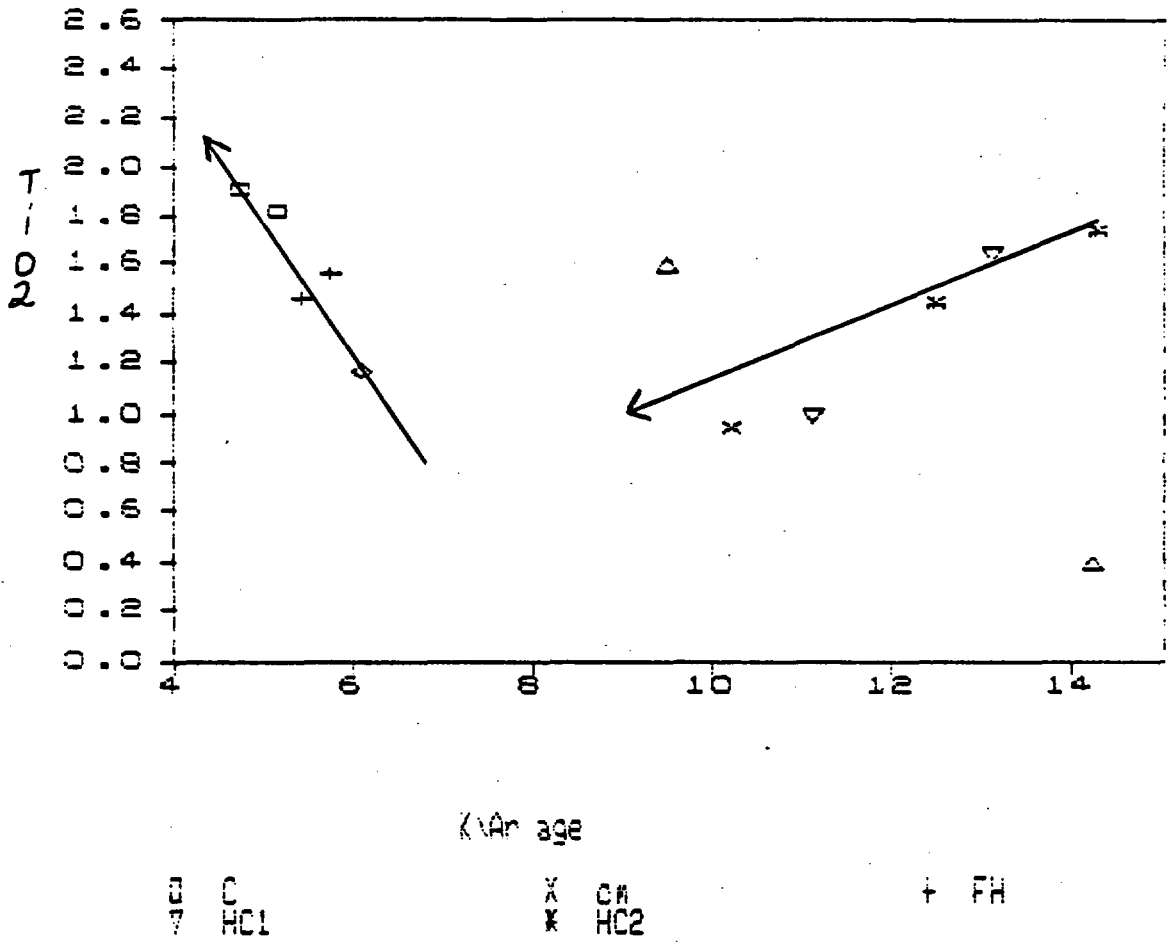


Figure 20. TiO_2 vs K-Ar age dates for Miocene to Pliocene volcanic rocks in the Lake Mead area. (Explanation same as Figure 19).

nearly constant with time during Hamblin-Cleopatra eruptions but decreases rapidly during the eruptions of the Fortification Hill basalts (Figure 21). Total REE decreases continuously from Hamblin-Cleopatra to Fortification Hill time (Figure 22).

STRUCTURAL CONTROL OF CONDUITS

The Lake Mead Fault Zone and associated north-northwest trending high-angle faults controlled the location of vents of post-13 Ma volcanoes in the area about Lake Mead (Figure 17). Although regional fault zones controlled the location of volcanic centers, in detail conduits are not always controlled by major faults associated with these fault zones. This is especially evident at the Lava Cascade and Fortification Hill.

At Lava Cascade, lava erupted from a cinder cone near the summit of the Black Mountains in an area nearly devoid of any major faults. Major north-northwest trending high-angle faults cut the range just to the west of the vent center. Basalt dikes north and south of the cinder cone are coplanar with the high-angle range bounding faults, but no mappable faults mark the extension of the dikes. One high-angle fault (striking N45W to N50W) trends toward the cinder cones in the vent zone, however dikes associated with the vent strike N20W to N5E. Eruption occurred very near the nose of a west-plunging synform in the Precambrian basement rocks. Lava flowed down a canyon cut parallel to the axis of the synform toward the present day Colorado River, however the synform does not control vent location. Dikes clearly cross-cut the foliation in the Precambrian gneiss and they are nearly perpendicular to the axis of the synform.

At Fortification Hill, dikes associated with the cinder cone, crop out north and south of the vent center. These dikes strike north-northwest and are coplanar with the

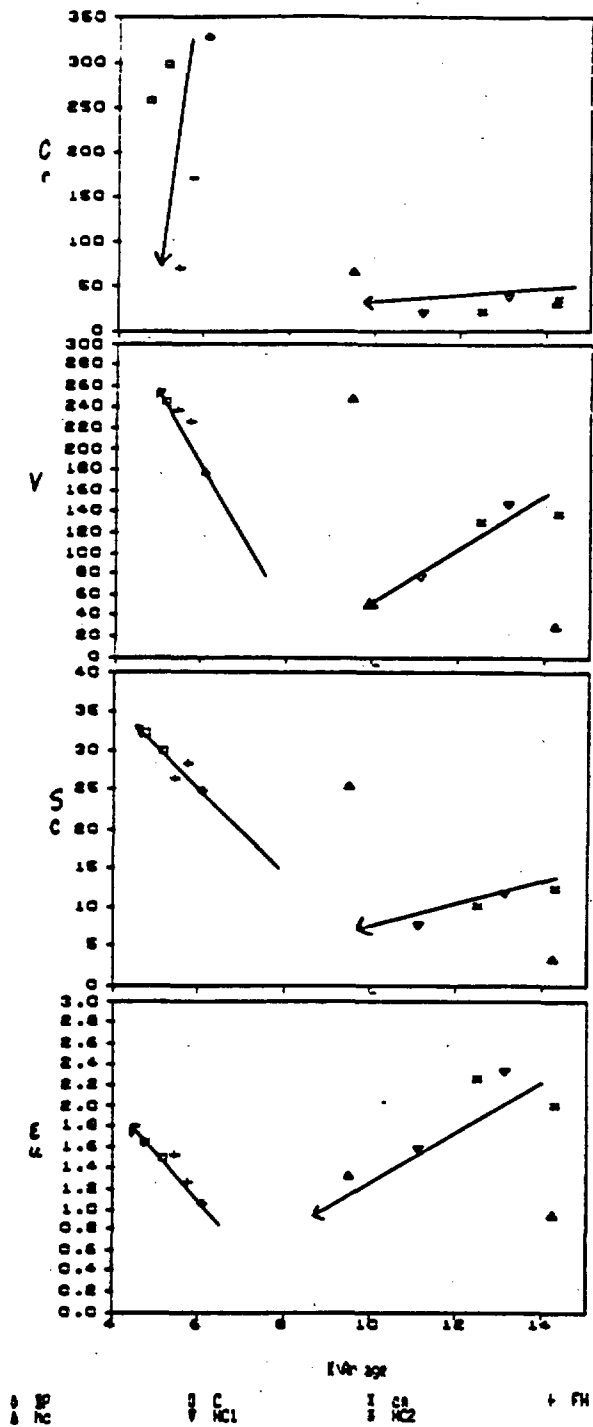


Figure 21. Cr, Y, Sc, and Eu vs K-Ar age dates for Miocene to Pliocene volcanic rocks in the Lake Mead area. (Explanation same as Figure 19).

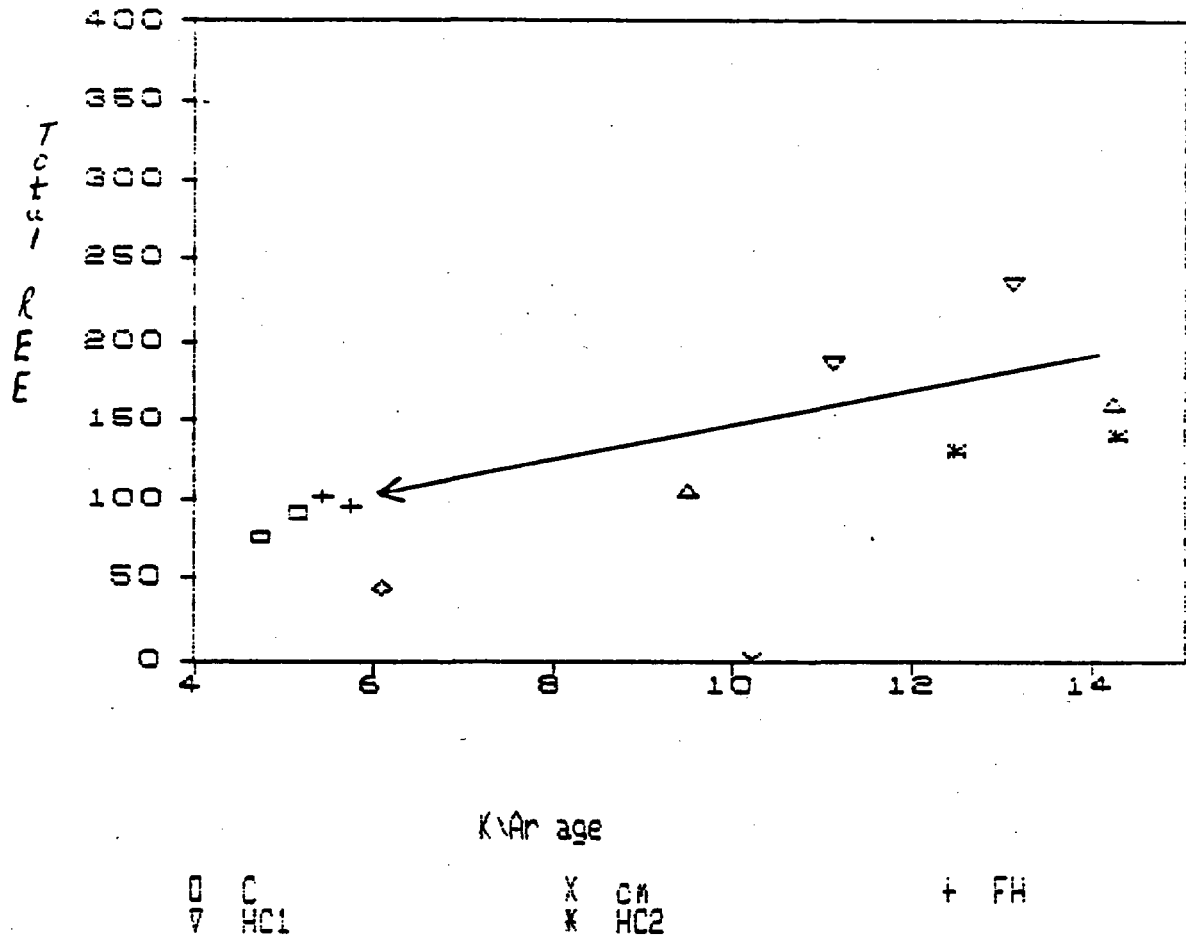


Figure 22. Total REE vs K-Ar age dates for Miocene to Pliocene volcanic rocks in the Lake Mead area. (Explanation same as Figure 19).

major high-angle normal faults in the area. Dikes intrude unbrecciated country rock within 100 m of major faults, however; these faults did not serve as conduits. The intrusive plugs within the Fortification Hill vent area are elongated parallel to dikes and regional faults. In fact, a major splay of the Fortification Hill fault projects beneath Fortification Hill, but it is uncertain whether this structure served as the conduit for eruptions at the cinder cone (Figure 17).

MAGMA EMPLACEMENT INTO THE CRUST

Basin-and-Range structures in the Fortification Hill-Lava Cascade area are bounded by fault zones formed of numerous sub-parallel moderate to high-angle normal faults. Even though the magnitude of displacement on individual faults may be small, total displacement of all the faults can be up to thousands of meters (Longwell et al., 1963). A possible scenario for magma emplacement in this structural setting is:

- 1) Magma intruded the network of faults and fractures related to the fault zone at depth. At Fortification Hill erosion exposed the vent zone to a depth of 1000 m below the surface of eruption. At this depth, dikes strike in the same direction as faults, but dikes do not occupy the fault zones.
- 2) Magma then rose toward the surface using fractures and faults which yielded the least resistance.
- 3) During ascent magma abandoned fault zones and rose along any available pathway to the surface. Certain faults were abandoned because the fault zone may have been sealed at a shallow depth due to hydrothermal mineralization (silicification of the fault zone). Another explanation is that the conduit did not have a large enough diameter to allow magma to rise to the surface. A dike must have a sufficient width to thermally insulate the magma from the cool country rocks in order to sustain flowage for a substantial period

of time prior to freezing (DeLeney and Pollard, 1982).

PETROGRAPHY

Fortification Hill and Lava Cascade

Basalt flows from Fortification Hill and Lava Cascade contain phenocrysts of subhedral to euhedral olivine (1-3% at Fortification Hill and 3-12% at Lava Cascade). Olivine is commonly resorbed and rimmed or replaced by iddingsite. The groundmass is pilotaxitic and occasionally intergranular in the coarser-grained varieties. Groundmass mineralogy consists of microlites of subhedral to euhedral plagioclase (50-60%), subhedral to euhedral augite and titanaugite (10-20%), and subhedral to euhedral iddingsitized olivine (4-11%).

The pyroxene-bearing plugs at Fortification Hill and Lava Cascade contain porphyritic olivine, augite, and plagioclase in an intergranular groundmass of olivine, plagioclase, augite, and titanaugite. Mineralogy of the plugs is similar to associated flows, however they contain large (0.5-2 mm long) subhedral, resorbed and zoned plagioclase (2-20%) and large (.3-3 mm long) subhedral and highly resorbed poikilitic augite (plagioclase included within the augite). These mineral phases along with olivine commonly appear in glomeroporphyritic clots. The olivine-bearing plugs are similar to the pyroxene-bearing plugs except that the large augite phenocrysts are rare to absent.

Black Point

Basalts at Black Point are porphyritic, containing euhedral to subhedral partially resorbed olivine (5-8%), subhedral poikilitic augite (13-19%), and subhedral poikilitic orthopyroxene (3-11%) in a pilotaxitic to intergranular groundmass. Groundmass is

composed of subhedral microlites and laths of plagioclase (52-63%), subhedral olivine (3-11%) and subhedral to anhedral augite (2-9%). Olivine phenocrysts are partially altered to chlorite and serpentine.

Petroglyph Wash

Basalt flows at Petroglyph Wash contain phenocrysts of subhedral partially resorbed olivine (1-12%), subhedral augite (<2%), subhedral partially resorbed zoned plagioclase (1-3%), and subhedral orthopyroxene (0-1%). Olivine is partially altered to iddingsite. Groundmass is pilotaxitic to intergranular containing microlites of subhedral plagioclase (51-63%), subhedral to euhedral augite and titanaugite (9-17%), and subhedral to euhedral iddingsitized olivine (9-14%). Some of the olivine crystals have incomplete rims of augite.

Callville Mesa

Basalt of Callville Mesa and West End Wash volcanoes contain phenocrysts of euhedral to subhedral partially resorbed and iddingsitized olivine (1-5%), subhedral, zoned, resorbed plagioclase (10-30%), subhedral, poikilitic augite (2-9%), and traces of subhedral orthopyroxene. Quartz and alkali-feldspar xenocrysts rimmed by glass and acicular clinopyroxene occur throughout this suite of rocks. Clots of large (1-1.5 mm) olivine, augite, and plagioclase are common. Occasional xenoliths of pyroxenite containing subhedral orthopyroxene and clinopyroxene occur within the flows.

GEOCHEMISTRY

Callville Mesa - West End Wash Volcanoes

Thirty-two whole rock, major-element chemical analyses are now available for the volcanic rocks of the Callville Mesa-West End Wash volcanoes. Twenty-three were

obtained during 1987-1988 (Table 4). Rocks of the Calville Mesa - West End Wash volcanoes are calc-alkaline basalts and andesites (Irvine and Baragar, 1971). Two rocks are alkalic-basalts and one is an Hawaiite (Figure 23).

Calville Mesa-West End Wash volcanic rocks vary in SiO_2 content from 52-57%. Fe_2O_3 , MgO, CaO and MnO decrease with increasing SiO_2 while P_2O_5 , Na_2O and Al_2O_3 remain constant (Figure 24). MnO is slightly depleted in the rocks associated with the West End Wash volcano.

All but three of the Calville Mesa-West End Wash volcanic rocks contain normative quartz (1-7%). All contain normative hypersthene and plagioclase (andesine).

Fortification Hill - Lava Cascade and Other Fortification Hill Aged Basalts

This year, we obtained thirty-five new major element analyses of Fortification Hill age basalts. These include 11 new whole rock chemical analyses from Petroglyph Wash and 6 from the alkali-basalt along U.S. 93 in Arizona (Table 5). Also major element data was obtained for kaurutite and ultramafic nodules in the alkali-basalts along U.S. 93.

All of the Fortification Hill aged rocks are alkalic except those from Malpais Flattop, and the south dike at Lava Cascade, and one of the lower flows at Fortification Hill which are subalkaline tholeiitic basalts (Irvine and Baragar, 1971) (Figure 26). For the most part, Fortification Hill aged volcanism produced alkali-basalts. The only exceptions are the north dikes at Lava Cascade and late-stage plugs at Petroglyph Wash which are picrites according to the Irvine and Baragar classification (Figure 26).

New chemistry from the stratigraphically lowest sections at Fortification Hill and the dikes at Lava Cascade suggest that these rocks are cogenetic with other rocks from

Sample	PG-20-91	PG-20-53	PG-20-54	PG-20-53	PG-20-56	PG-20-57	PG-20-58	PG-20-59	PG-20-60	PG-20-61	PG-20-62	PG-20-63	Sample	PG-20-64	PG-20-65	PG-20-66	PG-20-67	PG-20-68	PG-20-69	PG-20-70	PG-20-71	PG-20-72	PG-20-85	PG-20-86
Group 0	1.00	1.00	1.00	1.00	1.00	1.00	1.00	1.00	1.00	1.00	1.00	1.00	Group 0	1.00	1.00	1.00	1.00	1.00	1.00	1.00	1.00	1.00	1.00	1.00
Quartz	0	0	0	0	0	0	0	0	0	0	0	0	Quartz	0	0	0	0	0	0	0	0	0	0	0
Plagioclase	0	0	0	0	0	0	0	0	0	0	0	0	Plagioclase	0	0	0	0	0	0	0	0	0	0	0
Pyroxene	0	0	0	0	0	0	0	0	0	0	0	0	Pyroxene	0	0	0	0	0	0	0	0	0	0	0
Spinel	0	0	0	0	0	0	0	0	0	0	0	0	Spinel	0	0	0	0	0	0	0	0	0	0	0
Alumina	04.00	03.00	04.74	04.20	04.00	05.00	07.20	07.00	05.00	05.73	06.27	04.03	Alumina	05.00	06.00	05.04	05.00	05.10	05.01	07.20	06.01	05.00	04.00	05.27
TiO2	1.01	1.00	1.12	1.00	1.00	1.10	1.00	1.00	1.00	1.10	1.00	1.12	TiO2	1.20	1.00	1.11	1.10	1.07	1.00	1.00	1.20	1.10	1.20	1.20
Al2O3	10.01	10.20	10.00	10.00	10.20	10.20	10.07	10.70	10.01	10.04	10.00	10.23	Al2O3	10.10	10.00	10.10	10.02	10.04	10.01	10.07	17.10	10.07	10.47	10.40
FeO	10.21	10.00	0.27	0.00	0.00	0.02	0.70	0.47	0.00	0.00	0.00	0.00	FeO	0.00	0.17	0.00	0.11	0.40	0.00	0.00	0.10	0.20	0.00	10.14
MnO	0.14	0.10	0.11	0.12	0.14	0.14	0.12	0.12	0.11	0.12	0.12	0.12	MnO	0.10	0.13	0.11	0.12	0.10	0.11	0.12	0.00	0.10	0.10	0.10
MgO	3.22	3.20	4.00	0.00	4.20	4.74	4.01	4.07	4.00	4.24	4.20	4.42	MgO	4.00	4.24	4.04	4.43	4.20	4.20	4.10	2.00	4.00	4.70	3.00
CaO	0.27	0.00	0.01	0.70	0.01	0.34	0.40	0.20	0.01	0.00	0.77	0.20	CaO	0.17	0.03	0.13	0.20	0.04	0.10	0.70	0.00	0.77	0.20	0.20
Na2O	4.21	3.00	3.44	0.00	0.40	0.07	0.00	0.07	0.30	0.04	0.02	0.40	Na2O	0.00	0.07	0.00	0.70	0.02	0.00	0.01	0.00	0.00	0.00	0.00
K2O	2.01	1.00	2.00	2.00	2.00	2.40	2.40	2.40	2.30	2.74	2.24	1.72	K2O	1.00	2.20	1.00	2.20	2.04	2.22	2.40	3.00	2.40	2.00	2.42
P2O5	0.20	0.20	0.20	0.27	0.20	0.20	0.20	0.20	0.20	0.20	0.20	0.20	P2O5	0.22	0.20	0.20	0.20	0.20	0.21	0.20	0.20	0.21	0.20	0.20
Total	00.10	100.00	07.00	07.07	100.10	100.01	100.20	00.00	00.00	00.01	00.40	07.01	Total	00.21	100.04	07.42	100.00	00.01	07.72	100.24	00.02	100.20	101.21	101.07
Si	50	47	42	41	40	41	40	39	40	39	40	44	Si	43	41	42	40	40	43	41	30	30	40	42
O	2	2	2	2	2	2	2	2	2	2	2	2	O	2	2	2	2	2	2	1	2	2	2	2
Al	12	0	10	10	10	10	10	10	10	10	10	10	Al	11	14	12	10	10	10	10	10	10	11	10
Fe	30	20	20	20	21	20	20	20	20	20	21	20	Fe	20	20	20	20	20	20	20	22	20	20	20
Mn	20	20	21	21	20	21	20	20	21	20	20	20	Mn	20	21	20	21	20	21	20	20	20	20	20
Mg	7	0	10	0	11	11	0	0	0	11	0	0	Mg	0	0	0	0	0	0	0	0	0	0	0
Ca	10	10	10	10	10	10	10	10	10	10	10	10	Ca	0	0	0	11	0	10	10	10	10	10	10
Na	0	4	4	4	4	4	4	4	4	4	4	4	Na	17	10	10	10	10	10	10	0	10	10	0
K	3	2	2	2	2	2	2	2	2	2	2	2	K	0	0	0	0	0	0	0	0	0	1	0
P	1	1	1	1	1	1	1	1	1	1	1	1	P	0	0	0	0	0	0	0	0	0	0	0
P2O5	10.21	10.00	0.27	0.00	0.20	0.20	0.20	0.20	0.20	0.20	0.20	0.20	P2O5	0.00	0.17	0.00	0.11	0.40	0.00	0.00	0.10	0.24	0.00	10.14
P/P2O5	0.703	0.000	0.070	0.042	0.000	0.000	0.072	0.072	0.000	0.000	0.070	0.000	P/P2O5	0.000	0.077	0.001	0.070	0.000	0.042	0.000	0.704	0.004	0.072	0.000
SiO2	0.00	0.00	0.00	0.00	0.00	0.00	0.00	0.00	0.00	0.00	0.00	0.00	SiO2	0.00	0.07	0.00	0.00	0.00	0.00	0.00	0.00	0.00	0.00	0.00

Table 4. New whole rock major-element geochemistry and cation normative mineral compositions for basalts from the Callville Mesa and West End Wash volcanos.

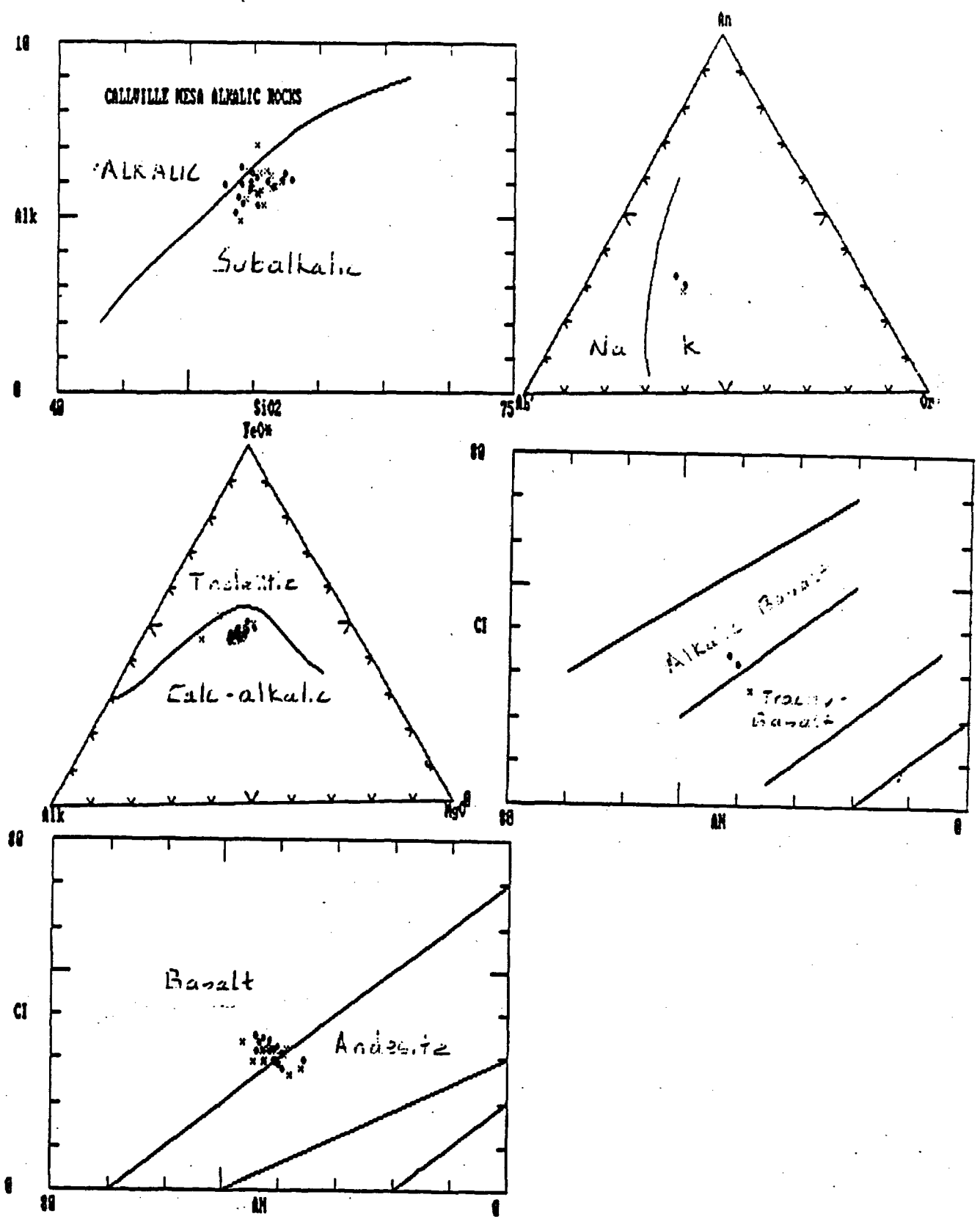


Figure 23. Irvine and Baragar (1971) classification of the basalts and andesites from Callville Mesa and West End Wash volcanos. Circles=Callville Mesa, X=West End Wash.

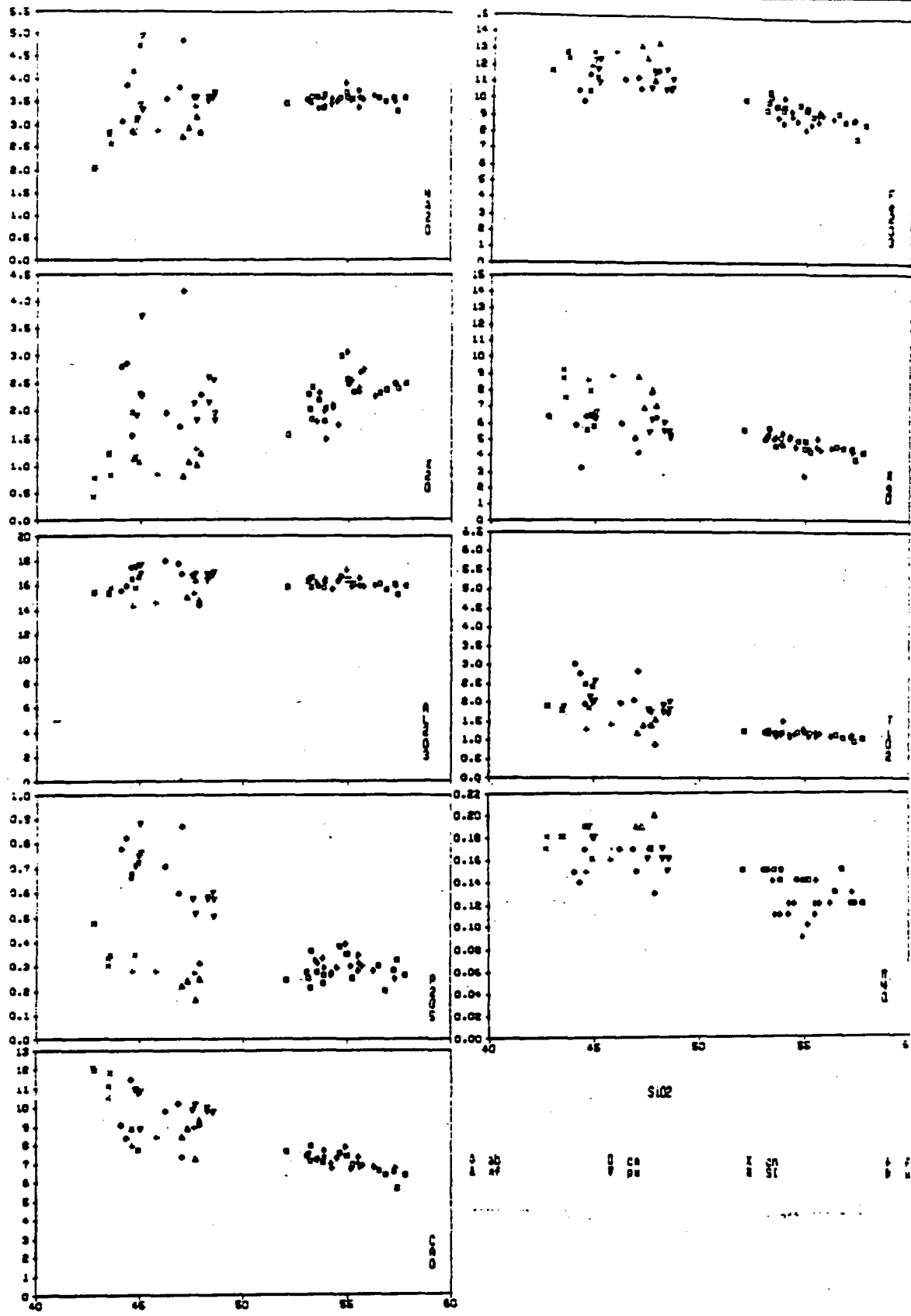


Figure 24. Harker variation diagrams. fhn=Fortification Hill, cn=Lava Cascade, mf=Malpais Flattop, pw-Petroglyph Wash, cm=Callville Mesa, we=West End Wash, and ab=U.S. 93 alkali-basalts.

File name C:\CPHRA86.DOC

Sample	FB-42-73	FB-42-74	FB-42-75	FB-42-76	FB-42-77	FB-42-78	FB-42-81	FB-42-82	FB-42-83	FB-42-84	FB-42-88	FB-42-92	FB-42-93	Sample	FB-42-94	FB-42-95	FB-42-96	FB-42-97	FB-42-98	
Group #	1.00	1.00	1.00	1.00	1.00	1.00	1.00	1.00	1.00	1.00	1.00	1.00	1.00	Group #	1.00	1.00	1.00	1.00	1.00	
Qua1	0	0	0	0	0	0	0	0	0	0	0	0	0	Qua1	0	0	0	0	0	
Key	2	2	2	2	2	2	2	2	2	2	4	3	3	Key	2	2	2	2	2	
Ref	0	0	0	0	0	0	0	0	0	0	0	0	0	Ref	0	0	0	0	0	
B102	44.78	45.02	44.98	45.00	45.48	45.22	45.20	47.52	48.24	47.64	46.24	38.87	44.31	B102	47.01	44.54	44.05	47.05	46.84	
T102	2.11	2.01	1.87	2.54	1.68	1.88	1.78	1.74	1.72	1.71	1.67	8.78	2.77	T102	2.82	1.84	2.07	8.88	2.03	
A1203	17.42	17.89	17.87	16.78	18.88	18.24	17.88	18.81	18.78	18.78	18.88	14.38	15.87	A1203	18.77	17.42	15.82	14.32	17.72	
FeO	12.23	12.28	11.88	10.88	10.84	11.78	10.88	10.88	10.88	10.88	11.45	11.11	10.28	0.88	FeO	10.87	11.38	10.48	11.88	11.28
MnO	0.18	0.18	0.18	0.18	0.18	0.17	0.18	0.18	0.18	0.17	0.17	0.18	0.14	MnO	0.18	0.17	0.18	0.18	0.17	
MgO	0.98	0.89	0.28	0.21	0.97	0.89	0.88	0.28	0.28	0.18	0.81	12.88	2.28	MgO	4.12	0.37	0.88	0.28	0.81	
CaO	10.88	10.78	10.88	0.78	0.72	0.72	0.72	0.78	0.82	10.87	0.78	11.38	0.34	CaO	7.31	11.48	0.07	0.07	10.17	
Na2O	3.11	3.32	3.42	4.04	3.88	3.48	3.81	3.87	3.84	3.87	3.84	2.82	3.88	Na2O	4.88	2.87	3.88	2.81	3.82	
K2O	1.88	2.25	2.27	3.78	2.54	2.88	1.82	2.11	2.12	1.81	1.85	1.81	2.85	K2O	4.18	1.84	2.88	2.27	1.71	
P2O5	0.71	0.78	0.75	0.88	0.88	0.87	0.87	0.87	0.88	1.71	0.71	0.84	0.82	P2O5	0.87	0.84	0.78	0.31	0.88	
Total	88.87	100.78	88.78	88.88	88.33	100.81	88.88	88.88	88.84	100.88	88.38	88.17	92.88	Total	88.88	88.34	84.81	88.47	88.27	
AN	78	78	74	78	82	84	88	82	82	48	88	188	47	AN	48	78	87	48	88	
or	11	13	13	22	18	18	11	12	13	11	12	0	17	or	28	8	17	13	18	
ab	12	0	0	4	28	18	28	21	22	25	18	0	28	ab	14	13	18	21	28	
en	28	28	28	13	22	21	24	23	23	24	27	22	17	en	12	38	28	28	28	
to	0	0	0	0	0	0	0	0	0	0	0	0	0	to	18	8	8	1	7	
no	0	18	11	21	8	8	3	5	5	3	8	12	7	di	15	18	18	18	17	
di	17	18	18	28	18	19	18	18	18	12	13	22	18	di	8	12	8	18	18	
hy	0	0	0	0	0	0	0	0	0	0	0	0	0	hy	8	5	7	3	5	
ol	13	13	12	8	18	11	18	18	18	18	12	17	3	ol	8	4	8	2	4	
et	5	5	5	5	5	5	5	5	5	5	5	8	8	et	2	2	2	1	1	
tl	4	4	4	5	3	4	3	3	3	3	4	8	5	tl	2	2	2	1	1	
hem	0	0	0	0	0	0	0	0	0	0	0	7	0	hem	10.87	11.38	10.48	11.88	11.28	
ep	2	2	2	2	1	1	1	1	1	4	2	0	2	ep	0.722	0.848	0.842	0.882	0.884	
para	0	0	0	0	0	0	0	0	0	0	0	3	0	para	2.83	2.72	2.88	2.88	2.88	
CO2	0	0	0	0	0	0	0	0	0	0	0	0	0	CO2	2.83	2.72	2.88	2.88	2.88	
FeO*	12.23	12.28	11.88	10.88	10.84	11.78	10.88	10.88	10.88	11.45	11.11	10.28	0.88	FeO*	10.87	11.38	10.48	11.88	11.28	
F/P-M	0.881	0.858	0.884	0.848	0.888	0.887	0.882	0.887	0.888	0.858	0.888	0.428	0.783	F/P-M	0.722	0.848	0.842	0.882	0.884	
den	2.13	2.72	2.71	2.87	2.88	2.88	2.88	2.87	2.88	2.88	2.88	2.82	2.88	den	2.83	2.72	2.88	2.88	2.88	

1. salt

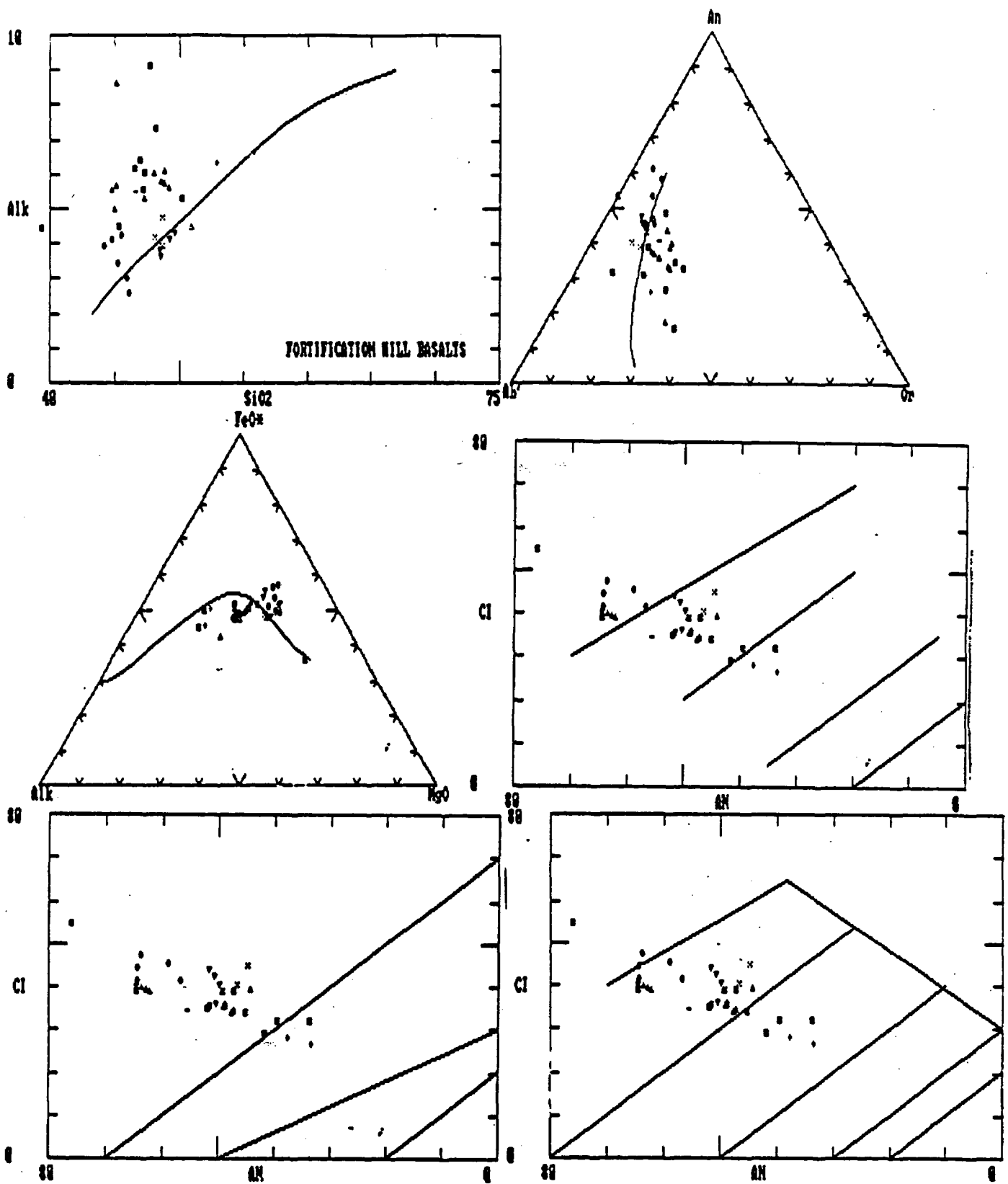


Figure 26. Irvine and Baragar chemical classification for the rocks from Lava Cascade (open circles), Fortification Hill (x), Petroglyph Wash (upward pointing triangle), U.S. 93 alkali-basalts (open squares), Malpais Flattop (downward pointing triangle), and Hamblin-Cleopatra volcano (crosses).

their respective localities.

The small plugs which crop out in Petroglyph Wash have lower SiO_2 (44-45%) contents compared to the rocks associated with the cinder cone complex (47-48%). The plugs also contain higher contents of P_2O_5 , MnO, Fe_2O_3 , TiO, CaO and MgO than the rocks erupted from the cinder cone (Figure 284).

The U.S. 93 alkali basalts contain 44-47% SiO_2 and are enriched in Na_2O , K_2O , P_2O_5 and TiO_2 compared to the rest of the Fortification Hill aged basalts. Basalts in Petroglyph Wash are nepheline (3-21%) and olivine (9-13%) normative and also contain normative labradorite. The U.S. 93 alkali basalts are nepheline (1-15%) and olivine (5-17%) normative with andesine and labradorite as the normative plagioclase.

Basalts from Lava Cascade and Fortification Hill are nepheline and olivine or hypersthene and olivine normative. Labradorite is the normative plagioclase. Basalt from Malpais flattop is olivine (8-17%) and hypersthene (6-16%) normative and contains labradorite as the normative plagioclase.

GEOCHEMISTRY OF THE FORTIFICATION HILL FIELD

(Eugene Smith)

Instrumental Techniques

Whole rock major element concentrations were determined by Inductively Coupled Plasma techniques (ICP) at Chemex Labs, Inc. (Sparks, NV) and by X-ray fluorescence (XRF) analysis in the Rock Chemistry Laboratory at the University of Nevada, Las Vegas. Cr, Ni, Cu, Zn, Rb, Sr, Y, Zr, Nb and Ba were analyzed by XRF.

Rare-earth elements and Sc, Rb, Sr, Ba, Ta, Hf, Zr, U, Th were analyzed by Instrumental Neutron Activation Analysis (INAA) at the Phoenix Memorial Laboratory, University of Michigan. The multi-element standards G-2, GSP-1, BHVO-1, and RGM-1 were used as internal standards. Precision for REE with concentrations less than 1000 ppm is 5%, except for Nd, Tb and Yb which is 10%.

Major Elements

Volcanic rocks of the Fortification Hill field are subdivided into four magma types on the basis of major-element chemistry (Table 6). They are:

1. Volcanic rocks of the Lava Cascade. Volcanic rocks of the Lava Cascade are alkali basalts and are low in SiO, total alkalis, and high in TiO₂, CaO, MgO and FeO. Lavas of this type crop out at the Lava Cascade and west of the Hamblin-Cleopatra volcano in the Boulder Wash area (north of Lake Mead).
2. Volcanic rocks of Fortification Hill. Compared to volcanic rocks of the Lava Cascade, the alkali basalts of Fortification Hill are higher in SiO₂, and lower in TiO₂, CaO and FeO. MgO contents are similar (Table 6). Volcanic rocks of the Fortification Hill type crop out at Fortification Hill and in Petroglyph Wash.
3. Volcanic rocks of Callville Mesa. Lavas on Callville Mesa and Black Mesa are basalts and basaltic andesites and are higher in SiO₂, but lower in MgO, TiO₂, CaO, FeO and P₂O₅ than either lavas of the Lava Cascade or Fortification Hill types. Lavas of the West End Wash volcano are very similar to those of the Callville Mesa volcano, however, at the present time they are not included in the chemical discussion.
4. Volcanic rocks of the Hamblin-Cleopatra volcano. Lavas of the Hamblin-Cleopatra volcano vary from andesite to dacite and are higher in SiO₂ and lower in MgO than

TABLE 6

COMPARISON OF CHEMICAL CHARACTERISTICS OF MAGMA TYPES
FORTIFICATION HILL VOLCANIC FIELD

ELEMENT	FORT HILL	CASCADE	CALLVILLE	HAMBLIN-CLEOPATRA
TiO ₂	1.4-1.6	1.8-2.0	0.9-1.2	0.8-1.9
CaO	8-10.5	10-12	6-8	3-8
Fe ₂ O ₃	10-12.5	11.5-14	8.5-10	2.5-9.5
MgO	5-8	5.5-9	4-5.5	0.5-4
Alkalis	4-5	3-4.5	5-6	6-8.5
P ₂ O ₅	0.3-0.5	0.3-0.55	0.2-0.3	0.15-0.65
Ce	40-65	45-70	60-80	80-220
Th	3-4	3.5-4.25	4-7	5-21
Co	33-45	35-50	20-30	5-25
V	200-260	220-300	120-180	30-180

Note: oxide concentrations in weight percent and element concentrations in ppm.

FORT HILL - Basalts of Fortification Hill

rocks of the other types.

Trace and Rare-Earth Elements

There is remarkable similarity of trace and REE abundances and REE distribution between and within the Fortification Hill and Lava Cascade magma types (Figure 27). Although the Lava Cascade magma type is slightly more enriched in REE compared to the Fortification Hill type, both have nearly identical elemental distributions with enriched light REE, depleted heavy REE and no Eu anomaly. Both types show a small increase in light REE with evolution (Figure 28). Trace-element contents are very similar, however, Sc content is higher in Lava Cascade lavas than those of Fortification Hill. Lavas of Calville Mesa and the Hamblin-Cleopatra volcano are higher in light and total REE content and Th, and lower in V, Co, and Cr than the Fortification Hill or Cascade types.

Differentiation Models

Introduction

We evaluated differentiation paths for the basalts of the Fortification Hill field using open-system models involving both Rayleigh fractionation and magma mixing. Major elements were modelled using the program XLFRAC (Stormer and Nicholls, 1978). XLFRAC solves a series of linear least squares mass balance equations to determine the proportions of added or subtracted phases required to produce a fractionated rock from a given parent. To evaluate the relative importance of mixing and fractionation, trace and REE were modelled using Rayleigh fractionation and by techniques that determine the change of the concentration of an element as a system undergoes concurrent mixing and fractionation (Depaulo, 1981; Thompson et al., 1986).

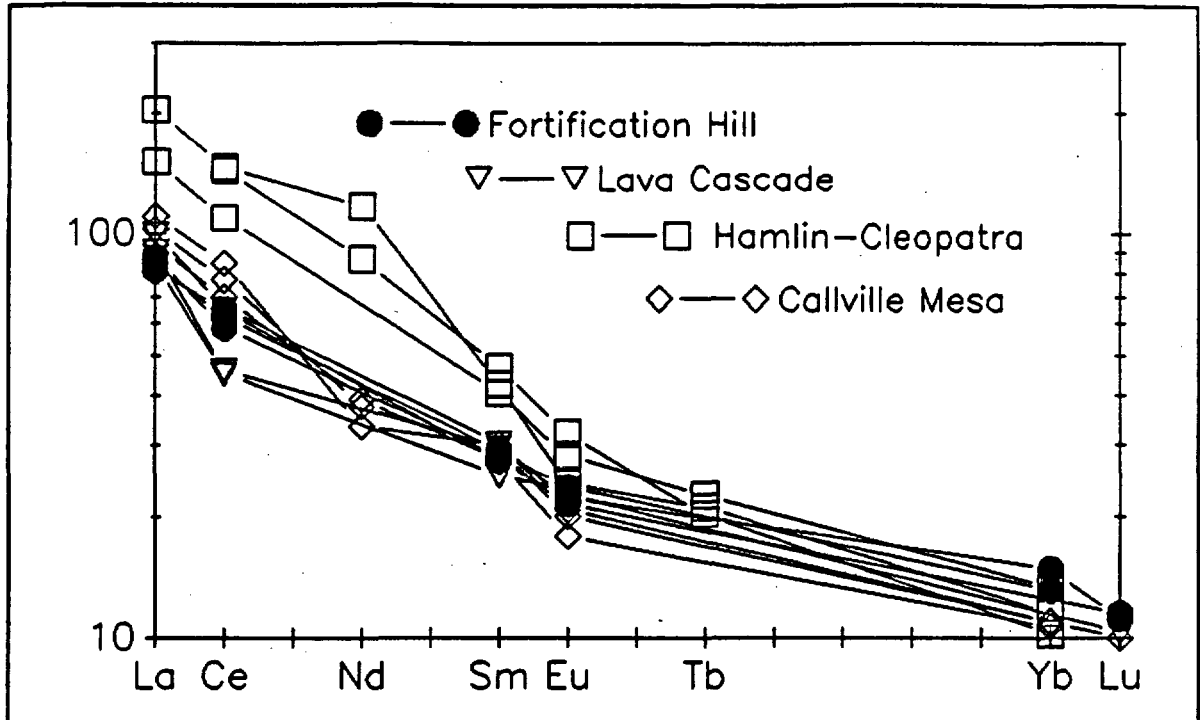


Figure 27. Comparison of REE distributions for the volcanic rocks of the Fortification Hill volcanic field.

Lava Cascade and Fortification Hill Magma Types

Models for the evolution of lavas at the Lava Cascade and at Fortification Hill must account for the following apparently contradictory observations:

1. No appreciable change in the contents of the REE, -V, FeO or total alkalis, and the lack of Eu anomalies.
2. Significant changes in MgO (5 to 9%) and Cr (75 to 325 ppm).
3. A decrease in Co (35 to 45 ppm), and increase in CaO (8 to 10.5%), TiO₂ (1.4 to 1.6%) and P₂O₅ with either decreasing MgO or Cr.

Fractionation of olivine, pyroxene or plagioclase will result in a derivative liquid with lower MgO, Cr, CaO, and V and higher SiO₂, alkalis, FeO and total REE abundance than the original liquid. REE content will increase with fractionation since the bulk

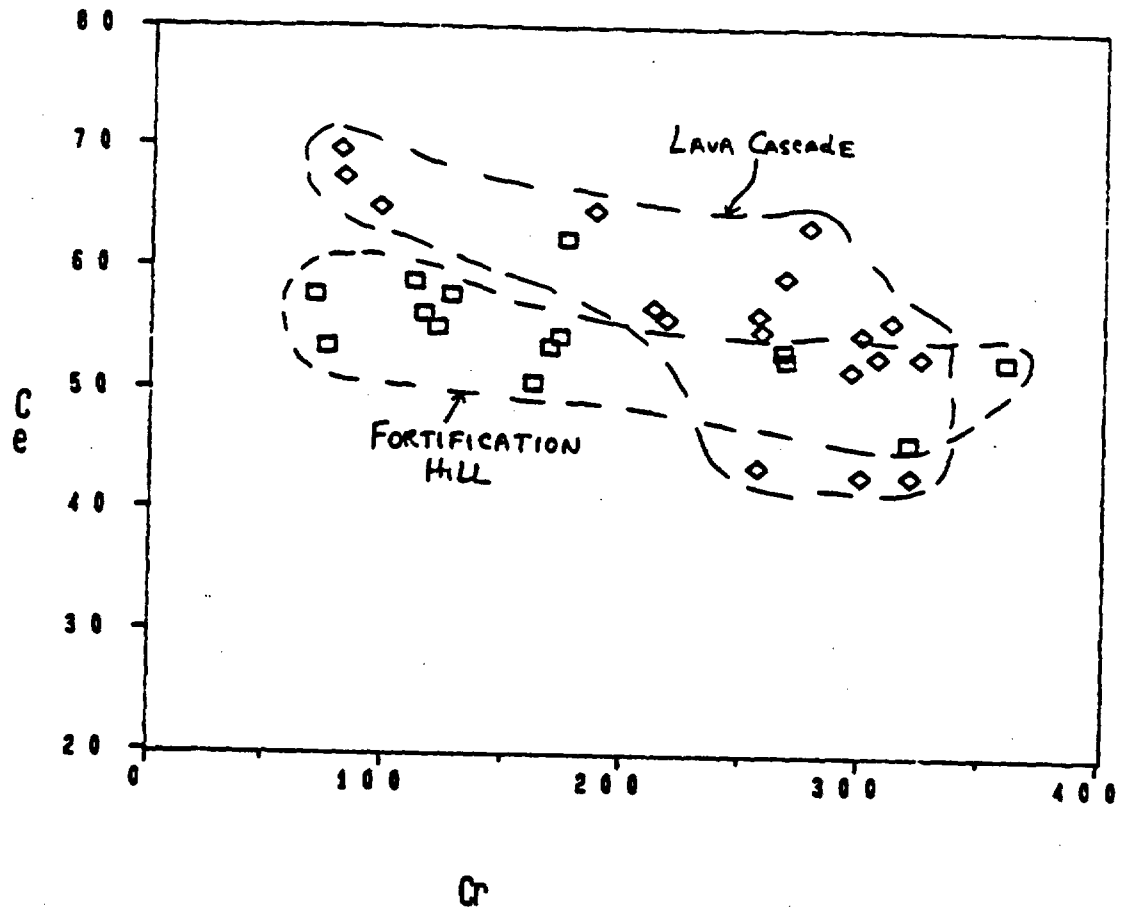


Figure 28. Ce vs. Cr plot for basalts of Fortification Hill and the Lava Cascade. Both magma types show a slight increase in Ce with evolution (decreasing Cr). Basalts of the Lava Cascade are more enriched in the light REE than those of Fortification Hill.

distribution coefficient for each REE for clinopyroxene, and olivine is much less than 1. Also, plagioclase fractionation will result in increasing REE abundances and an Eu anomaly; bulk distribution coefficients are less than one for each REE (0.13 to 0.06; but 0.34 for Eu). Relatively constant REE abundances and increasing CaO with decreasing MgO and Cr are not compatible with simple fractionation processes. On the other hand, mixing or assimilation of independently derived end-member magmas accompanied by fractional crystallization may explain the apparently contradictory observations. For example, the mixing of two basaltic magmas with similar REE abundances, but different MgO and Cr contents will result in hybrid magmas that display a wide range of MgO and Cr but relatively constant REE values. End-member compositions for open-system processes are represented by pyroxene plugs and dikes (sample 143 and 107, Fortification Hill and Lava Cascade respectively) and olivine basalt flows (samples 13 and 114, Fortification Hill and Lava Cascade respectively).

Using major-elements, two models successfully describe the range of compositions at Fortification Hill. The first requires the mixing of pyroxene and olivine bearing end members and the fractionation of 4.5% olivine (Model 1, Table 7). R (the ratio of mixed component to fractionated component) for this model is 2.37. The second successful model involves 6% olivine fractionation alone (Model 2, Table 7). Evolution vectors for trace elements were calculated by assuming a value of R (obtained from major element models) and allowing F (the amount fractionated) to vary. Models assuming R values of 3 to 10 with olivine fractionation account for the compositional variation at Fortification Hill (Figure 29). Olivine fractionation alone is not

TABLE 7
SUMMARY OF MAJOR ELEMENT MODELS

MODEL NO.	<u>FORTIFICATION HILL</u>		<u>CASCADE</u>
	1	2	3
OLIVINE	4.54	5.51	8.04
PLAGIOCLASE	----	----	2.30
CLINOPYROXENE	----	----	----
MIXED COMPONENT	10.8 (143)	----	----
OTHER	----	----	----
----- TOTAL FRACTIONATED	4.54	5.51	10.34
R VALUE	2.37	----	----
RESIDUALS	0.946	0.961	0.515

MODEL NO.	<u>CASCADE</u>		<u>CALLVILLE</u>
	4	5	6
OLIVINE	6.87	5.50	----
PLAGIOCLASE	----	4.74	4.44
CLINOPYROXENE	----	----	4.81
MIXED COMPONENT	----	65.8 (107)	54.8 (368)
OTHER	----	----	----
----- TOTAL FRACTIONATED	6.87	10.24	9.25
R VALUE	----	6.42	5.72
RESIDUALS	0.641	0.296	1.590

MODEL NO.	7
OLIVINE	5.00
PLAGIOCLASE	5.00
CLINOPYROXENE	15.0
MIXED COMPONENT	7.50 (368)
OTHER	----

TOTAL FRACTIONATED	25.0
R VALUE	0.3
RESIDUALS	1.00 (ESTIMATED)

NOTE: MINERAL VALUES ARE PERCENT FRACTIONATED. THE MIXED COMPONENT VALUE IS PERCENT ADDED. THE SAMPLE NUMBER OF THE MIXED COMPONENT USED IN THE MODEL IS IN PARENTHESES.

Models 1 to 6 were calculated using the program XLFRAC. Model 7 is based on trace and REE using the program MELT. The error (residual) for model 7 is based on a visual comparison of model and actual rock data.

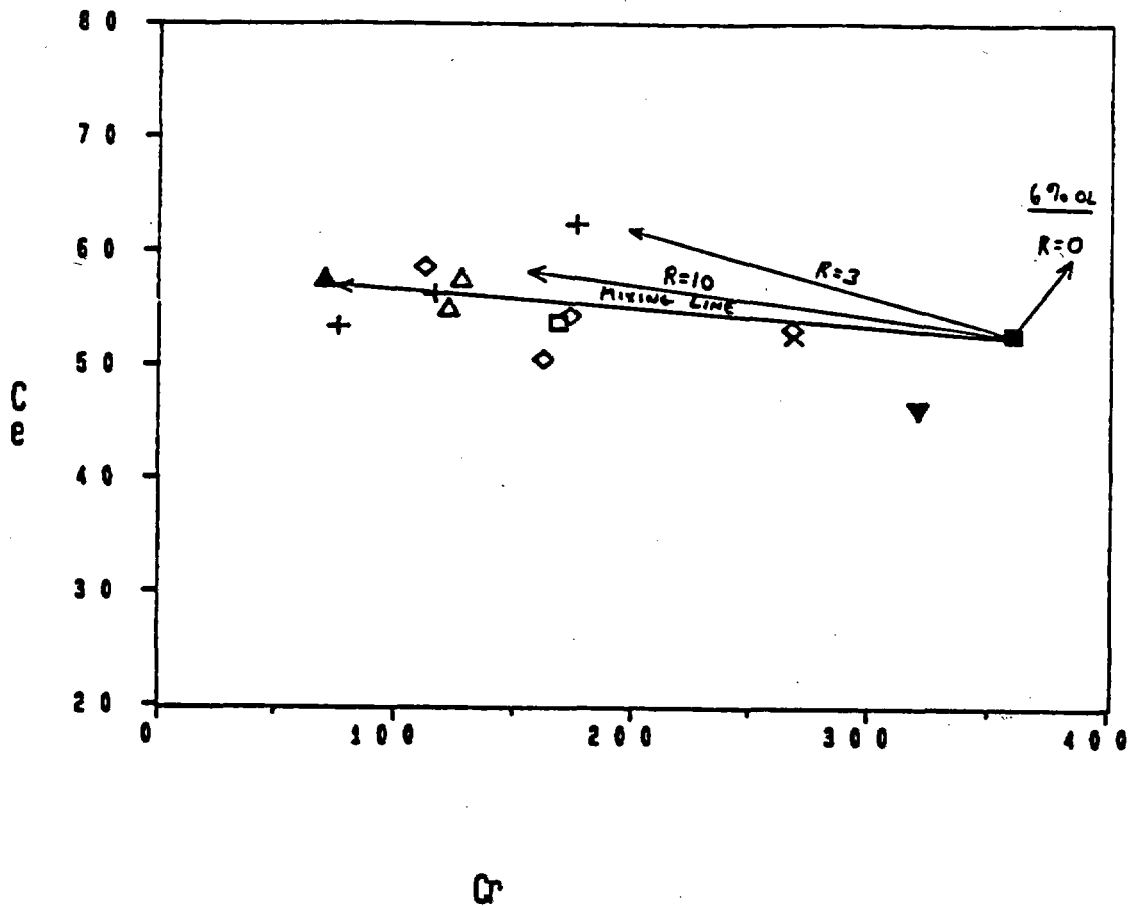


Figure 29. Evolution vectors for basalts of Fortification Hill on a Ce vs. Cr plot indicate that models that involve the mixing of pyroxene (sample 143, solid upward triangle) and olivine basalt (sample 13, solid square) magmas and about 6% olivine fractionation reproduce the nearly 300 ppm decrease in Cr and slight increase in Ce. Models that assume fractional crystallization alone produce liquids with high Cr and Ce values (R=0 vector). The mixing line displays hybrid compositions produced by mixing of pyroxene and olivine basalt magmas. R = the ratio of mixed to fractionated components; R=0 indicates fractionation and no mixing. Diamonds = dikes, boxes and down-pointing triangle = flows, x and + = intrusions and plugs.

supported by trace element models since olivine removal will not sufficiently reduce the concentration of Cr. In fact, small amounts of olivine fractionation ($F < 10\%$) will increase Cr, since the bulk distribution coefficients of Cr in olivine are less than 1 for small values of F (Figure 29). In order to decrease Cr by the amount observed, as much as 50% clinopyroxene must be removed, but this amount of clinopyroxene fractionation is not supported by field or petrographic studies. Also, since the bulk distribution coefficients for REE in clinopyroxene are less than 1, this large amount of fractionation would significantly increase the total REE content. Also, because Co and Cr decrease and V and Sc increase with degree of evolution, olivine and not clinopyroxene must be the major fractionated phase, since the bulk distribution coefficient is greater than 1 for Co in olivine, but less than 1 for clinopyroxene.

Models for the evolution of the Lava Cascade are complicated due to the variable compositions of both the pyroxene and olivine bearing basalts (Figure 30). The evolution of the pyroxene and olivine basalts are modelled separately since olivine basalts do not show evidence of mixing or assimilation, while clinopyroxene basalts display ample petrographic and field evidence of contamination. These observations rule out a single differentiation process.

End members of the olivine basalt series are sample 114 the lowermost flow, and sample 111 one of the latest flows. Major-element models involving the fractional crystallization of 8% olivine and 2.3% plagioclase (Model 3, Table 7) or 6.8% olivine (Model 4, Table 7) successfully reproduce the range of compositions of the olivine series. Trace-element models, however, do not support fractional crystallization as the only differentiation process. Fractionation of olivine and plagioclase in the amounts

indicated by the major element models will result in increasing Cr (322 to 360 ppm) and small increases in Ce (43 to 47 ppm), however, observed differences between sample 114 and 111 indicate a large decrease in Cr (322 to 175) and increase in Ce (43 to 65). Also, FeO/FeO + MgO ratios remain relative constant in the olivine series (0.60 to 0.57). This observation is not consistent with a fractional crystallization model since olivine fractionation should result in substantial increases in this ratio. The mixing of pyroxene basalt (107) with olivine basalt (114) and 10% fractionation of olivine (8%) and plagioclase (2%) successfully models the variation of the olivine series (Figure 30), however, the lack of mixing of textures in the olivine basalts urges caution and careful reevaluation before accepting this model.

The evolution of the pyroxene basalts was modelled by the mixing of olivine and pyroxene basalt and fractionation. A successful model involves the fractionation of 5.5% olivine and 4.7% plagioclase from olivine basalt (sample 114) and the addition (either by liquid-liquid or liquid-solid mixing) of pyroxene basalt (sample 107) to form the compositional range observed in the pyroxene series. The R value for this model is 6.42 (Model 5, Table 7). Trace element models support large R values. Evolution vectors plotted on a Ce vs. Cr diagram suggest that R values of 6 to 8 provide a reasonable fit to the observed elemental distributions (Figure 30).

Mixing of magmas at both the Lava Cascade and Fortification Hill is also supported by element ratio-element plots. If magma mixing is an important differentiation process, samples will fall on a hyperbolic curve on a ratio-ratio or ratio-element plot (Langmuir et al., 1978). End member compositions can be approximated on ratio-ratio and ratio-element plots since the hyperbola will become asymptotic to

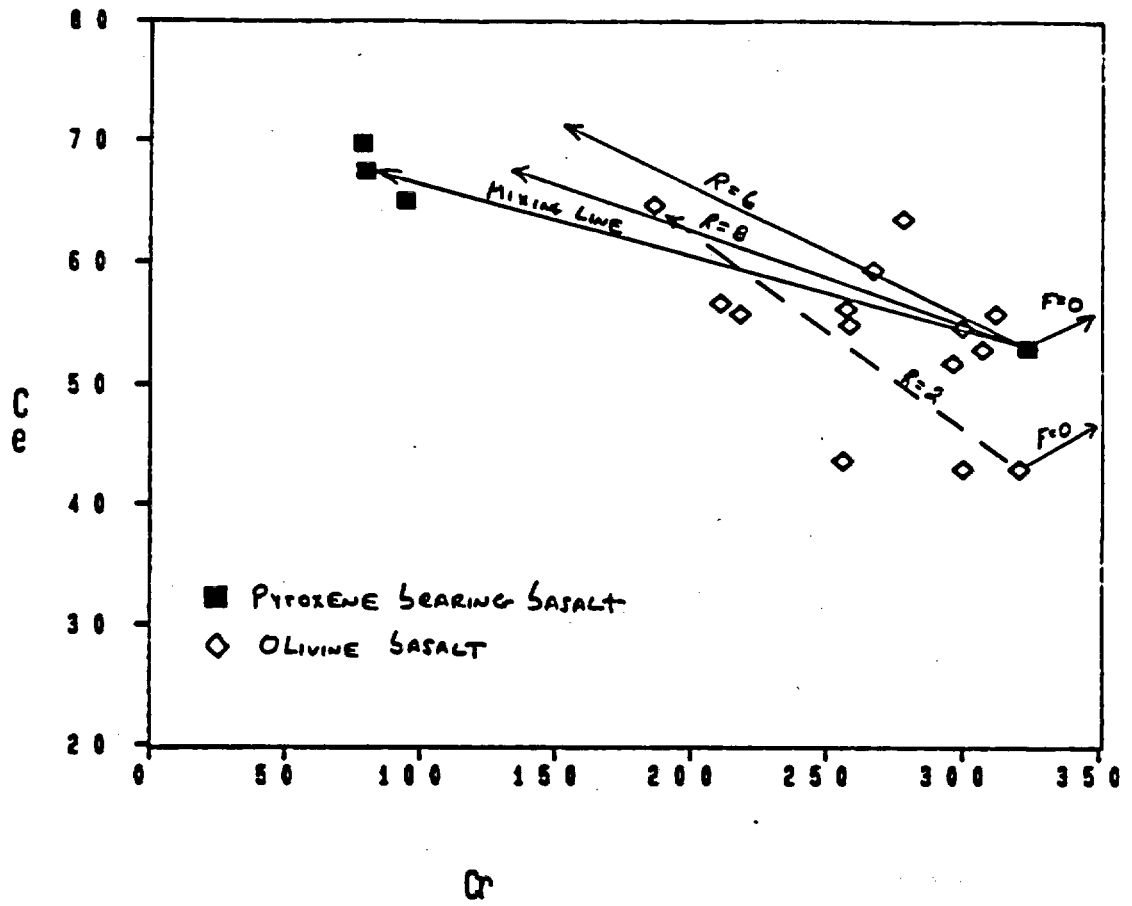


Figure 30. Ce vs. Cr plot for basalts of the Lava Cascade. Both olivine series (open diamonds) and pyroxene series (filled squares) show variation in Cr and Ce (and other light REE). Solid lines are evolution vectors for the pyroxene series, and dashed lines are vectors for the olivine series. See caption for Figure 28 for explanation of mixing line and R values.

the X and Y coordinates at ratios that approximate the elemental ratios of the end members (Langmuir et al., 1978). A plot of Fe/Cr vs. Cr for samples of basalt from the Lava Cascade and Fortification Hill displays a nearly perfect hyperbolic curve confirming that mixing is an important process in the evolution of lavas in both areas (Figure 31).

Callville Mesa

Models for the evolution of the basalts and basaltic andesites of Callville Mesa must explain:

1. The higher SiO₂ contents (51 to 56%) when compared to Fortification Hill and Lava Cascade rocks. Also the higher Th, REE content and total alkalis, and the lower TiO₂, CaO, FeO, Co, and V concentrations.
2. The positive correlation of TiO₂ and MgO abundance, as compared to the negative correlation for Fortification and Lava Cascade rocks (Figure 32).
3. The observation that an evolution vector drawn from the least evolved to most evolved rock points toward the field occupied by average upper crustal compositions. If the vector is extended back toward more primitive compositions, it intersects the field of the pyroxene basalt of Fortification Hill (Figure 32).

We suggest that the lava compositions at Callville Mesa were generated by first mixing magma with the composition of the pyroxene basalt of Fortification Hill (either samples 143 or 107) with an upper crustal contaminant such as the quartz monzonite of the Tertiary Wilson Ridge Pluton (sample 368) (Smith et al., 1988) to produce the most primitive Callville Mesa magma (sample 46). This mixing may have been accompanied by as much as 9% fractionation of clinopyroxene and plagioclase from

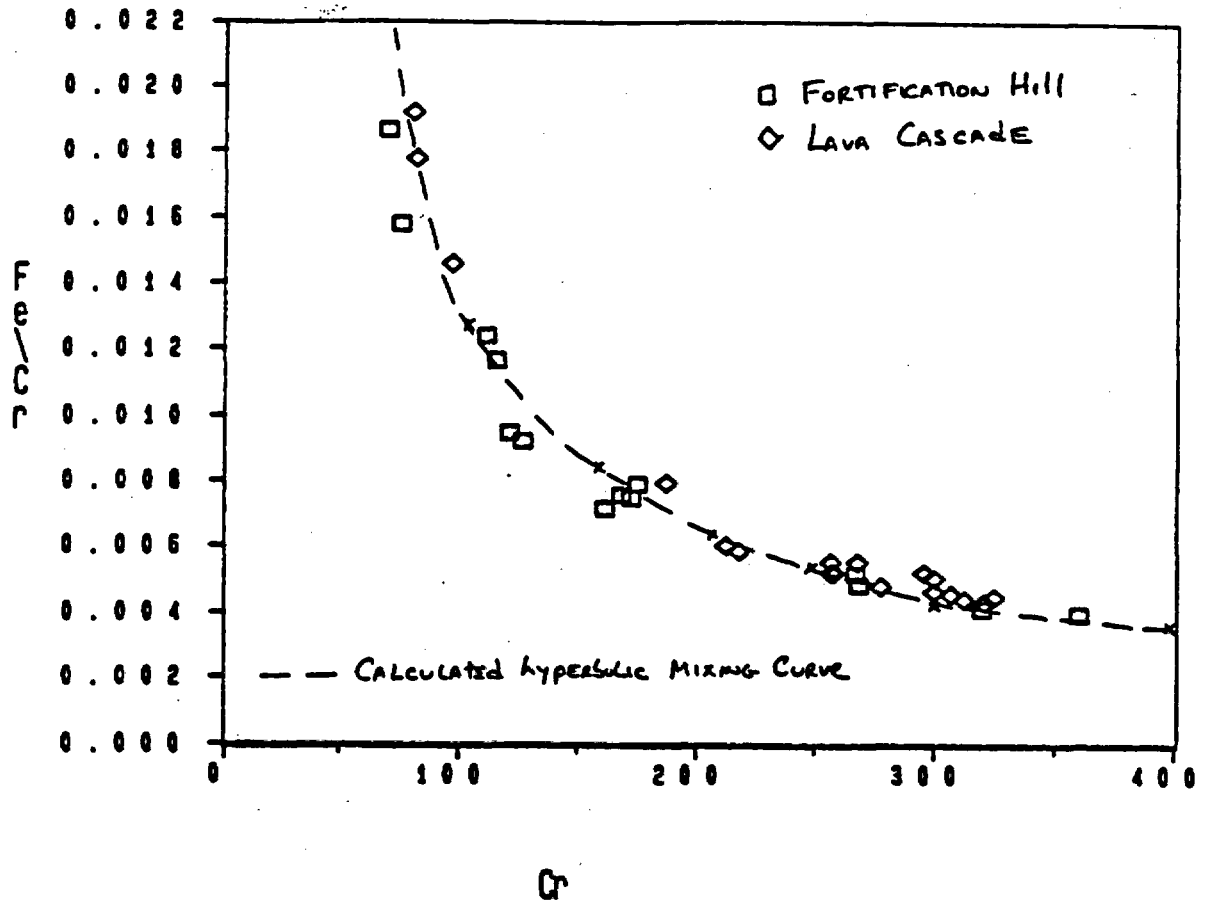


Figure 31. Ratio-element plot for Fortification Hill and Lava Cascade basalts. If magma mixing is an important differentiation process, samples will fall on a hyperbolic curve on a ratio-ratio or ratio-element plot (Langmuir et al., 1978). The nearly perfect hyperbolic curve confirms that mixing is an important process in the evolution of lavas in both areas. Note that this curve was calculated using the equations of Langmuir et al. (1978), it is not a statistical best-fit curve.

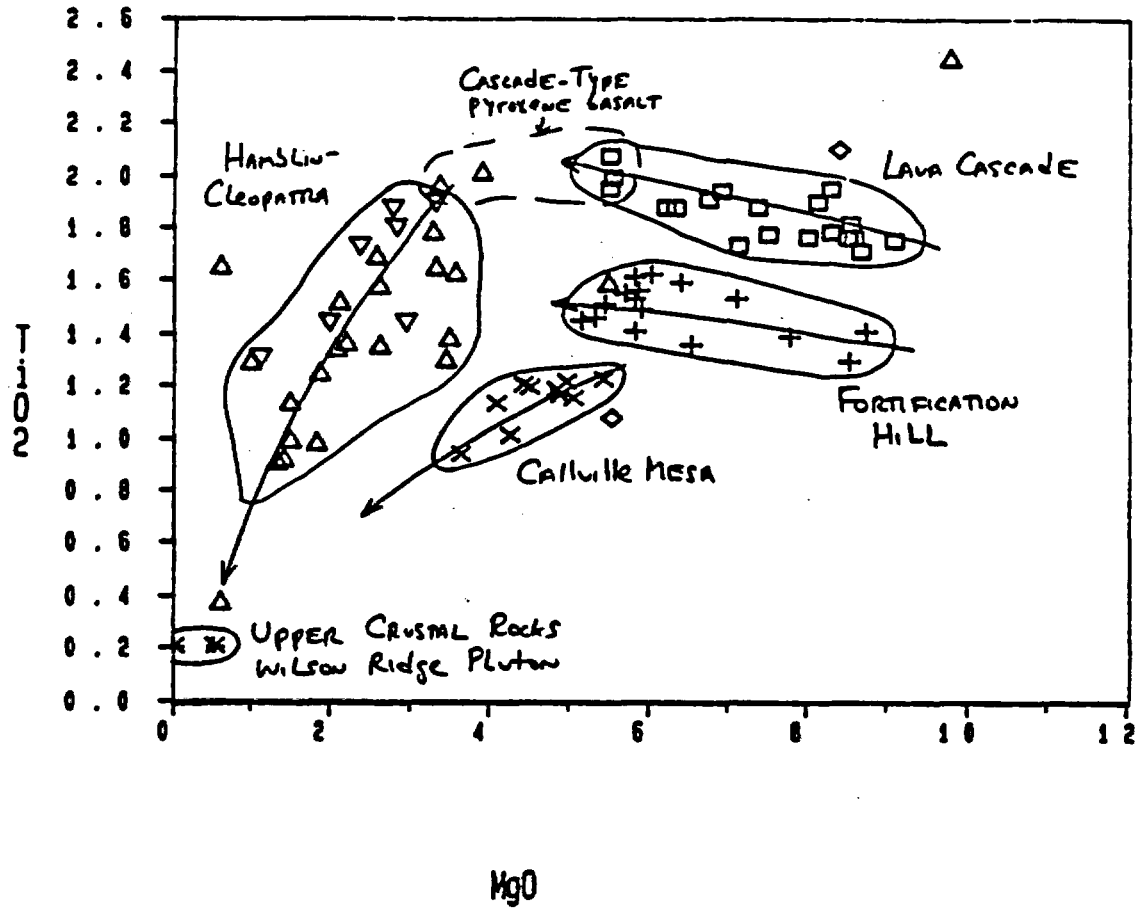


Figure 32. TIO₂ vs. MgO diagram for volcanic rocks of the Fortification Hill field. Open squares = basalts of the Lava Cascade, + = basalts of Fortification Hill, X = basalts and basaltic andesites of Callville Mesa, triangles (both upward and downward pointing; upward pointing triangles are stage 1 and downward pointing triangles are stage 2 of Thompson, 1986) = volcanic rocks of the Hamblin-Cleopatra volcano. Also plotted are granites and quartz monzonites of the Wilson Ridge Pluton (*), and alkali basalts in River Mountains (diamonds). Data for pluton rocks and alkali basalts is in Smith et al. (1988). Arrows are observed evolution vectors.

the mafic end member (143 or 107) (Model 6, Table 7). Further differentiation (sample 46 to 50) is modelled by fractionation of olivine, clinopyroxene, and plagioclase accompanied by the addition of crustal material; here assumed to be Wilson Ridge pluton (sample 368) ($R=0.3-0.4$) (Figure 33) (Model 7, Table 7).

Hamblin-Cleopatra Volcano

Lavas of the Hamblin-Cleopatra volcano display a positive correlation between TiO_2 , and MgO contents and vary in composition from andesite to dacite (Thompson, 1985). Evolution vectors (Figure 32) qualitatively show that Hamblin-Cleopatra compositions lie between the fields of Lava Cascade type pyroxene basalt and an upper crustal composition. Mixing of these end members along with fractionation of clinopyroxene, hornblende and possibly biotite may produce the observed variation. Evolution of the volcano is complex and activity may be subdivided into at least two cycles (Thompson, 1985). The compositional range of the cycles overlap suggesting repetition of the open-system processes. The two end-members required for modelling are locally available. Basalts of Lava Cascade type, dated at about 9 Ma (Thompson, 1985), crop out just to the west of the volcano. The most highly evolved lavas of the Hamblin-Cleopatra volcano fall within the field of compositions related to the Wilson Ridge Pluton. The field observations, as well as abundant mixing textures (Thompson, 1985), indicate that mixing/assimilation was important in the magmatic development of the Hamblin-Cleopatra volcano.

Formation of Parent Magmas

Our modelling suggests that at least 4 parent basaltic magmas and a crustal contaminant are required to produce the observed compositional variations of the

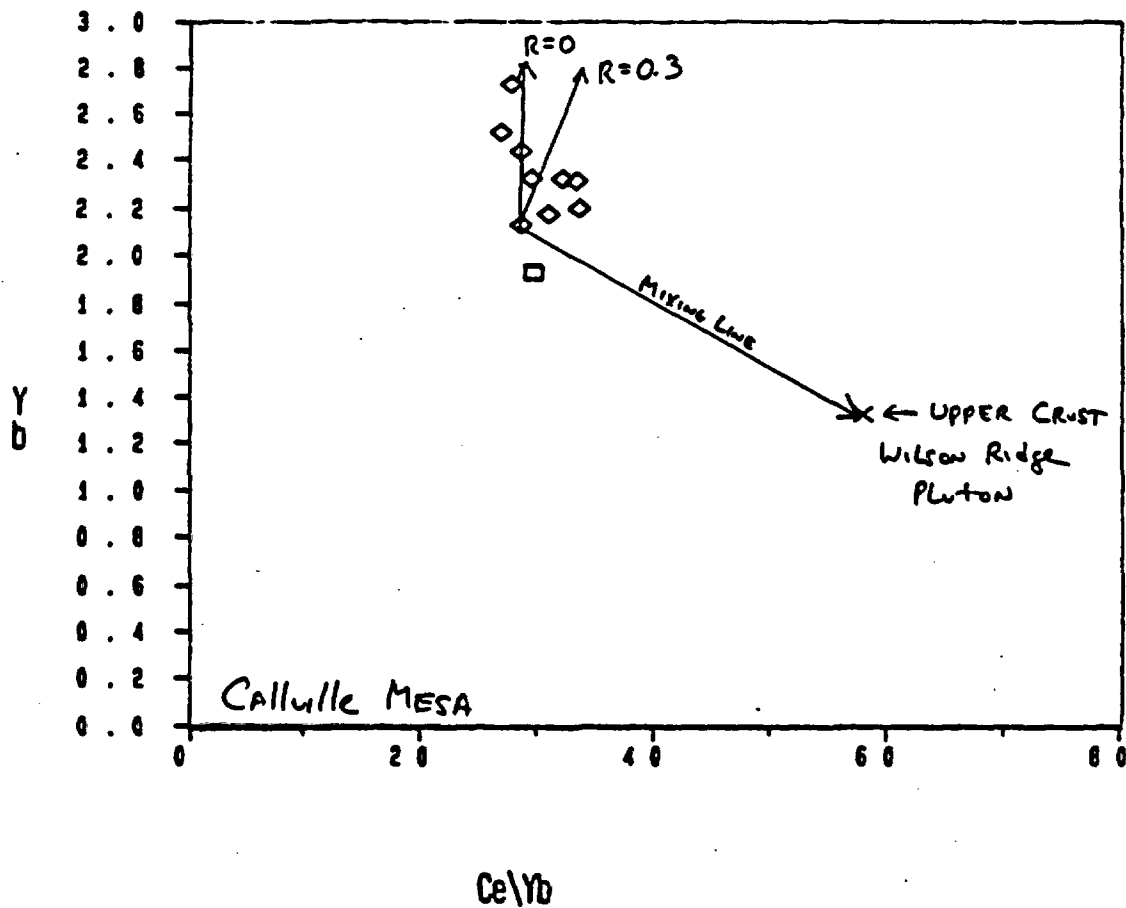


Figure 33. Yb vs. Ce/Yb for volcanic rocks of Calville Mesa (diamonds). Also plotted is Fortification Hill basalt 143 (box) and Wilson Ridge Pluton quartz monzonite (348) (X). Modelling suggests that fractional crystallization of olivine, clinopyroxene, and plagioclase accompanied by the addition of crustal material (Wilson Ridge Pluton) ($R=0.3$) may be responsible for the compositional variation of the Calville Mesa basalts.

Fortification Hill basalt field. We suggest that these parent magmas were generated by a complex process of partial melting of a compositionally heterogeneous mantle composed of spinel peridotite accompanied by fractional crystallization of the resultant partial melt. The spinel peridotite is assumed to contain clinopyroxene (30%), orthopyroxene (12%), spinel (5%), and olivine (53%) and is enriched 4 times that of chondrite for light REE and 2 times chondrite for heavy REE. Modal batch melting of this spinel peridotite alone will not yield magmas of the proper FeO/FeO+MgO (Fe') ratio. However, fractional crystallization of 30 to 45% olivine from the partial melts will produce the observed ratios (Figure 34). The generation of the pyroxene bearing parents are modelled by 3% partial melting followed by 40% olivine fractionation. Olivine bearing parent magmas probably formed by about 15% partial melting followed by 30% olivine fractionation (Figure 34). A comagmatic relationship between the Lava Cascade and Fortification Hill magma types is ruled out since Lava Cascade lavas are higher in REE content and Th, and also higher in TiO₂, CaO, FeO and V and lower in total alkalis than Fortification Hill lavas. These contradictory trends suggest generation of each type by independent melting of a heterogeneous mantle source, rather than the formation of one from the other by a fractional crystallization process.

Igneous Activity and Extensional Tectonics

Volcanism during active extension in the Lake Mead area was alkali-calcic or calc-alkalic with intermediate rock types predominating. Following the transition at about 10 Ma to a period of tectonic quiescence, alkalic basalt was the major eruptive product. Smith et al. (1988) suggested that the intermediate compositions formed during extension were a product of the mixing of the end-members of a bimodal

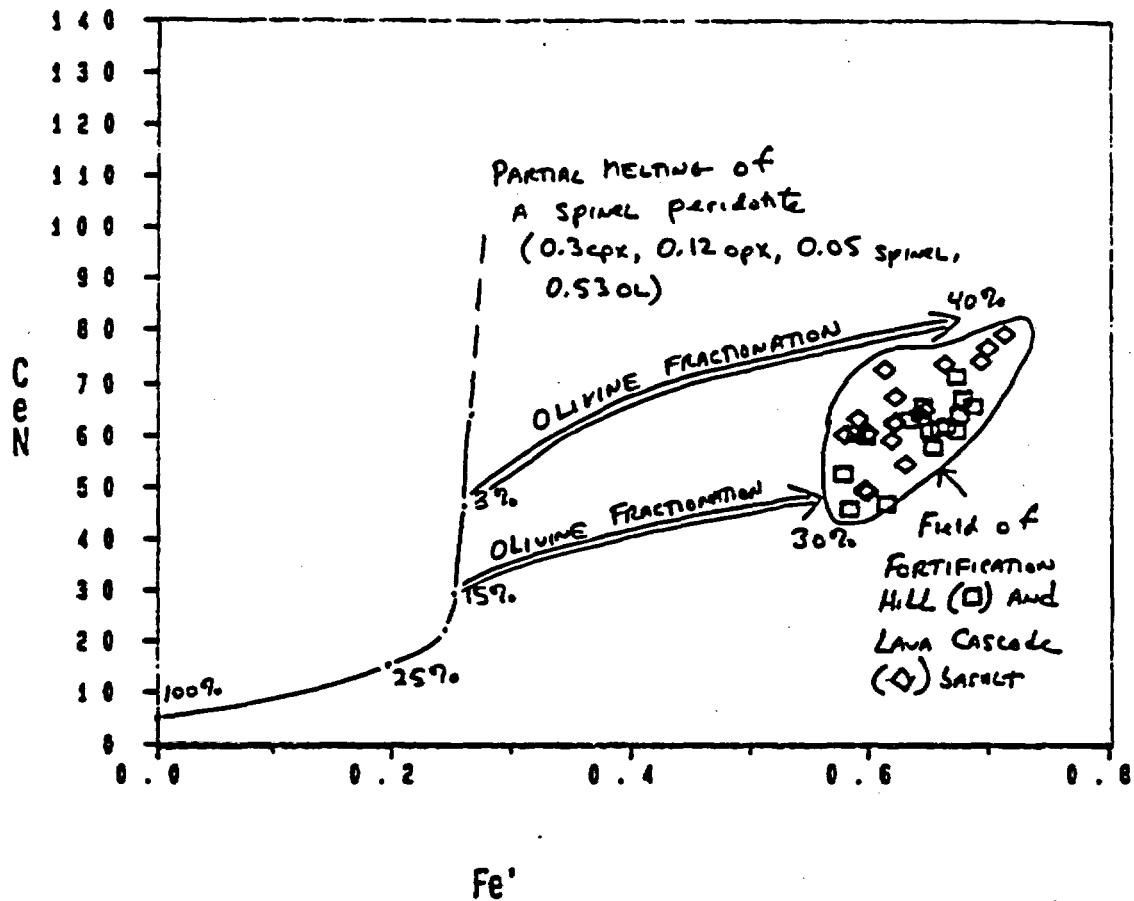


Figure 34. Ce (chondrite normalized) vs. Fe' ($FeO/FeO+MgO$) plot of basalts of the Lava Cascade (diamonds) and Fortification Hill (box). Curved line shows liquid evolution line during partial melting of a spinel peridotite source. Double arrows are evolution tracks for fractionation of liquids formed by 3% and 15% partial melting. Note that Fortification Hill and Lava Cascade basalt "primary magmas" can not be produced by partial melting alone; both partial melting and olivine fractionation are required.

basalt-rhyolite (or basalt-dacite) suite. The mixing of these magma types may have been enhanced by the presence of abundant brittle and/or ductile low-angle faults or shear zones in the upper crust. These low-angle zones probably acted as traps and "mixing" chambers for rising magma. During the waning stages of extension, high-angle faults penetrated deeper into the crust thus allowing end-member magmas to reach the surface (Smith et al., 1988). In the Fortification Hill field the waning of extension is marked by the removal of the felsic crustal component as an end-member for mixing processes. This event is recorded by the change of compositions from intermediate to mafic and graphically by the change in slope on a MgO vs. TiO₂ plot. Magmas produced during extension plot in fields that lie between an upper crustal composition and a mafic parent. After 10 Ma, during the waning stages of extension, magma compositions no longer show any relationship to upper crustal compositions and the slopes of evolution vectors on MgO vs. TiO₂ reverse (Figure 32).

The removal of the upper crustal component may be related to how effectively rising magma can be isolated from country rock. Rising magma will chill upon contact with colder country rock and produce a lining or coating that should effectively insulate the conduit (Myers, 1988). During active extension, faulting may preclude the formation of a vent lining, thus facilitating contamination. During a period of tectonic quiescence when the frequency of faulting decreases, vent linings may form and effectively isolate the rising magma from the upper crustal contaminant.

ROCK CHEMISTRY LABORATORY

(Ed Thomas)

Introduction

The goal of the rock chemistry laboratory in this last year was to develop an approved set of technical procedures for the processing and analyzing of samples for major elements (SiO_2 , Al_2O_3 , Fe(total), MgO, CaO, Na_2O , K_2O , TiO_2 , MnO and TiO_2) and some trace elements (Sr, Rb and Zr). Achieving this goal will then allow us a greater degree of independence from outside contractors and will allow better internal control of samples and analytical parameters. The lab will provide a high degree of analytical precision and accuracy through the use of both an upgraded Dapple Systems x-ray fluorescence (XRF) system and a modern Perkin Elmer model 3030B atomic absorption spectrophotometer (AAS).

Progress

Acid Digestion Techniques

Initially, our goal was to establish a technique for sample preparation and analysis by AAS. Because of the numerous problems encountered in the analysis the major elements by AAS and the ease of analysis with the XRF, only aluminum, sodium and potassium will be analyzed by AAS. The first sample preparation techniques that we used were standard acid digestion bomb (ADB) methods for dissolving powdered rock samples. The ADB method involves digesting the powdered sample in a solution of hydrofluoric acid (HF), aqua regia, and boric acid in a heated, pressurized teflon container. Besides the obvious problems in handling the materials used on a daily basis, this method also proved unacceptable in its reliable digestion of the sample. Because of problems with chemical complexing, especially between HF and silicon, accurate analysis of samples prepared in this manner was not possible. These

problems then resulted in the abandonment of this technique.

Standards

Standard preparation was another major problem. Two different types of standards were considered; multi-element standards prepared from digested USGS rock standards and single-element standards prepared from single-element atomic absorption standards. Preparation of the multi-element standards posed the same problems as the preparation of the unknowns. As a result, we decided to use single-element standards. The single-element standards are as similar as possible to the samples and contain all of the sample chemicals (acids, fluxes, etc.) as the samples to be analyzed. However, many of the matrix problems encountered with the multi-element standards are eliminated. Storage of standards also posed a problem because many of the standard solutions are unstable. The solutions will often precipitate depending especially on the length of storage time. Because the AAS is only being used for aluminum, magnesium and sodium at this time, it is only these standards that must be dealt with. These standards are best prepared on a daily basis.

Alkali-Fusion Methods

We next used alkali-fusion techniques. The sample is fused at a high temperature with an alkali flux such as sodium peroxide or lithium metaborate. A glass bead is formed which readily dissolves in hydrochloric acid (HCl). Lower temperature fusions (i.e., fusion over a burner flame) in a zirconium crucible with reagents such as sodium peroxide were tested first and proved useful for at least some of the elements. However elements such as sodium and potassium could not be analyzed by this

method because of their presence in the flux. Thus, a higher temperature fusion technique suggested by Perkin-Elmer was chosen. This procedure requires that 100 mg of the powdered rock sample is fused with 0.6 g of lithium metaborate at 1000°C in a platinum crucible for 15 minutes. Once fused, the glass bead is dissolved in the crucible with concentrated hydrochloric acid. The resulting solution is transferred into a 200 ml volumetric flask. Enough lanthanum solution form a 0.1% lanthanum solution is added, and the solution is brought to a final volume of 200 ml. The lanthanum solution is added to reduce ionization effects in the AAS flame. This solution is used, unaltered, in the analysis of aluminum. A five-times dilution of the initial solution with an adjusted lanthanum content of 0.1%, is used for the analysis of magnesium and sodium.

X-ray Fluorescence Techniques

In the past couple of months, we initiated major element analyses by XRF. Our XRF unit was recently modified by the addition of solid-state electronics and will soon be retrofitted with an automated system. The new solid-state system resulted in a precise, accurate and rapid system for analyzing the oxides of Si, Fe, Ca, K, Ti, Mn and the trace elements like Zr, Sr, Rb, and Ni. The analytical technique involves the production of a compressed sample pellet made from a small amount of finely powdered sample backed with a binding material such as methyl cellulose (Hutchinson, 1974). All of the powdered samples are currently being run through a micronizing mill in order to insure that there is a constant grain size for all of the

samples. This step all but eliminates matrix corrections.

Loss On Ignition Techniques (LOI)

LOI determinations of the concentration of volatile components, such as water and other volatile elements or compounds, in a sample. The analytical procedure involves the weighing out of a random amount of the sample in a platinum crucible. The crucible with sample is placed in an oven at 1000 degrees celsius for 15 minutes and then the sample is reweighed as soon as it has cooled. The resulting sample weight is divided by the initial weight and the resulting percentage is the weight percent of the volatiles in the rock. The technique is also briefly outlined in Hutchinson (1974).

IMPLICATIONS FOR THE VOLCANISM NEAR YUCCA MOUNTAIN

1. Multiple age dates on single volcanic centers are more meaningful than single dates. Multiple dates provide estimates of the duration of volcanic activity at an individual volcanic center and provide a better understanding of the periodicity of eruptions and the length of periods of quiescence between eruptions. Age dating of basalt in the Fortification Field suggests that volcanic activity may continue at a single center for between 50 and 680 Ka. Our estimate of the duration of volcanic activity agrees with that of Crowe based on work at Crater Flat. Crowe and others (1988) indicated that many "small volume basaltic centers are polycyclic with intermittent activity that extends for periods of up to several hundred thousand years." These observations suggest that basaltic centers younger than several hundred thousand years may be the focus of future eruptions. If the Lathrop Wells cone, south of Yucca Mountain, is less than 100 Ka, it may be a dormant volcano or may be part of a

dormant volcanic field. Thus, there is potential for future activity. This work relates directly to the licencing of the Yucca Mountain site as a nuclear waste repository, since the presence of potentially active volcanoes within 100 km of the site is a potentially adverse condition that might disqualify it as a candidate site.

2. Stratigraphic and geochemical studies indicate the nature of chemical changes during the lifetime of a volcanic field. This work is useful for evaluating conclusions of Foland et al. (1987) who suggested that basaltic eruptions in the Reveille-Pancake Range become more highly alkalic and nepheline normative in their waning stages any particular geographic locality. This observation has important implications for volcanism at Crater Flat adjacent to the proposed Yucca Mountain repository. Since the youngest eruptive products at Crater Flat are nepheline normative, no further eruptions would be expected at this locality if Foland's geochemical model is correct.

Our studies in the eastern Reveille Range based on detailed study of the Hyde Springs volcanic complex and in the Fortification Hill field suggest that chemical changes are cyclic and that the trend toward nepheline normative magmas may not be a sign of waning volcanism. At the present time, we have not identified any chemical criteria that positively signal the termination of volcanism.

3. The emplacement of volcanic vents (dikes, plugs, sills) is not directly controlled by the location of mappable faults or joints. In the Hyde Spring area (Reveille Range) dikes commonly cut across the regional joint set. In the Fortification Hill area, dikes and plugs are commonly elongated in the direction of major fault zones, but they do not crop out within these zones. We suggest a model where magma rises along zones of structural weakness at depth (> 1000 m), but because hydrothermal activity

near the surface tends to seal fault zones and joints, magma abandons the regional structures and rises along any available pathway to the surface. Scott and Bonk (1984) indicate that the proposed Yucca Mountain repository would be situated in an area relatively free of faults. Fault density increases both to the west and east of the repository site. Our studies at the Lava Cascade suggest that renewed volcanic activity related to the Crater Flat field may not use existing structure, but magma might move into areas not presently faulted by creating its own pathway to the surface. Therefore the paucity of faults may not guarantee safety from future volcanic disruption.

REFERENCES CITED

- Anderson, R.E., Longwell, C.R., and Armstrong, R.L., 1972, Significance of K-Ar ages of Tertiary rocks from the Lake Mead region, Nevada-Arizona: *Geological Society of America Bulletin*, v. 83, p. 273-288.
- Anderson, R.E., 1973, Large-magnitude late Tertiary strike-slip faulting north of Lake Mead, Nevada: U.S. Geological Survey Professional Paper 794, 18 p.
- Anderson, R.E., 1978, Geological Map of the Black Canyon 15' Quadrangle, Arizona and Nevada: U.S. Geological Survey Map GQ-1394.
- Anderson, R.E., 1982, Miocene structural history south of Lake Mead, Nevada-Arizona: *Geological Society of America Abstracts with Programs*, v. 14, no. 4, p. 145.
- Bohannon, R.G., 1983, Geologic map, tectonic map and structure sections of the Muddy and northern Black Mountains, Clark County, Nevada: U.S. Geological Survey, Map I-1406.
- Bohannon, R.G., 1984, Mesozoic and Cenozoic tectonic development of the Muddy, North Muddy, and northern Black Mountains, Clark County, Nevada, in Miller, D.M., Todd, V.R., and Howard, K.A., eds., *Tectonic and Stratigraphic studies in the eastern Great Basin: Geological Society of America, Memoir 157*, p. 125-148.
- Campbell, I., and Schenk, E.T., 1950, Camptonite dikes near Boulder Dam, Arizona: *American Mineralogist*, v. 35, nos. 9-10, p. 671-692.
- Carr, W.J., 1982, Volcano-tectonic history of Crater Flat as suggested by new evidence from drill hole USW-VH-1 and vicinity, Crater Flat, southwestern Nevada: U.S. Geological Survey Open File Report 74-176, 53 p.
- Christiansen, R.L. and Lipman, P.W., 1972, Cenozoic volcanism and plate-tectonic evolution of the western United States, II, Late Cenozoic: *Philos. Transactions Royal Society of London Series A*, v. 271, p. 249-284.

- Crowe, B.M., Perry, F.V., Turrin, B.D., Wells, S.G., and MacFadden, L.D., 1988, Volcanic hazard assessment for storage of high-level radioactive waste at Yucca Mountain, Nevada: Geological Society of America, Abstracts with Programs, v. 20, no. 3, p. 153.
- DeLaney, P.T., and Pollard, D.D., 1982, Solidification of basaltic magma during flow in a dike: American Journal of Science, v. 282, p. 856-885.
- Deubendorfer, E.M., Sewall, A.J., and Smith, E.I., 1988, The Saddle Island detachment: an evolving shear zone in the Lake Mead area, Nevada: Geological Society of America Special Paper (in press).
- Dohrenwend, J.C., Turrin, B.D., and Diggies, M.F., 1985, Topographic distribution of dated basaltic lava flows in the Reville Range, Nye County Nevada: Implications for Late Cenozoic erosion of upland areas in the Great Basin: Geological Society of America Abstracts with Programs, v. 17, no. 6, p. 352.
- DePaulo, D.J., 1981, Trace element and isotopic effects of combined wall-rock assimilation and fractional crystallization: Earth and Planetary Science Letters, v. 53, p.189-202.
- Ekren, E.B., Rogers, C.L. and Dixon, G.L., 1973, Geologic and Bouguer gravity map of the Reville Quadrangle, Nye County, Nevada: U.S. Geological Survey Miscellaneous Geologic Investigations Map I-806.
- Feuerbach, D.L., 1986, Geology of the Wilson Ridge pluton; a mid-Miocene quartz monzonite intrusion in the northern Black Mountains, Mohave County, Arizona and Clark County, Nevada: (M.S. Thesis): Las Vegas, University of Nevada, 79 p.
- Foland, K.A., Kargel, J.S., Lum, C.L., and Bergmann, S.C., 1987, Time-spatial-composition relationships among alkali basalts in the vicinity of the Lunar Crater, south central Nevada: Geological Society of America Abstracts with Programs, v. 19, no. 7, p. 666.
- Irvine, T.N., and Baragar, W.R.A., 1971, A guide to the chemical classification of the common volcanic rocks: Canadian Journal of Earth Sciences, v. 8, p. 523-548.
- Langmuir, C.H., Vocke, R.D., Jr, Hanson, G.H., Hart, S.H., 1978, A general mixing equation with applications to Icelandic basalts: Earth and Planetary Science Letters, v. 37, p. 380-392.
- Lipman, P.W., Prostka, H.J., and Christiansen, R.L., 1972, Cenozoic volcanism and plate-tectonic evolution of the western United States, I, Early and middle Cenozoic: Philos. Transactions Royal Society of London Series A, v. 271. p. 217-248
- Longwell, C.R., Pampeyan, E.H., Bowyer, Ben and Roberts, R.J., 1965, Geology and mineral deposits of Clark County, Nevada: Nevada Bureau of Mines and Geology Bulletin 62, 218p.
- Mills, J.G., 1985, The geology and geochemistry of volcanic and plutonic rocks in the Hoover Dam 7 1/2 quadrangle, Clark County, Nevada and Mohave County, Arizona (M.S. Thesis): Las Vegas, University of Nevada, 119 p.
- Myers, J.D., 1988, Possible petrogenetic relations between low and high-MgO Aleutian basalts: Geological Society of America Bulletin, v. 100, p. 1040-1053.
- Scott, R.B., and Bonk, Jerry, 1984, Preliminary geologic map of Yucca Mountain, Nye County, Nevada with geologic sections: U.S. Geological Survey Open File Report 84-494.
- Smith, E.I., Feuerbach, D.L., Naumann, T.R. and Mills, J.G., 1988, Mid-Miocene igneous rocks in the Lake Mead area of Nevada and Arizona: Production of intermediate igneous rocks in an extensional

environment: In Anderson, J.L., Cordilleran Magmatism, Geological Society of America Special Paper (In press).

Stormer, J.C., Jr., and Nicholls, J., 1978, XLFRAC: a program for the interactive testing of magmatic differentiation models: *Computers and Geoscience*, v. 4, p. 143-159.

Suneson, N.H. and Lucchitta, Ivo, 1983, Origin of bimodal volcanism, southern Basin and Range province, west-central Arizona: *Geological Society of America Bulletin*, v. 94, p. 1005-1019.

Thompson, K.G., 1985, Stratigraphy and petrology of the Hamblin-Cleopatra volcano, Clark County, Nevada: Unpublished Master's Thesis, University of Texas, Austin, 306 p.

Thompson, R.A., Dungan, M.A. and Lipman, P.W., 1986, Multiple differentiation processes in Early-Rift Calc-Alkalic volcanics, northern Rio Grande Rift, New Mexico: *Journal of Geophysical Research*, v. 91, no. B6, p. 6046-6058.

Vaniman, D. and Crowe, B., 1981, Geology and petrology of the basalts of Crater Flat: applications to volcanic risk assessment for the Nevada Nuclear Waste Storage Investigations: Los Alamos National Laboratory manuscript, LA-8845-MS, 67 p.

Vaniman, D., Crowe, B., and Gladney, E.S., 1982, Petrology and geochemistry of hawaiite lavas from Crater Flat, Nevada: *Contributions to Mineralogy and Petrology*, v. 80, p. 341-357.

Weber, M.E., and Smith, E.I. 1987, Structural and geochemical constraints on the reassembly mid-Tertiary volcanoes in the Lake Mead area of southern Nevada: *Geology*, v. 15, p. 553-556.

Eruptive probability calculation for the Yucca Mountain site, USA: statistical estimation of recurrence rates*

Chih-Hsiang Ho¹, Eugene I Smith², Daniel L Feuerbach², Terry R Naumann²

¹ Department of Mathematical Sciences and ² Center for Volcanic and Tectonic Studies, Department of Geoscience, University of Nevada, Las Vegas, NV 89154, USA

Received July 23, 1990/Accepted June 5, 1991

Abstract. Investigations are currently underway to evaluate the impact of potentially adverse conditions (e.g. volcanism, faulting, seismicity) on the waste-isolation capability of the proposed nuclear waste repository at Yucca Mountain, Nevada, USA. This paper is the first in a series that will examine the probability of disruption of the Yucca Mountain site by volcanic eruption. In it, we discuss three estimating techniques for determining the recurrence rate of volcanic eruption (λ), an important parameter in the Poisson probability model. The first method is based on the number of events occurring over a certain observation period, the second is based on repose times, and the final is based on magma volume. All three require knowledge of the total number of eruptions in the Yucca Mountain area during the observation period (E). Following this discussion we then propose an estimate of E which takes into account the possibility of polygenetic and polycyclic volcanism at all the volcanic centers near the Yucca Mountain site.

Introduction

The Yucca Mountain region is located within the Great Basin portion of the Basin and Range physiographic province, a large area of the western USA characterized by alternating linear mountain ranges and alluvial valleys. Crowe and Perry (1989, Figure 1) divide the Cenozoic volcanism of the Yucca Mountain region into three episodes that include (1) an older episode of large volume basaltic volcanism (12 to 8.5 Ma) that coincides in time with the termination of silicic volcanic activity; (2) the formation of five clusters of small volume basalt scoria cones and lava flows (9 to 6.5 Ma), all located north and east of the Yucca Mountain site; and (3) the

formation of three clusters of small volume basalt centers (3.7 to 0.01 Ma), all located south and west of the Yucca Mountain site. The two youngest episodes form northwest-trending zones that parallel the trend of structures in the Spotted Range-Mine Mountain section of the Walker Lane belt. Crowe and Perry (1989) suggest a southwest migration of basaltic volcanism in the Yucca Mountain area based on this structural parallelism, a pattern that may reflect an earlier southwest migration of silicic volcanism in the Great Basin. Smith et al. (1990a) suggest that there is no preferred migration trends for post-6-Ma volcanism in the Yucca Mountain region.

Concern that future volcanism might disrupt the proposed Yucca Mountain repository site motivated the assessment of the volcanic risk to the Yucca Mountain area, located within the Nevada Test Site (NTS). Crowe and Carr (1980) calculate the probability of volcanic disruption of a repository at Yucca Mountain, Nevada using a method developed largely by Crowe (1980). Crowe et al. (1982) refine the volcanic probability calculations for the Yucca Mountain area using the following mathematical model:

$$Pr [\text{disruptive event before time } t] = 1 - e^{-\lambda tp},$$

where λ is the recurrence rate of volcanic events and p is the probability of a repository disruption, given an event. The parameter p is estimated as a/A , where a is the area of the repository and A is some minimal area that encloses the repository and the area of the volcanic events. Crowe et al. (1982) develop a computer program to find either the minimum area circle or minimum area ellipse (defined as A) that contains the volcanic centers of interest and the repository site. A is defined to accommodate tectonic controls for the localization of volcanic centers and to constrain λ to be uniform within the area of either the circle or ellipse. The rate of volcanic activity is calculated by determination of the annual rate of magma production for the NTS region and by cone counts using refined age data. Resulting probability values using the refined mathematical model are calculated for periods of 1 year and 100,000 years. Two

* Paper financed by the Nuclear Waste Project Office, State of Nevada, USA

Offprint requests to: C-H Ho

procedures (explained below) are used for the rate calculations (Crowe et al. 1982). As calculated by Crowe et al. (1982), the probability of volcanic disruption of a waste repository located at Yucca Mountain falls in the range of 3.3×10^{-10} to 4.7×10^{-8} during the first year, which increases approximately linearly with isolation time.

Issues that arise in connection with the work of Crowe et al. (1982)

Although the procedure outlined in Crowe et al. (1982) represents a more formal approach to this problem than ever attempted previously, flaws exist. The method must be modified because the existing data base is inadequate to reasonably constrain λ . Despite the fact that there are well-recognized means of gathering data in the NTS region (field mapping; determinations of the eruptive history of basaltic centers; petrology; geochemistry; geochronology, including magnetic polarity determinations; tectonic setting; and geophysical studies) many considerations are still unknown, e.g., age of volcanism and vent counts.

Present understanding of eruptive mechanisms is not yet advanced enough to allow deterministic predictions of future activity. The only attempts at long-term forecasting have been made on statistical grounds, using historical records to examine eruption frequencies, types, patterns, risk, and probabilities. Reliable historical data make possible the construction of activity patterns for several volcanoes (Wickman 1966, 1976; Klein 1982, 1984; Mulargia et al. 1987; Condit et al. 1989; Ho 1990). Unfortunately, detailed geologic mapping of volcanic centers is in its infancy in the Yucca Mountain area. A formal structure, with conclusions depending on the model assumptions, needs to be developed to evaluate volcanic risk for the NTS.

This paper investigates important parameters required to calculate the probability of site disruption and provides estimates for the unknown parameter(s) that are meaningful both statistically and geologically, taking into account the limited availability of precise ages in the NTS region.

The Poisson model

The application of statistical methods to volcanic eruptions is put onto a sound analytical footing by Wickman (1966, 1976) in a series of papers that discuss the applicability of the methods and the evaluation of recurrence rates for a number of volcanoes. Wickman observes that, for some volcanoes, the recurrence rates are independent of time. Volcanoes of this type are called "Simple Poissonian Volcanoes." Theoretically, the probability formula (Crowe et al. 1982) is derived for this type of volcanic activity from the following assumptions:

1. Volcanic eruptions in successive time periods of length t for each period are independent and should

follow a Poisson distribution with a constant mean (average rate) λt , i.e. a simple Poissonian volcano.

2. Every eruption has the same probability of repository disruption p . That is, there is no heterogeneity with respect to disruptiveness.

3. The disruptiveness of the eruptions are independent of one another.

This very brief description is purely mathematical and has no direct interpretation in geologic terms. Since the Poisson model is both the state-of-the-volcanological-art (e.g. Wickman 1966, 1976) and used in actual risk assessment (e.g. Gardner and Knopoff 1974; McGuire and Barnhard 1981), we do not question the above assumptions in this article. Therefore, the following statistical development is based on the assumptions of a simple Poisson model. Of course, exploring alternative models derived from different assumptions based on detailed geologic data and statistical analysis would be valuable as well (e.g. see Ho 1991).

Probability formula

The probability model of Crowe et al. (1982) is based on the following relationship:

$$Pr [\text{disruptive event before time } t] = 1 - e^{-\lambda tp}.$$

The power series expansion for $\exp^{-\lambda tp}$ (Ellis and Gullick 1986, p. 545) is:

$$e^{-\lambda tp} = \sum_{k=0}^{\infty} \frac{(-\lambda tp)^k}{k!} = 1 - \lambda tp + \frac{(\lambda tp)^2}{2!} - \frac{(\lambda tp)^3}{3!} + \dots$$

Therefore, the final probability calculation can be simplified as:

$$Pr [\text{disruptive event before time } t]$$

$$= \lambda tp - \frac{(\lambda tp)^2}{2!} + \frac{(\lambda tp)^3}{3!} - \dots$$

$$\doteq \lambda tp, \text{ for small } \lambda \text{ and } p \text{ relative to } t.$$

The approximation is reasonable and is true for virtually all of the calculations in Crowe et al. (1982) since all of their estimated values of both λ ($< 10^{-5}$) and p ($< 10^{-3}$) are small. Therefore, the accuracy of estimating the unknown parameters λ and p directly influences the significance of values for the probability of repository disruption.

Recurrence rate

The Poisson process is used to describe a wide variety of stochastic phenomena that share certain characteristics and phenomena in which some "happening" takes place sporadically over a period of time in a manner that is commonly thought of as "at random." We will refer to a "happening" as an event. If events in a Poisson process occur at a mean rate of λ per unit time (1 year, 10^5 year, etc.), then the expected number (long-run average) of occurrences in an interval of time in t units is λt . In quantifying volcanism at Yucca Moun-

tain, we define a volcanic eruption as an event. Therefore, the collection of data is directly or indirectly based on the number of eruptions.

Crowe et al. (1982) try three methods to calculate λ in their probability calculations. These are: (1) evaluation of intervals of volcanic activity for evidence of periodicity; (2) counts of volcanic events in Quaternary time; and (3) evaluation of the ratio of magma production rate and mean magma volume. Based on method 1, they conclude that the data suggest no distinct patterns or periodicity of basaltic volcanism in late Cenozoic time. Therefore, the data are insufficient to analyze interval patterns and thus cannot be used to calculate future rates of volcanic activity (Crowe et al. 1982). We believe, however, that according to the Poisson model assumptions, intervals of volcanic activity should follow an exponential distribution and thus λ can be estimated statistically. We shall demonstrate such statistical sampling and estimation techniques in the following section.

Based on method 2, Crowe et al. (1982) calculate λ as N/T where N is the number of scoria cones and T is the period of time represented by the age of the cones or some other specified time period. Thus λ is the average number of eruptions per unit time. In their calculation of N/T , they define no statistical sampling technique that is associated with the assumed model. Moreover, they do not provide evidence that counting cones is equivalent to counting eruptive events. Crowe et al. (1989) and Wells et al. (1990) now recognize and classify the Lathrop Wells volcanic center as a polygenetic volcano and suggest that some cones may have erupted more than once. Note that the Lathrop Wells volcanic center is only 12 miles away from the proposed Yucca Mountain repository site. We shall introduce a statistical estimation procedure to interpret the estimator.

Based on method 3, Crowe et al. (1982) determine the rate of magma production for the NTS region by fitting a linear regression line to a data set of four points collected from four volcanic centers. Each value thus represents magmatic volume of a single eruption at a corresponding volcanic center. The mean magma volume for 4 m.y. is calculated by taking the average of these four values. The ratio (rate/mean) is then calculated as an estimate for the annual recurrence rate λ . Similarly, the annual recurrence rate for Quaternary time is obtained using only the two Quaternary data points. We consider this approach questionable, since a simple Poisson model requires a constant rate of occurrence, which is not the same as steady-state magma production in a volume-predictable model (e.g. see Wickman 1966, 1976; Wadge 1982). We shall show that such calculations based on magma volume duplicate those of method 2, if the rate of magma volume is constant. Moreover, we shall also point out that, in this case, they apparently assume only four (two) eruptions in the NTS region during the last 4 m.y. (Quaternary time). This apparent assumption explains why their final probabilities based on magma volume are consistently smaller than those based on cone counts (Crowe et al. 1982, tables IV and V).

The rate of volcanic eruption, λ is a critical parameter for the probability calculation. We shall now examine various statistical methods for calculating λ , how the geologic record of volcanism in the Yucca Mountain can be used to estimate values of λ , and the limitations in calculating λ .

Estimation based on Poisson count data

In dealing with distributions, repeating a random experiment several times to obtain information about the unknown parameter(s) is useful. The collection of resulting observations, denoted x_1, x_2, \dots, x_n , is a sample from the associated distribution. Often these observations are collected so that they are independent of each other. That is, one observation must not influence the others. If this type of independence exists, it follows that x_1, x_2, \dots, x_n are observations of a random sample of size n . The distribution from which the sample arises is the population. The observed sample values, x_1, x_2, \dots, x_n , are used to determine information about the unknown population (or distribution).

Assuming that x_1, x_2, \dots, x_n represent a random sample from a Poisson population with parameter λ , the likelihood function is:

$$L(\lambda) = \prod_{i=1}^n f(x_i; \lambda) = e^{-n\lambda} \lambda^{\sum_{i=1}^n x_i} / \prod_{i=1}^n x_i!$$

Many good statistical procedures employ values for the population parameters that "best" explain the observed data. One meaning of "best" is to select the parameter values that maximize the likelihood function. This technique is called "maximum likelihood estimation," and the maximizing parameter values are called "maximum likelihood estimates," also denoted MLE, or $\hat{\lambda}$. Note that any value of λ that maximizes $L(\lambda)$ will also maximize the log-likelihood, $\ln L(\lambda)$. Thus, for computational convenience, the alternate form of the maximum likelihood equation,

$$\frac{d}{d\lambda} \ln L(\lambda) = 0$$

will often be used, and the log-likelihood for a random sample from a Poisson distribution is:

$$\ln L(\lambda) = -n\lambda + \sum_{i=1}^n x_i \ln \lambda - \ln \left(\prod_{i=1}^n x_i! \right).$$

The maximum likelihood equation is:

$$\frac{d}{d\lambda} \ln L(\lambda) = -n + \sum_{i=1}^n \frac{x_i}{\lambda} = 0,$$

which has the solution $\hat{\lambda} = \sum_{i=1}^n \frac{x_i}{n} = \bar{x}$. This is indeed a maximum because the second derivative:

$$\frac{d^2}{d\lambda^2} \ln L(\lambda) = - \sum_{i=1}^n \frac{x_i}{\lambda^2},$$

is negative when evaluated at \bar{x} .

Let us demonstrate this estimation technique. Let X denote the number of volcanic eruptions for a 10^5 -year period for the NTS region from this assumed Poisson process. Then X follows a Poisson distribution with average recurrence rate μ , with $\mu = \lambda t = 10^5 \lambda$. If we wish to estimate λ for the Quaternary using the Poisson count data for the NTS region, the successive number of eruptions from the last 16 consecutive intervals of length 10^5 years ($16 \times 10^5 = 1.6 \times 10^6 =$ Quaternary period) must be estimated. The number of observed eruptions per interval are denoted as x_1, x_2, \dots, x_{16} . Thus, these 16 values represent a sample of size 16 from a Poisson random variable with average recurrence rate μ . Estimating the mean of the Poisson variable from these count data gives:

$$\hat{\mu} = \bar{x} = \sum_{i=1}^{16} x_i / 16,$$

and

$$\hat{\lambda} = \hat{\mu} / 10^5 = \sum_{i=1}^{16} x_i / (1.6 \times 10^6)$$

This shows that the estimated annual recurrence rate, $\hat{\lambda}$, is the average number of eruptions during the observation period (in years). Based on this estimation technique, $\hat{\lambda}$ can be defined as:

$$\hat{\lambda} = E/T, \quad (1)$$

where E = total number of eruption during the observation period,
and T = observation period.

Note that for the estimation of λ in this model, an individual observation x_i is not required. However, the distribution of x_i 's can provide information for model selection, for model-adequacy checking, and for parameter estimation in general.

Estimation based on repose times

With any Poisson process there is an associated sequence of continuous waiting times for successive occurrences. If events occur according to a Poisson process with parameter λ , then the waiting time until the first occurrence, T_1 , follows an exponential distribution, $T_1 \sim \text{Exp}(\theta)$ with $\theta = 1/\lambda$. Furthermore, the waiting times between consecutive occurrences are independent exponential variables with the same mean time between occurrences, $1/\lambda$ (Parzen 1962, p. 135). Several simplifying assumptions must be made in treating eruptions as events in time. Although the onset date of an eruption is generally well-defined as the time when lava first breaks the surface, the duration is harder to determine because of such problems as slowly cooling flows or lava lakes, and the gradual decline of activity. We adopt the same definition for repose time as used by Klein (1982). Therefore, we ignore eruption duration, we choose the onset date as the most physically meaningful parameter, and we measure repose times from one onset date to the next. Thus, our definition of "repose time" differs from the classic one as a noneruptive

period. This procedure seems justified because most eruption durations are much shorter than typical repose intervals. The mean time between two events (eruptions), θ , is inversely related to the volcanic recurrence rate λ . Assumptions of the Poisson process are rather restrictive, but at least a very tractable and easily analyzed model can be proposed. The maximum likelihood estimator for θ (Hogg and Tanis 1988, p. 336) is:

$$\hat{\theta} = \bar{t} = \sum_{i=1}^m t_i / m, \text{ and } \hat{\lambda} = \hat{\theta}^{-1} = \bar{t}^{-1},$$

where t_1, \dots, t_m represent values of a random sample of size m from an exponential population with parameter θ . For the NTS region, the exact values of t_i 's (repose times) are difficult to obtain because the precise date of each eruption is not known. However, based on the definition of repose times we can calculate:

$$\sum_{i=1}^m t_i = \text{time between the first and last eruptions during the observation period,}$$

and

m = total number of repose times = $E - 1$, which gives

$$\hat{\lambda} = (E - 1) / (T_0 - T_y), \quad (2)$$

where

E = Total number of eruptions between T_0 and T_y , inclusive,

with

T_0 = age of the oldest eruption,

T_y = age of the youngest eruption.

Note that the numerical values of E in both Eqs. 1 and 2 are identical for the same observation period of length T . In practice, however, the observation period for the exponential model (Eq. 2) must be trimmed to a period between T_0 and T_y , inclusive, to reflect that exactly $m (= E - 1)$ repose times (t_1 through t_m) are obtained. Theoretically, the two estimates obtained for λ (Eqs. 1 and 2) should be consistent, but not identical.

Estimation based on magma volume

Let V be the total volume of basaltic magma erupted at the surface in the NTS region during the observation period of length T . From Eq. 1, we obtain:

$$\hat{\lambda} = E/T = EV/TV = (V/T)/(V/E) = r/\bar{v} \quad (3)$$

where

$r = V/T$, the annual rate of magma production,

and

$\bar{v} = V/E$, the mean volume of magma during the observation period of length T .

Equation 3 is valid, but it also requires an accurate estimate of E for \bar{v} . If E (or r) is underestimated, so is λ . The most efficient way to calculate r is V/T . Crowe and Perry (1989) present a refined method to calculate r .

They evaluate r as the slope of the curve of cumulative magma volume plotted versus time. It is essentially identical to V/T , assuming a constant rate of magma volume (an assumption that Crowe et al. (1982) and Crowe and Perry (1989) have been striving to prove). In this case, the degree of erosional modification of volcanic landforms should be studied to estimate volumes of missing volcanic deposits. The overall error, which is multiplicative, is compounded in the values of Crowe and Perry (1989) for r . Moreover, E must be estimated when calculating \bar{v} , the mean volume of magma. Therefore, we see no economy in Eq. 3 and consider it to duplicate Eq. 1. We derive Eq. 3 merely to demonstrate that the estimation procedures used by Crowe et al. (1982) and Crowe and Perry (1989) are flawed and therefore must be modified.

Estimation of E

All of the statistical estimation methods considered for λ (Eqs. 1-3) require knowing the value of E (total number of eruptions during the observation period). An accurate count of E is possible for volcanoes with a complete historical record. Identifying E , however, depends strictly on a clear understanding of eruptive processes and reliable dating techniques for the NTS region, since no historical record is available. Scientists differ in their opinions of volcanism at the NTS area. The following is the view of Crowe et al. (1983):

"Basalt centers are composed of multiple vents, each marked by a scoria cone. In the NTS region the cones are divided into two categories: large central cones, referred to as the main cones, and satellite cones. The average number of cones at a single center, based on cone counts of seven Quaternary basalt centers in the NTS region, is about two to three cones. Thus, field data suggest a general eruption pattern where the initial breakthrough of magma to the surface is marked by the development of an eruptive fissure with two or three loci of effusion. Each of these vents becomes the site of small scoria cones. As the eruption proceeds, activity shifts or concentrates at a single vent that becomes the site of the main scoria cone."

The above description indicates that a main scoria cone is the final stage of a single eruption, and a single eruption could have several small vents to accompany the main cone. However, the possibility of polycyclic volcanism at all the volcanic centers needs to be evaluated. λ would be underestimated if nearby vents have distinguishable ages. We, therefore, estimate E as follows:

Let I denote the number of volcanic centers under investigation, and let J_i be the number of main cones in the i th volcanic center, where $i = 1, \dots, I$. The proposed estimate of E is:

$$\hat{E} = \sum_{i=1}^I \sum_{j=1}^{J_i} (m_{ij} + e_{ij}), \quad (4)$$

where m_{ij} = number of multiple, time-separate eruptions of the j th main cone in the i th volcanic center,

and e_{ij} = number of vents that are separate in space and time (with distinguishable age measurements) from the j th main cone in the i th volcanic center.

The rationale for this estimate is that significant information has emerged that some of the volcanic centers are polygenetic volcanoes (e.g. Lathrop Wells center (Wells et al. 1990)). This estimation for parameter E (total number of eruptions) given by Eq. 4 takes into account such a possibility for the NTS area. Studies are in progress to attempt to evaluate the values of m_{ij} 's and e_{ij} 's for the Quaternary volcanic centers of the Yucca Mountain.

Empirical results

Specifying the observation period (T) is important in modeling the volcanism at NTS. Most of the volcanic risk assessment studies in the Yucca Mountain area are centered around the post-6-Ma (Pliocene and younger) and Quaternary (<1.6 Ma) volcanism (Crowe et al. 1982, Smith et al. 1990a, and Wells et al. 1990). We shall use a preliminary data set based on the Quaternary volcanism to demonstrate the estimation techniques of the recurrence rate.

According to Crowe and Perry (1989), the younger zone of basaltic activity in the vicinity of Yucca Mountain is characterized by basaltic centers occurring as clusters of scoria cones and lava flows. There are seven Quaternary volcanic centers: the sequence of four 1.2-Ma centers in Central Crater Flat, two centers of the 0.28-Ma Sleeping Butte site, and the Lathrop Wells center. The age of the Lathrop Wells center has been refined from the original 0.27 Ma (Crowe et al. 1982) to 0.01 Ma (Crowe and Perry 1989). This date (0.01 Ma) is in the range of 0 to 0.02 Ma, the period of the most recent volcanic activity of the Lathrop Wells Cone as reported by Wells et al. (1990). The sequence of four 1.2 Ma centers in central Crater Flat includes Red Cone, Northern Cone, Black Cone, and two Little Cones (Fig. 1). Smith et al. (1990a) concentrate on this group of five cinder cone complexes in the central part of Crater Flat in Fig. 1. Based on their discussion, the cones form a 12-km-long arcuate chain. Details of vent alignment are best observed on Black Cone and Red Cone in the central part of the chain. In the Black Cone complex, the cinder cone is the most prominent topographic feature (about 100 m high and 500 m in diameter), but it may only account for a small volume of flows. A larger volume of basalt erupted from at least ten vents located north, south and east of Black Cone. These vents are commonly represented by scoria mounds composed of cinder, ash, and large bombs. Vents are aligned along two sub-parallel zones that strike approximately N35° E. One zone includes Black Cone and four scoria mounds; the other zone lies 300 m to the southeast of Black Cone and contains at least seven mounds. Dikes exposed in eroded mounds strike northeast and parallel the trend of the vent zones. The Red Cone complex contains three vent zones; two trend approximately N45° E and a third zone strikes N50° W (Fig. 2). This

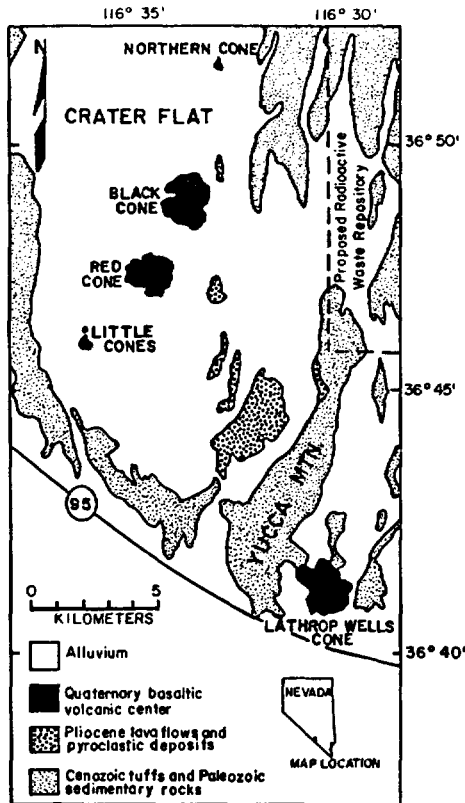


Fig. 1. Generalized geologic map of Crater Flat volcanic field area and boundary of proposed radioactive waste repository; inset map shows location of the Crater Flat volcanic field. (Source: Wells et al. 1990, figure 1)

provides substantive justification of our treatment of the total number of eruptions (E), and demonstrates that data for the Yucca Mountain region are incomplete at this preliminary stage of the site characterization studies.

Another key issue in the volcanic risk assessment studies is the disagreement over age-dating of the rocks. For example, the K-Ar dates for Red Cone presented by Smith et al (1990b, table 4) are: 0.98 ± 0.10 Ma for dike, 1.01 ± 0.06 Ma for amphibole-bearing unit, and 0.95 ± 0.08 for basalt on top of Red Cone. Until more reliable dating techniques are available, we have no way to distinguish the ages of the cones within each cluster of volcanic centers. Notice that, although an individual observation (x_i or t_i) is not required for the estimation of E developed in this article, the limited availability of precise ages would affect the counts of both m_{ij} and e_{ij} in Eq. 4.

Consistent with the notations used in the previous sections, the Quaternary volcanism yields:

$$T = 1.6 \text{ Ma}, E = 8, T_0 = 1.2 \text{ Ma}, \text{ and } T_y = 0.01 \text{ Ma.}$$

Therefore, based on Eq. 1,

$$\hat{\lambda} = E/T = 8/(1.6 \times 10^6) = 5 \times 10^{-6}/\text{yr}$$

Based on Eq. 2,

$$\hat{\lambda} = (E - 1)/(T_0 - T_y) = (8 - 1)/(1.2 \times 10^6 - 0.01 \times 10^6) = 5.9 \times 10^{-6}/\text{yr}$$

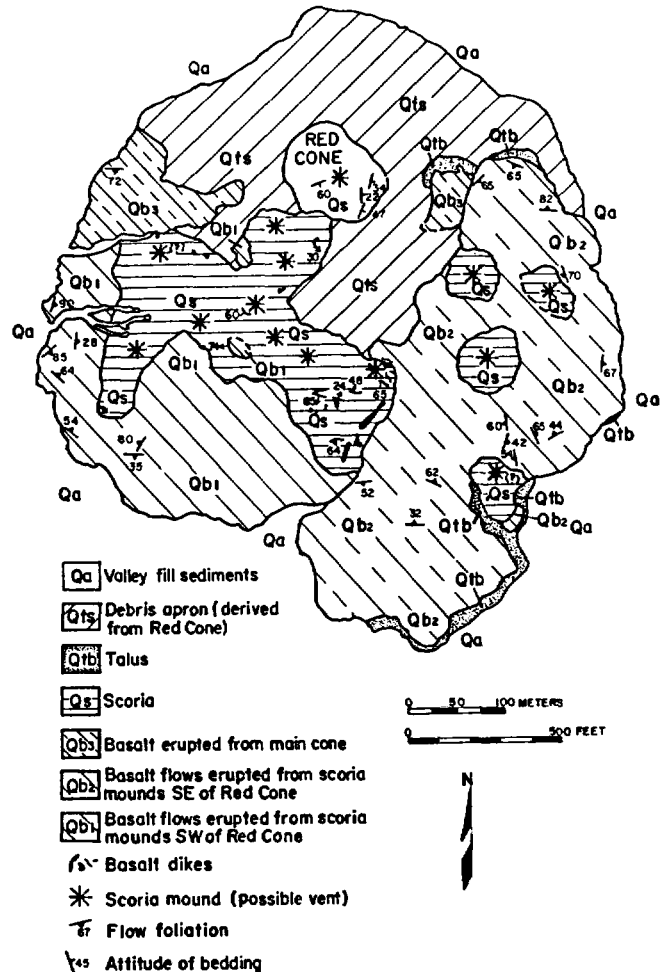


Fig. 2. Geologic map of Red Cone, Crater Flat, Nevada

Of course, the estimated rate based on Eq. 3 is $5 \times 10^{-6}/\text{yr}$ regardless of the value of V , since the magma volume is really never needed in this calculation.

Discussion and conclusion

The statistical estimation of recurrence rate λ requires a reliable count of distinguishable vents. This approach is based on the geologic record of volcanism at the NTS region. The methods of the approach are supported by sound statistical sampling theory. Crowe and Perry (1989), however, object that vent counts record only the recognition of a volcanic event, not its magnitude, and so they refine the parameter estimation by concentrating on the cumulative magma volume, which is a continuous variable. Nonetheless, their model assumptions and development are still based on a discrete simple Poisson model, which treats each eruption equally in order to calculate the final probability.

We now conclude this section with a few comments and point to some further work.

1. Their recommended method for estimating λ is to construct a curve of cumulative magma volume versus time, which is also affected by the counts of vents (\hat{E}) in

the observation period (T). Their ignorance of the critical factor E in Eq. 3 leads them to believe that estimation based on magma volume is the most acceptable method (Crowe and Perry 1989); this questionable belief, in turn, handicaps their estimates for \bar{v} and thus for λ .

2. All of the published results that demonstrate statistical sampling techniques for volcanic activity require a representative sample and a sufficiently large sample size to calculate a reliable long-run average with precision at a desired level (flipping a coin twice does not tell the whole story of the fairness of the coin).

3. Their recognition of the fact that short periods of eruptive activity are bounded by long periods of inactivity at NTS indicates that their choice of a simple Poisson model should be adequately checked based on more detailed geologic data. So far, the problems of model assumptions and parameter estimations have been treated only separately by Crowe et al. (1982) and Crowe and Perry (1989), despite the fact that the model (simple Poisson, or Volume-predictable model) assumptions and parameter (occurrence rate, or magma effusion rate) estimation methods virtually always depend on each other in volcanic hazard and risk calculations.

Yucca Mountain is remote from human habitation. There is no historical record of volcanism near Yucca Mountain. Therefore, the volcanic record must be developed by detailed field, geomorphic, and geochronologic studies. Precise ages are critical for volcanic rate calculations, but traditional K-Ar dating commonly has a large error in the age range recorded by the volcanoes near Yucca Mountain (1.1 Ma to 20 Ka). Until more precise techniques are developed, there will be uncertainties with regard to the age and duration of volcanism. Since predictions are needed, one possible improvement would be to reconfirm all of the crucial assumptions using data that are the only basis we have for making necessary plans, calculations, and model selections. We have no choice but to form our notion of governing laws on the basis of data and to act accordingly. This is particularly true in volcanic studies, where data are rare and expensive (\approx \$300-\$600 per age of a vent at Yucca Mountain). Our efforts for future studies will be devoted to considerably more detailed data collection and statistical modeling. At this preliminary stage of our work, all we can conclude is that the probabilistic results of Crowe et al. (1982) are based on idealized model assumptions, a premature data base, and inadequate estimates of the required parameters. For the reasons discussed, we think that Crowe et al. underestimate the risk of volcanism at the proposed Yucca Mountain repository site.

Acknowledgements. We wish to thank Dr. Donald A. Swanson for his useful and thoughtful suggestions to this work. We also thank Nate Stout for drafting the figures.

References

Condit CD, Crumpler LS, Aubele JC, Elston WE (1989) Patterns of volcanism along the southern margin of the Colorado plateau: the Springville Field. *J Geophys Res* 94:1975-1986

- Crowe BM (1980) Disruptive event analysis: volcanism and igneous intrusion. Battelle Pacific Northwest Laboratory Rep PNL - 2882
- Crowe BM, Carr WJ (1980) Preliminary assessment of the risk of volcanism at a proposed nuclear waste repository in the Southern Great Basin. US Geol Survey Open-File Rep 80-375, 15 p
- Crowe BM, Johnson ME, Beckman RJ (1982) Calculation of the probability of volcanic disruption of a high-level radioactive waste repository within Southern Nevada, USA. *Radioactive Waste Management* 3:167-190
- Crowe BM, Self S, Vaniman D, Amos R, Perry F (1983) Aspects of potential magmatic disruption of a high-level radioactive waste repository in Southern Nevada. *J Geol* 91:259-276
- Crowe BM, Harrington C, Turrin B, Champion D, Wells S, Perry F, McFadden L, Renault C (1989) Volcanic hazard studies for the Yucca Mountain Project. *Waste Management* 89, Vol 1. High Level Waste and General Interest, pp 485-491
- Crowe BM, Perry FV (1989) Volcanic probability calculations for the Yucca Mountain site: estimation of volcanic rates. Focus '89, Nuclear waste isolation in the unsaturated zone, September, 1989, hosted by the Nevada section of the American Nuclear Society, pp 326-334
- Ellis R, Gulick D (1986) *Calculus* (3rd) Harcourt Brace Jovanovich, New York
- Gardner JK, Knopoff L (1974) Is the sequence of earthquakes in Southern California, with aftershocks removed, Poissonian? *Bull Seismol Soc Am* 64:1363-1367
- Ho CH (1990) Bayesian analysis of volcanic eruptions. *J Volcanol Geotherm Res* 43:91-98
- Ho CH (1991) Time trend analysis of basaltic volcanism for the Yucca Mountain site. *J Volcanol Geotherm Res* 46:61-72
- Hogg RV, Tanis EA (1988) *Probability and statistical inference*, 3rd edn. Macmillan, New York
- Klein FW (1982) Patterns of historical eruptions at Hawaii volcanoes. *J Volcanol Geotherm Res* 12:1-35
- Klein FW (1984) Eruption forecasting at Kilauea volcano, Hawaii. *J Geophys Res* 89:3059-3073
- McGuire RK, Barnhard P (1981) Effects of temporal variations in seismicity on seismic hazard. *Bull Seismol Soc Am* 71:321-334
- Mulargia F, Gasperini PI, Tinti S (1987) Identifying different regimes in eruptive activity: an application to Etna volcano. *J Volcanol Geotherm Res* 34:89-106
- Parzen E (1962) *Stochastic processes*. Holden-Day, San Francisco
- Smith EI, Feuerbach DL, Naumann TR, Faulds JE (1990a) The area of most recent volcanism near Yucca Mountain: Implications for volcanic risk assessment. Proceedings of the International Topical Meeting, High-Level Radioactive Waste Management: American Nuclear Society/American Society of Civil Engineers, Vol 1, pp 81-90
- Smith EI, Feuerbach DL, Naumann TR, Faulds JE (1990b) Annual Report of the Center for Volcanic and Tectonic Studies for the period 10-1-89 to 9-30-90. The Nuclear Waste Project Office, Report No 41
- Wadge G (1982) Steady state volcanism: evidence from eruption histories of polygenetic volcanoes. *J Geophys Res* 87:4035-4049
- Wells SG, McFadden LD, Renault CE, Crowe BM (1990) Geomorphic assessment of late Quaternary volcanism in the Yucca Mountain area, southern Nevada: implications for the proposed high-level radioactive waste repository. *Geolog* 18:549-553
- Wickman FE (1966) Repose-period patterns of volcanoes. *Ark Mineral Geol* 4:291-367
- Wickman FE (1976) Markov models of repose-period patterns of volcanoes. In: Merriam DF (ed) *Random processes in geology*. Springer, New York Berlin Heidelberg, pp 135-161

Editorial responsibility: Y. Kastui